Parameter optimisations of a marine ecosystem model in the Southern Ocean

Author:
Kidston, Mehera

Publication Date:
2010

DOI:
https://doi.org/10.26190/unsworks/23571

PARAMETER OPTIMISATIONS OF A MARINE ECOSYSTEM MODEL IN THE SOUTHERN OCEAN

by

Mehera Kidston

A thesis submitted in fulfilment of the requirements for the degree of Doctor of Philosophy within the University of New South Wales, Australia

2010

Abstract

The Southern Ocean plays a central role in global biological production (Sarmiento et al., 2004). Quantifying the mechanisms that regulate magnitude and variability in plankton biomass in the Southern Ocean is a key challenge in understanding controls on global climate (Busalacchi, 2004). Numerical models are an integral means of understanding large scale views of seasonal plankton cycles (Fasham et al., 1990). Marine biogeochemical models are characterised by non-linear dynamics and the annual model trajectories are highly sensitive to the parameters used to run them. Experiments were performed to select a stochastic inverse method to objectively estimate the parameters of a simple four component nitrogen based mixed-layer marine ecosystem model for the Southern Ocean. Twin experiments using the Metropolis-Hastings algorithm and simulated annealing show that simulated annealing holds promise as a standard means of assigning the parameters of marine biogeochemical models in a way that improves the model agreement to available observations.

SeaWiFS surface chlorophyll estimates in the Sub-Antarctic Zone show low concentrations south west of Tasmania and high concentrations south east of Tasmania. Simulated annealing was used to estimate the model parameters at two locations in the Sub-Antartic Zone (station P1 at $140^{\circ}\mathrm{E}$, $46.5^{\circ}\mathrm{S}$ and station P3 at $152^{\circ}\mathrm{E}$, $45.5^{\circ}\mathrm{S}$) through assimilation of SeaWiFS chlorophyll observations. Model parameter estimates were compared to in situ parameter estimates from the SAZ-Sense (Sub-Antarctic Zone Sensitivity to environmental change) project stations P1 and P3 in the austral summer of 2007.

The parameter estimates suggest that different ecosystems are present within the Sub-Antarctic Zone. Station P3 has higher regenerated production with an *f*-ratio of 0.57 compared to P1 which has an *f*-ratio of 0.70, indicating larger size fractionated phytoplankton at P1 with a greater capability to sink and smaller size fractioned organisms at P3 with greater recycling ability. Different biological processes rather than different physical conditions between the two sites are responsible for the difference in

ecosystem function in our experiments. At P3 the optimisation results in satisfactory estimates of recycling rates but underestimates primary production, zooplankton biomass and zooplankton grazing. We conclude that the same ecosystem model structure is not applicable at both stations and we need additional processes at P3 to reproduce the observed seasonality of phytoplankton and the observed primary productivity. We hypothesize that the missing processes in the ecosystem model at P3 are iron limitation of phytoplankton and the seasonal variations in atmospheric deposition of iron.

SeaWiFS surface chlorophyll estimates and Levitus nitrate estimates in the Southern Ocean south of Australia (140°E) show that this region is characterised by a high-nitrate low-chlorophyll (HNLC) regime typical of Southern Ocean waters. The HNLC conditions become more prominent moving south from the Sub-Antarctic Zone, with surface chlorophyll generally decreasing and nitrate increasing with latitude. Simulated annealing was used to fit the ecosystem model to SeaWiFS surface chlorophyll data in the Sub-Antarctic Zone, Polar Frontal Zone and Antarctic Zone. We hypothesise that bio-availability of iron limits phytoplankton growth in this region. The most reliable physiological indicator of iron availability was investigated by optimising the model parameters for maximum photosynthetic growth and maximum photosynthetic efficiency of phytoplankton.

The parameter optimisations indicate that phytoplankton growth rates in the Polar Frontal Zone and Antarctic Zone are limited by some process not explicitly included in this model, with iron availability being the most likely candidate. In our experiments variations in ecosystem functioning caused by iron availability are more significant than differences caused by light availability. Based on these optimisations we support the contention that micronutrient availability, such as iron, is the primary cause of the HNLC conditions in the Australian sector of the Southern Ocean.

Unification of the information provided by observationalists and modellers is a valuable approach for improving understanding of marine ecosystem dynamics. Measurements of atmospheric deposition of iron, phytoplankton growth rates, primary production, *f*-ratio

and processes contributing to regenerated production throughout the year are needed to support Southern Ocean modelling studies.

Acknowledgements

I would like to thank my supervisors Richard Matear and Mark Baird for their time and effort in supporting my research over the past three and a half years, and for the opportunities they have presented me with. The continued enthusiasm they have provided has been indispensable to my development as a marine scientist.

I would also like to thank the biogeochemical modelling group at CSIRO – Thomas Moore, Andrew Lenton and Mathieu Mongin for helpful advice and constructive discussions.

I am grateful to the captain and crew of RSV *Aurora Australis* for their expertise in supporting the work at sea during SAZ-Sense, and am grateful to many colleagues for on board measurements and analysis. Thanks to my supervisors, and to Brian Griffiths and Steve Rintoul for giving me the opportunity to participate in two marine science research voyages. The volunteer work at sea allowed me some fantastic adventures and provided insight into many aspects of marine biogeochemistry and oceanography that I would not have otherwise experienced.

I am grateful for the financial support provided by the Northcote Graduate Scholarship scheme administered by the Menzies Centre for Australian Studies, the Australian Government's Endeavour Europe Award and the CSIRO Wealth from Oceans Flagship Collaboration Fund. My graduate studies would not have been possible without this assistance.

I also thank the NASA Ocean Biology Processing Group at the GSFC, Greenbelt, MD 20771 for the production and distribution of the SeaWiFS ocean colour data.

I thank all my friends and family for continual positive encouragement. The advice and perception they have given me has been highly appreciated in my efforts to finish this thesis.

TABLE OF CONTENTS

Abbreviations

AESOPS	Antarctic Environment and Southern Ocean Process Study
AZ	Antarctic Zone
ACC	Antarctic Circumpolar Current
BATS	Bermuda Atlantic Time-series Study (64°W, 31°N)
C	Carbon
CHL	Chlorophyll
CO_2	Carbon dioxide
dFe	Dissolved iron
DIC	Dissolved inorganic carbon
DIN	Dissolved inorganic nitrogen
HOTS	Hawaii Ocean Time-Series
HNLC	High nitrate – low chlorophyll
IPCC	Intergovernmental Panel on Climate Change
JGOFS	U.S. Joint Global Ocean Flux Study
MLD	Mixed layer depth
NABE	North Atlantic Bloom Experiment (20°W , 47°N)
NCAR	National Center for Atmospheric Research
N-P-D-Z	Dissolved inorganic nitrogen – phytoplankton – zooplankton – detritus
OG99	Oschlies and Garcon, 1999
OWSI	Ocean Weather Ship India (19°W , 59°N)
P1	Station P1 (140°E , 46.5°S)
P3	Station P3 (152°E , 45.5°S)
PAR	Photosynthetically available radiation
PF	Polar Front
PFZ	Polar Frontal Zone
SACCF	Southern Antarctic Circumpolar Current Front
SAF	Sub-Antarctic Front
SAMW	Sub-Antarctic Mode Water

SAZ	Sub-Antarctic Zone
SAZ-Sense	Sub-Antarctic Zone Sensitivity to change
Sea-WiFS	Sea-viewing Wide Field of view Sensor
SO03	Schartau and Oschlies, 2003a
SOIREE	Southern Ocean Iron Release Experiment
SST	Sea surface temperature
SSH	Sea surface height
STF	Subtropical Front
Station P	Ocean Station Papa (145°W, 50°N)

Chapter 1: Introduction

The ocean plays an integral role in the climate system by regulating the amount of carbon dioxide in the atmosphere. Carbon dioxide (CO_2) from the atmosphere dissolves in the surface waters of the ocean where it undergoes rapid chemical reactions. The carbon dioxide and the associated chemical forms are collectively known as dissolved inorganic carbon (DIC).

The oceans are responsible for the uptake of 2.2 ± 0.4 Pg C yr . (Takahashi et al., 2002) and contain 60 times more carbon than the atmosphere. As well as being transported around the globe by ocean currents, DIC is used by ocean biology; carbon fluxes in the ocean are often described in terms of the solubility pump and biological pump.

1.1 Plankton and the Biological pump

Phytoplankton are the most numerous organisms on the planet (Hallegraeff, 2006), and are the basis of most ocean food chains. For the past 3.5 billion years they have been controlling Earths climate through oxidation (Lee and de Mora, 1999; Falkowski et al., 1988) and the trapping of carbon dioxide (Riebesell et al., 1993).

The Earth's store of materials is fixed and finite; biologically important elements must be constantly recycled. During recycling the form of these elements continually changes as one chemical compound is transformed into another. Through the process of photosynthesis, phytoplankton produce organic compounds in the sun lit surface oceans from dissolved carbon dioxide and nutrients. Much of the organic matter produced is recycled within the surface waters through the food web structure of phytoplankton, zooplankton and bacteria but some survives and is transported out of the photic zone towards the ocean floor through sinking of dead organisms or faecal pellets. At depth remineralisation processes such as bacterial respiration transform the organic carbon back into DIC hence there is a net transfer of carbon from surface to depth A small fraction of this carbon is transported below the thermocline, where currents transport it to the deep ocean and it is 'buried' for hundreds to thousands of years. This process is known as the 'soft tissue pump'. Some species of phytoplankton and zooplankton form mineral

calcium carbonate shells in the upper ocean waters. When they die their shells sink and dissolve either in the water column or in sediments. This process adds to the downward transport of DIC from the surface to the abyss and is termed the ‘carbonate pump’. Together the soft tissue pump and the carbonate pump make up the ‘biological pump’.

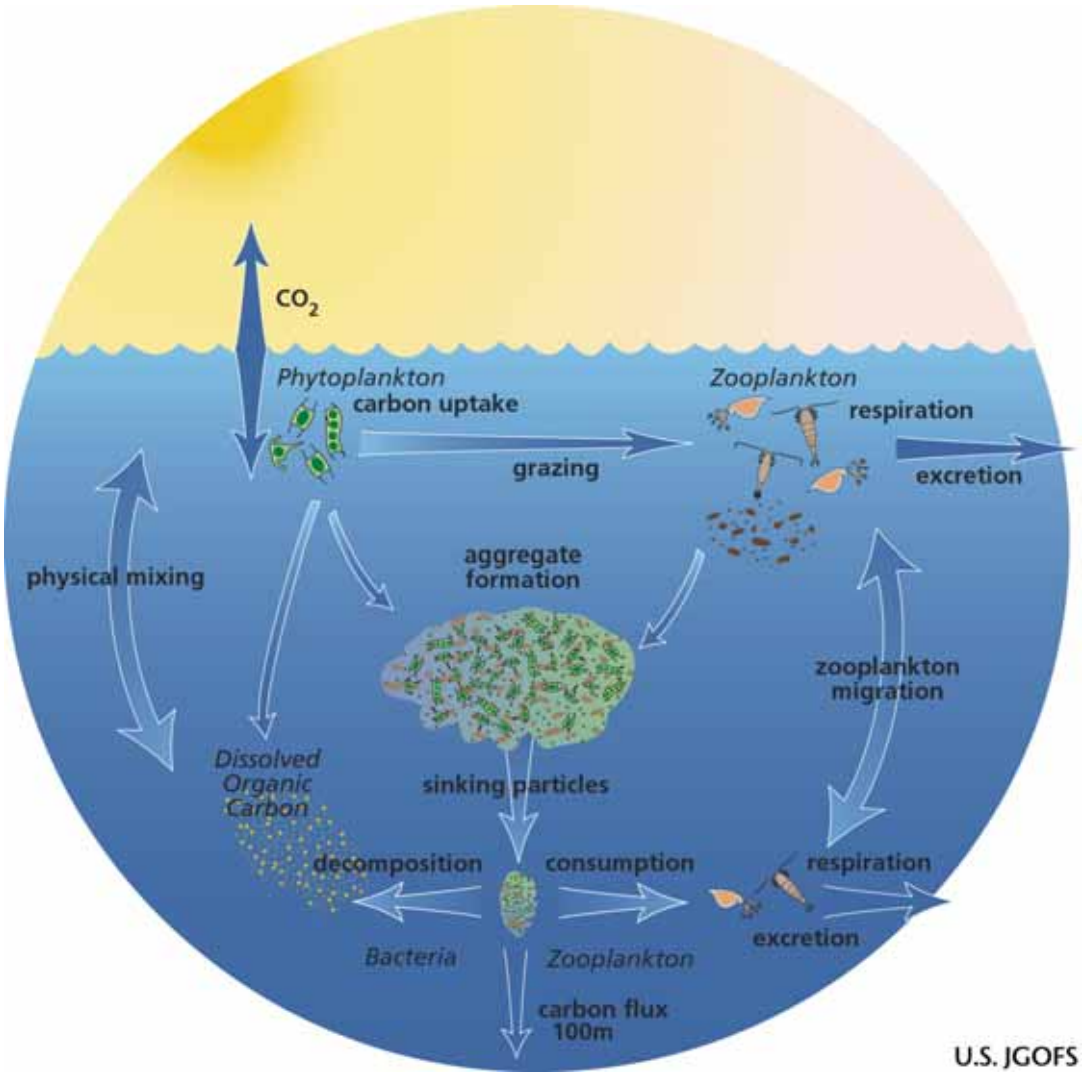

Figure 1.1: The ocean biological pump

Current literature suggests that photosynthetic carbon fixation by phytoplankton leads to the formation of approximately 45 Gt C yr^{-1} of which about 16 Gt are transported to the ocean interior through dissolved and particulate matter (Falkowski et al., 1998)
Given that air – sea carbon fluxes controlling the ocean carbon concentration have historically been in balance - a conjecture verified by ice core data of atmospheric CO_2 concentrations, which were remarkably stable for 10000 years before the industrial revolution (Neftel et al., 1982), it is assumed that the biological pump had been operating in steady state for many thousands of years preceding the eighteenth century. In addition, of the main chemical constituents that make up the soft tissue of all organisms (oxygen, hydrogen, carbon, nitrogen and phosphorus) nitrogen and phosphorus have the potential to limit phytoplankton productivity because they are not always found in forms that are biologically available (Ayres, 1997). Carbon, as well as oxygen and hydrogen, is abundant everywhere and does not limit growth of phytoplankton; therefore it is also widely assumed that the biological pump has continued operating in steady state since industrialisation despite the associated increase in atmospheric CO_2 levels (Anderson and Totterdell, 2004). However it cannot be assumed that this steady state will continue forever, and it has been suggested that the steady state assumption needs to be re-evaluated (Sarmiento and Gruber, 2006; Riebesell et al., 2007) .

Anthropogenic CO_2 causes changes in the inorganic aspects of ocean chemistry which effect the biological uptake of CO_2. Taylor et al. (2002) demonstrate that biological systems may respond to climate signals other than those that dominate the driving variables. Sarmiento et al. (1998) caution that biological changes may already be occurring and that they could easily modify the ocean carbon sink substantially between now and the middle of the twenty-first century. They report the largest potential modification is found in the Southern Ocean where increased stratification could decrease upward transport of excess DIC and cause an increase in biological pump efficiency. Conversely Maier-Reimer et al. (1996) report that the potential slowing of the thermohaline circulation could result in reduced nutrient upwelling and a reduction in biological pump efficiency.

In general it is clear that future climate driven changes could modify biogeochemical cycles and it is not known how ecosystems will respond to increasing CO_2 levels in the ocean. It is essential to investigate ocean biogeochemical cycles to understand the evolving role of the ocean in the face of environmental change.

1.2 The Southern Ocean

The Southern Ocean plays a central role in regulating ocean-atmosphere carbon exchanges, the climate system and biological production (Marinov et al., 2006) and is recognised as the body of water most sensitive to climate change (Sarmiento et al., 1998); furthermore different regions within the Southern Ocean have responded differently to climate change (Kohfeld et al., 2005).

Composed of three major masses of water - Antarctic Surface Water, Antarctic Bottom Water and Circumpolar Deep Water, the Southern Ocean produces over half of the world's deep ocean water (Trewby, 2002). The Southern Ocean's northern boundary is the Subtropical Front which is characterised by steep surface gradients in sea surface temperature and salinity (Hill et al., 2006). At this major biological barrier the Southern Ocean's mainly eastward flowing waters known as the Antarctic Circumpolar Current (the largest ocean current in the world and the only current to flow around the globe without encountering any continuous land barrier) meet the Atlantic, Pacific and Indian Oceans. Hence the Southern Ocean is the formation region of a global network of ocean currents that redistributes heat and nutrients around the earth.

The Southern Ocean is notorious for having some of the strongest winds and largest waves on the planet leading to the formation of a deep mixed layer of up to 800 metres in winter (Rintoul and Trull, 2001) that subsequently leads to a significant amount of upward mixing of nutrients from depth potentially sustaining large phytoplankton populations.

The Southern Ocean includes distinct regions which differ with respect to their hydrological, chemical and biological features (Treguer and Jacques, 1992). Despite the

favourable environment and plentiful macro-nutrient concentrations, vast areas of the Southern Ocean have surprisingly low phytoplankton populations with no distinct spring bloom. This phenomenon is also observed in areas of the Pacific Ocean, and determining the cause of these "high nitrate-low chlorophyll" (HNLC) conditions has been the subject of many studies in recent years (Boyd, 2002; Coale et al., 2004).

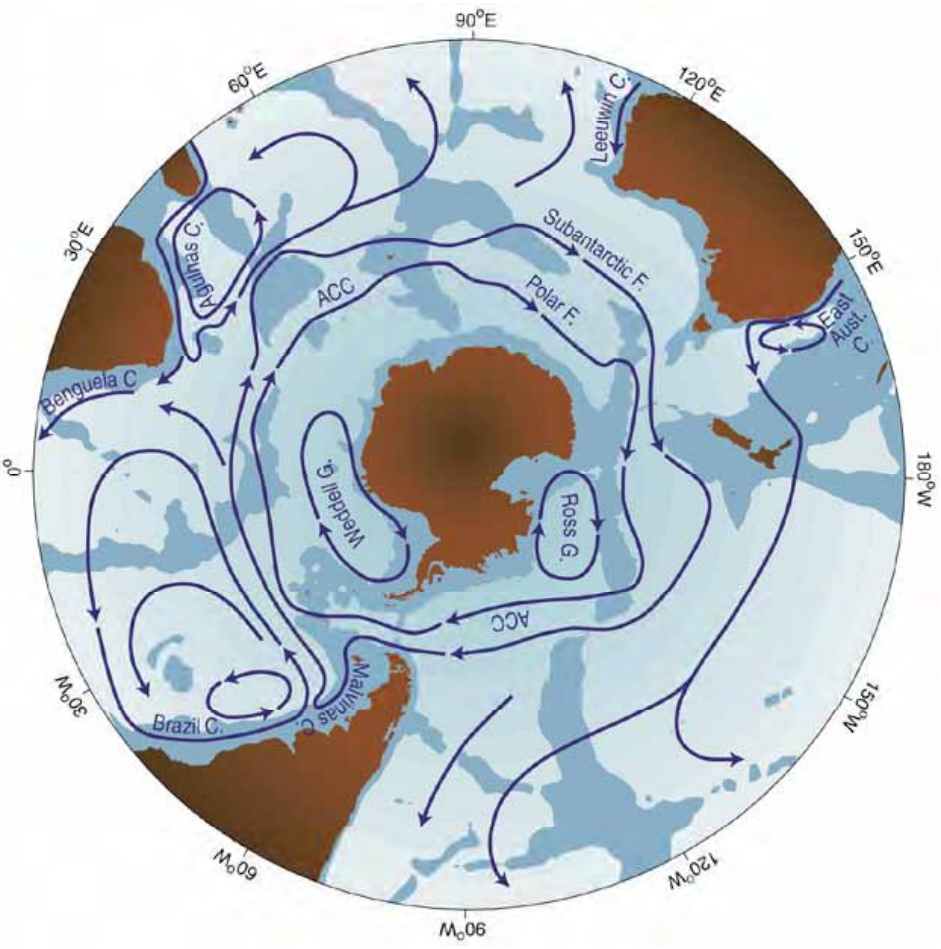

Figure 1.2: Map of the Southern Ocean showing the Antarctic Circumpolar Current (ACC), the Sub-Antarctic Front and the Polar Front.

Southern Ocean phytoplankton abundance is highly variable seasonally as well as spatially (Smith and Lancelot, 2004). In austral summer the Southern Ocean acts as an

intense sink for atmospheric CO_2, primarily due to photosynthetic utilization of CO_2 (Takahashi et al., 2002), however there is great variability in CO_2 ocean-atmosphere exchanges, largely linked to the activity of the biological pump (Treguer and Jacques, 1992). The relative contributions of physical conditions (such as mixing) and biological factors (sinking of detritus) in the uptake of carbon dioxide are still poorly constrained (Takahashi, et al., 2002), it is thought that vertical gradients of DIC are largely due to biological processes and thermodynamical effects alone explain only about one quarter of the observed gradients (Maier-Reimer and Hasselmann, 1987; Volk and Hoffert, 1985).

Predicting the responses of the physical and biological systems of the ocean to warming (Sarmiento and LeQuéré, 1996), and elucidating mechanisms describing processes such as the magnitude and variability in primary production in the Southern Ocean remain important issues to be resolved in understanding the controls on global climate. However until recently detailed study of the Southern Ocean has been problematic due to the limited number of shipboard observations south of 30°S (Gille, 2002).

1.3 The Sub-Antarctic Zone

The circumpolar Sub-Antarctic Zone (SAZ) is the body of water between the Subtropical Front and the Sub-Antarctic Front. The SAZ represents more than half the areal extent of the Southern Ocean (Orsi et al., 1995). SAZ surface waters have the potential to act as a large sink for atmospheric CO_2 due to seasonally low carbon dioxide partial pressures relative to atmospheric levels (Metzl et al., 1999). The SAZ is the region of formation of Sub-Antarctic Mode Water (SAMW) which supplies nutrients to the sub-tropical and tropical oceans on decadal to century timescales (Toggweiler et al., 1991). Up to 75% of global oceanic production may rely on this nutrient supply (Sarmiento et al., 2004). Thus the SAZ represents a key interface that mediates the influence of the Southern Ocean on the global oceans, and equally represents the first Southern Ocean region affected by circulation changes to the north (Griffiths et al., 2006).

1.3.1 Sub-Antarctic Zone Sensitivity to change

SAZ-Sense is the study of the sensitivity of Sub-Antarctic Zone waters to global environmental change. A scientific research voyage took place from 17th January to 20th February 2007 to examine biogeochemical processes in SAZ waters south of Australia. The overall goal was to understand the controls on Sub-Antarctic Zone productivity and carbon cycling and their sensitivity to future changes including climate warming (Griffiths et al., in press).

The survey included a wide range of measurements of biogeochemical and microbial community structure, carbon transports and ecosystem processes (Westwood et al., in press; Pearce et al., in press; Cavagna et al., in press; Lannuzel et al., in press; de Salas et al., in press; Wright et al., in press; Bowie et al., 2009). The process-orientation of the project allows ecosystem and biogeochemical models to benefit from realistic estimates of the key ecosystem processes such as *f*-ratios and primary production.

I participated as a volunteer on the SAZ-Sense voyage as part of the Conductivity-Temperature-Depth (CTD) team, and also learnt about how some of the many measurements used in this thesis, such as the maximum photosynthetic efficiency of phytoplankton, are made.

1.4 Remote Sensing

Quantification of phytoplankton biomass in the surface oceans can be derived from remote sensing measurements of the spectral distribution of sunlight reflected from below the sea surface. Phytoplankton contain the photosynthetic pigment chlorophyll-*a*, which mainly absorbs red and blue-violet light and reflects green light. When phytoplankton concentrations are high they predominate in determining the spectral absorption of sea water (Robinson and Sanjuan-Calzado, 2006) thus allowing satellite detection of phytoplankton distributions.

There has been a significant growth in satellite systems over the recent decades since the first ocean remote sensing satellites were launched by the US in the 1970s.
The most extensive global ocean colour data sets have been provided by the Sea-viewing Wide Field-of-view Sensor (Sea-WiFS) carried on a SeaStar spacecraft. Launched in August 1997 as part of NASA's Mission To Planet Earth, Sea-WiFS is a 'sequel' to Coastal Zone Colour Scanner which ceased operation in 1986.

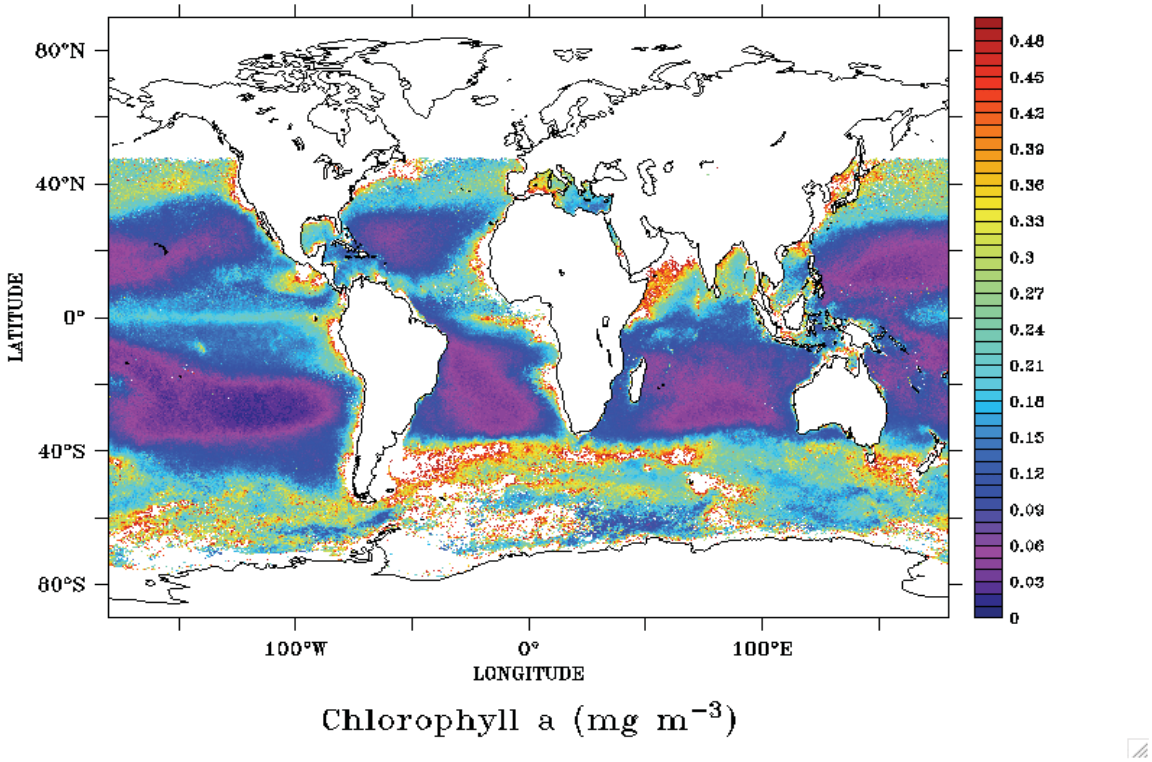

Figure 1.3: Surface chlorophyll concentrations (mg m^{-3}) in February from 1998 – 2008 Sea-WiFS climatology computed from 8-day composites.

Satellite data is crucial for validating model simulations of basin or global scale processes, as it is the only source of such large scale observations. While attractive in

principle it should be noted that use of this data is subject to several limitations. Measurement errors average about 30% due to cloud cover obstructing the satellite view and the presence of dissolved organic matter which strongly absorbs blue light, and interferes with measurements of chlorophyll. In addition satellites only detect the surface activity and field data from the Southern Ocean show chlorophyll-*a* typically exhibits maximum values at sub surface depths. For a full discussion on the use, and limitations, of satellite ocean colour data in marine ecosystem models see Robinson and Sanjuan-Calzado (2006).

Since satellite data provides the only large-scale synoptic observations of the Southern Ocean, the most advantageous use of Sea-WiFS observations would be to combine them with the relatively sparse data provided by in-situ measurements to collectively gain as much information as possible.

1.5 Numerical Modelling

Numerical modelling is a fundamental method of understanding the ocean biological pump. Marine biogeochemical models usually attempt to describe the movement of inorganic chemical tracers through the ecosystem by partitioning the chemistry and biology into a number of compartments such as nitrate, phytoplankton, zooplankton and detritus. Using mass conservation as an underlying concept the compartments simulate standing stocks, and transferral between compartments, of matter or energy. In this thesis the term ecosystem model is often used as a synonym for the entire biogeochemical model.

There are a large number of marine biogeochemical models available of varying complexities. (E.g. Evans and Parslow, 1985; Fasham et al., 1990; Oschlies and Garcon 1998; Palmer and Totterdell, 2001; Moore et al., 2002; Baird et al., 2006). These can broadly be divided into two categories:

1) Simple models, termed *N-P-Z-D* models (Evans and Parslow, 1985; Wroblewski et al., 1988; Doney et al., 1996; Denman and Pena, 2002; Kantha, 2004). These

models describe the non-linear interactions between populations of phytoplankton, zooplankton, nutrients and detritus. They may contain a few more compartments such as bacteria or ammonium (Fasham et. al., 1990) and are usually calculated in terms of nitrogen. Nitrogen is generally the limiting nutrient, and understanding the nitrogen cycle is a necessary prerequisite to modelling the carbon cycle (Fasham et al., 1995). Typically these models have 10 to 30 parameters.

2) Complex models, termed plankton functional type models, incorporating many different components of the intricate food web structure capable of capturing complex processes such as the export flux. There are about 5000 species of marine phytoplankton and there are models that include many functional types such as diatoms, coccolithophorids, picophytoplankton, phytoflagellates and dinoflagellates (Bissett et al., 1999; Totterdell et al.,1993; Moore et al., 2002; Gregg et al., 2003). These models typically have more than a hundred parameters.

In developing a marine ecosystem model the particular choice of compartments and the parameterisation of fluxes between compartments contains an element of subjectivity. In contrast to the modelling of physical ocean properties where the underlying equations of fluid dynamics are well known (Gill, 1982), the governing equations for biogeochemical models are unknown. Typically they use numerous parameters, for example even the relatively simple seven compartment model of Fasham et al. (1990) has 27 parameters. The model solutions significantly depend on the choice of these biological parameters, only a few of which are derived from observational data. Parameters derived from laboratory studies may be dependent upon the conditions in which biological samples are grown and dependent on different methodologies used in different laboratories. As the model complexity increases the number of parameters that must be fitted surpasses our ability to constrain them from observations (Matear, 1995).

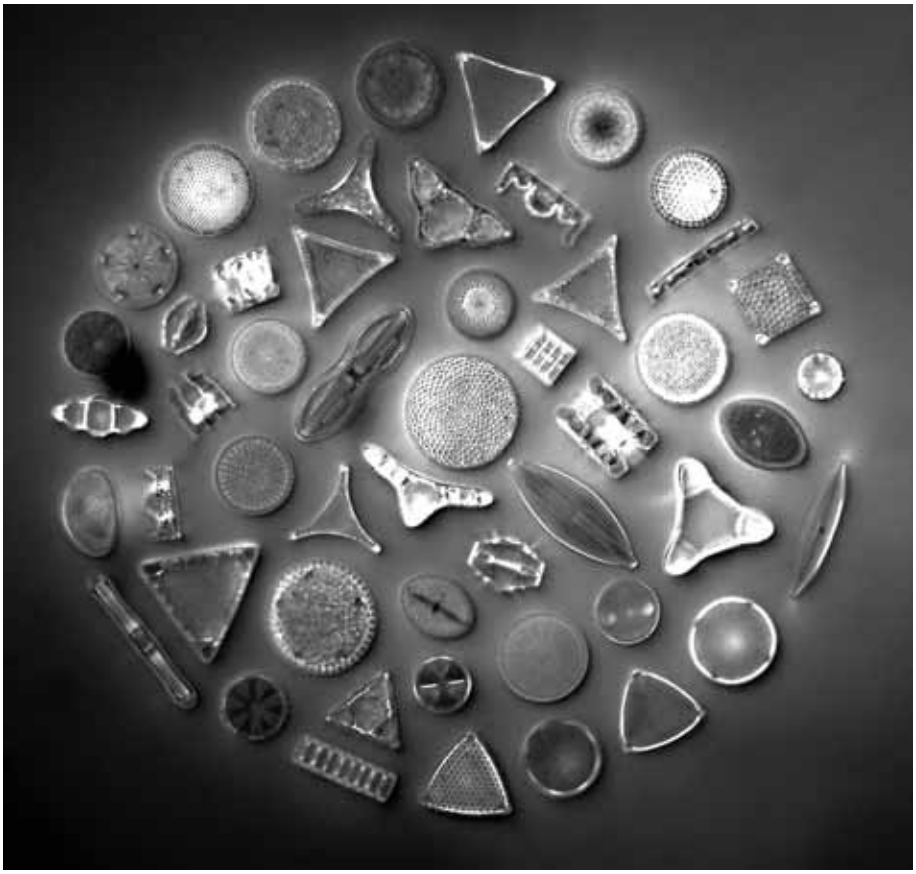

Figure 1.4: A photomicrograph depicting the siliceous frustules of fifty species of diatoms (the main primary producers in the Southern Ocean).

How much complexity is required to accurately simulate major observed biogeochemical cycles is a subject of debate (Anderson, 2005; le Quere, 2006). Although simple *N-P-Z-D* models cannot adequately explain all of the diverse measurements available for well sampled sites in the ocean such as the Bermuda Atlantic Time-series Study (BATS), they are capable of providing many insights into ocean biology such as the timing and magnitude of phytoplankton blooms. The choice of model complexity will ultimately depend on the purpose it is being used. It has not been demonstrated that models of greater complexity will inherently produce the best estimates of bulk biogeochemical fluxes. Indeed Friedrichs et al. (2006) showed that in fitting various models to

biogeochemical observations of DIN, chlorophyll, , zooplankton, primary production and export flux, the additional complexity of a multiple size class model is minimal. For the purpose of simulating phytoplankton distribution in a region of few biogeochemical observations, such as the Southern Ocean, a simple aggregated model is most appropriate.

One of the *N-P-Z-D* models most commonly used for its simplicity is that of Fasham et al. (1990). Despite its simplicity this model can reproduce the main features of the mixed layer at several locations and assist understanding of the fundamental biological interactions in the ocean (Fasham et al., 1995; Ryabchenko et al., 1997; Popova et al., 2002). It has become a standard model used in various studies ranging from zero-dimensional mixed-layer applications to coupled three-dimensional ecosystem circulation models (Matear, 1995; Sarmiento et al., 1993). However it has been shown by Spitz et al. (1998) that not all the parameters can be constrained by observations for BATS. Similarly it was shown by Matear (1995) that data sets for Station P (Ocean Station Papa) could not validate a seven compartment model, and a three-component configuration is adequate for explaining the observations of nitrate, phytoplankton and mesozooplankton concentrations and primary production.

Oschlies and Garcon (1999) simplified the model of Fasham et al. (1990) to a four component model, achieving quite realistic simulations of seasonal ecosystem dynamics in different biological provinces of the North Atlantic, however their model analysis indicated some deficiencies such as an overestimation of zooplankton grazing and an underestimation of phytoplankton mortality. Overcoming such deficiencies by increasing complexity is outweighed by the penalty of lowered accuracy due to inadequate parameterisations (Anderson 2005). One approach to the question of how to make models more realistic is to utilize the growing quantity of synoptic data to increase model agreement to the observed state.

1.6 Data Assimilation

Data assimilation is a versatile methodology for estimating oceanic variables. The estimation of a quantity of interest via data assimilation involves the combination of observational data with the underlying dynamical principles governing the system under observation (Robinson and Lermusiaux 2000).

There are two main uses of data assimilation:

1) forecasting to allow forward extrapolation of observations in order to improve the predictive power of models, a familiar application in the context of meteorological forecasting and widely used for physical ocean modelling (Oke et al., 2008). This application is only just emerging in ocean biogeochemical modelling (Mattern et al., 2010; Fontana et al., 2009).
2) parameter estimation, the determination of an optimal set of parameter values for a specified model, a rapidly growing field of research (Hemmings, 2009).

The standard approach when tuning ocean ecosystem models involves running the model forward in time, retrospectively comparing the results to the data, and then modifying the parameters accordingly – a process which always allows the possibility of tuning poorly defined parameters to force model output to the desired result. Data assimilation (sometimes termed inverse modelling), in the parameter estimation context, is a systematic means of comparing the output of the model with observations to obtain the underlying model parameters which statistically are most likely to have produced the data.

Minimising parameter uncertainty in marine ecosystem models is important since model dynamics can change substantially with different parameter values. A poor fit between model output and data can be because of a poor choice of parameter values or because of inappropriate model structure. This ambiguity between parameter uncertainties and model uncertainties makes it difficult to distinguish superiority between two or more contending models and explains the overabundance of models describing the same processes such as phytoplankton growth (Vallino, 2000).

The assimilation process can reduce the uncertainties (errors) associated with using either data or model alone; highlight where uncertainty is not reduced which is an indication of where model improvement needs to be made (Hurtt and Armstrong 1999); and investigate which parameters are well constrained by the data and which are not (Matear, 1995). Many parameter optimisation experiments have overlooked error estimation (Fasham et al., 2006), however measures of uncertainty are an essential aspect of parameter optimisation to avoid erroneous results (Fennel et al., 2001).

1.7 Objectives of this thesis

This thesis contributes toward understanding of two main issues in marine biogeochemical modelling. The factors that influence zonal and meridional variability in phytoplankton dynamics in the Southern Ocean are investigated, and suitable methodologies for parameter optimisation are evaluated.

More specifically the objectives of this thesis are:
1) Evaluate stochastic parameter estimation methods by optimising the parameters of a simple four-component nitrogen based marine ecosystem model using simulated annealing and the Metropolis-Hastings algorithm.

- Apply the algorithms in a set of twin experiments to determine their suitability for the problem and select the most advantageous of the two methods to optimise the model parameters.
- Identify the cost function sensitivity to each parameter value. Determine the parameters which are well constrained and those that are not
- Assess the suitability of using solely chlorophyll observations for data assimilation.

2) Investigate zonal differences in ecosystem dynamics in the Southern Ocean by performing parameter optimisation experiments at two contrasting locations in the Sub-Antarctic Zone south of Tasmania.

- Evaluate parameter optimisation estimates in terms of model fit to Sea-WiFS surface chlorophyll data as well as in situ estimates from the SAZ-Sense project.
- Investigate possible causes for the differences in phytoplankton biomass between the two contrasting sites by comparing optimised parameters, modelled *f*-ratios and primary productivity for the two locations.
- Determine whether the zonal variability in the ecosystem functioning is due to differences in the biological parameters or differences in the physical forcing.

3) Examine meridional variation in phytoplankton distributions south of Australia by performing parameter optimisations in the Sub-Antarctic Zone, Polar Frontal Zone and Antarctic Zone at 140°E.

- Consider the role of iron availability as a possible cause for the HNLC conditions of the Australian sector of the Southern Ocean by optimising phytoplankton growth parameters.
- Evaluate parameter optimisation estimates in terms of model fit to Sea-WiFS surface chlorophyll data as well as in situ estimates from published literature.
- Investigate meridional differences in ecosystem functioning by comparing the optimised parameters, *f*-ratios, primary production and zooplankton grazing between the three zones.
- Determine whether meridional variability in the estimated phytoplankton growth rates is due to differences in solar radiation, temperature, mixed layer depth or some other cause such as bio-availability of iron.

Chapter 3 of this thesis has been prepared in the form of a manuscript for submission to a peer-reviewed journal. Subsequently some aspects of the introduction and methodology are repeated for comprehensiveness.

Chapter 2:

Data assimilation methods for optimising the parameters of a marine ecosystem model

2.1 Introduction

Biogeochemical models provide an essential tool for numerical experimentation, such as the assessment of how marine ecosystems may respond to, or influence, changes in climatic conditions (e.g. McNeil and Matear, 2008; Matsumoto, 2007). They are a valuable tool for defining sampling strategies for measurement programs (Lenton et al., 2009) and are useful for filling in the gaps between oceanographic samplings (e.g. The Joint Global Ocean Flux Study).

The combination of biogeochemical models with observational data is an effective methodology that can provide insights into marine ecosystems that might not be feasible using either approach alone. Data assimilation can provide an improved representation of biological variables, where the errors and deficiencies of both models and data are reduced in a complementary fashion (Gregg et al., 2009).

The result of any biogeochemical modelling study is dependent upon the parameters chosen to run the model, and thus it is imperative that their allocated values are chosen critically. Assigning the values of the biological parameters is especially difficult as, unlike many chemical or physical parameters, they cannot strictly be regarded as constants (Fasham et al., 1990). There exists large variability in field estimates of parameters, and in some regions very few measurements exist. The use of data assimilation methods to determine the most suitable biological parameters has been the focus of much research over the past decade (Fennel et al., 2001; Eknes and Evensen, 2002; Schartau and Oschlies, 2003a; Hemmings et al., 2004; Oschlies and Schartau, 2005; Friedrichs et al., 2006; Nerger and Gregg, 2007; Zhao and Lu, 2008; Anderson, 2009).

Schartau and Oschlies (2003a) (SO03 hereafter) optimised the parameters of a four component reduced version of the Fasham et al. (1990) ecosystem model developed by Oschlies and Garcon (1999). They improved the model performance compared with the

initial parameterisation at three locations in the North Atlantic. The Southern Ocean ecosystem is crucial in global biogeochemical cycles and climate regulation. Running the models described in SO03 or Oschlies and Garcon (1999) in the Southern Ocean produces estimates of annual phytoplankton distributions very different from those estimated by satellites. Here we use the optimised parameters from SO03 as a starting point to perform parameter optimisation experiments for the Southern Ocean.

There are several techniques that can be used for parameter optimisation (gradient descent methods, conjugate gradient algorithms, newtons method, stochastic search algorithms). Despite numerous studies utilising data assimilation methods there is no consensus on the best approach. In the parameter estimation framework the most common implementation in ecosystem modelling is with the use of the adjoint method (essentially a gradient descent method). An adjoint model is used to compute the gradient of a model-data misfit function (known as the liklihood function or cost function) with respect to the parameters. Lawson et al. (1996) were the first to assimilate data into a biogeochemical model applying the variational adjoint method in a twin experiment to a five component zero-dimensional model. Subsequently the adjoint technique has been used for numerous studies ranging from twin-experiments using zero dimensional models (Spitz et al., 1998; Schartau et al., 2001) to fitting coupled physical-biological models to satellite ocean colour data (Xu et al., 2008).

Estimating the parameters of a marine biogeochemical model is a strongly non-linear problem (Athias et al., 2000). The adjoint method relies on iteratively solving linear inverse problems. The problem is solved by progressively computing local gradients of the model-data misfit function from a prior solution that must lie close enough to the real solution for the linearised equations to hold. Since the likelihood function (cost function) need not be quadratic, it is possible to have more than one optimal parameter set, i.e. the cost function may have more than one minimum. A minimum is said to be a global minimum if no other lesser or equal minima exist, otherwise it is considered a local minimum. The need to specify an initial guess for the parameters leads to the possibility

of convergence to a local minimum – the value of which will be influenced by the initial guess chosen.

The lack of prior knowledge about the parameters, and the fact that the cost functions associated with these problems exhibit several local extrema and saddle points, makes methods which rely on determining gradients of the cost function inappropriate (Athias et al., 2000). The use of stochastic search algorithms, which can explore large regions of the parameter space and reduce the chance of getting stuck in local minima, are better suited for highly non-linear systems.

Matear (1995) applied the stochastic method of Simulated Annealing to fit data from Station P to three different zero-dimensional marine ecosystem models and found the method to be robust and effective at determining optimal parameters while a conjugate gradient algorithm failed to find the optimal model parameters. Hurtt and Armstrong (1996; 1999) also used simulated annealing to reduce model-data misfit for a four-component reduced version of the Fasham et al. (1990) model, and were confident that they had found the "global" optima. The genetic algorithm is another stochastic method, used by Schartau and Oschlies (2003a) to optimise the parameters of the four-component model developed by Oschlies and Garcon (1999). Both simulated annealing and the genetic algorithm provide robust results however convergence to the global minimum cannot be proven.

Approaching the parameter optimisation problem from a Bayesian perspective Harmon and Challenor (1997) used the Metropolis-Hastings algorithm, which relies on Markov Chain Monte Carlo simulation. This approach allows determination of the posterior probability density distribution of parameter estimates; summary statistics such as the mean along with measures of uncertainty can then be derived. Furthermore this algorithm is proven to converge to the target distribution and directly accounts for covariance among uncertain parameters by storing the parameter distributions (Dilks et al, 1992). This approach of presenting a full statistical description of parameters, in the context of marine ecosystem models, has to the best of our knowledge, not been used in

optimisation experiments assimilating real data. Harmon and Challenor (1997) and Dowd and Meyer (2003) found the technique to be very successful in twin experiments and a promising framework for ecosystem inverse problems.

Assimilation of satellite ocean colour data into biogeochemical models is an approach with scope for much development. With over a decade of satellite ocean colour observations the range of data products is expanding as sensors become more sophisticated (McClain, 2009). The Argo float program is expanding to include biogeochemical observations (Gruber et al., 2007). These data sets allow data assimilation experiments in remote regions (such as the Southern Ocean) where annual in situ measurements are not practical. Inverse techniques will become more important in the future as more and more comprehensive data sets become available. It is important to identify the best methodology to integrate these observations with models.

A comparison of the Metropolis-Hastings algorithm and simulated annealing for optimising the parameters of a NPZD model has, to the best of our knowledge, not been done before. Twin experiments, in which model-generated data are assimilated into the model are used for addressing methodological issues (Spitz et al., 1998; Fennel et al., 2001; Friedrichs, 2001; Xu et al., 2008; Hemmings et al., 2008; Simon and Bertino, 2009), and are the first step in robust ecosystem modelling studies. In this study we test the performance of the two optimisation methods under idealised conditions in the Polar Frontal Zone (PFZ) of the Southern Ocean (146°E, 54°S). We identify the model parameters that are well determined in this location, and those that are not, and assess the suitability of assimilating satellite derived surface chlorophyll measurements as the only data constraint – an important consideration when performing data assimilation studies in the Southern Ocean.

The rest of this Chapter is organised as follows: Section 2.2 provides a description of the biological model and the data constraints used to run it. Section 2.3 describes the optimisation problem and the methods used to solve it. Section 2.4 describes the experimental design of the optimisations performed. The results of applying the

Metropolis-Hastings algorithm are presented and discussed in Section 2.5. The simulated annealing results are presented and discussed in Section 2.6. Section 2.7 summarises this Chapter.

2.2 The ecosystem model

2.2.1 Model structure

Following SO03 a simplified version of the Fasham et al. (1990) model with a reduced number of parameters is used. It is a four component *N-P-Z-D* (Nitrate-Phytoplankton-Zooplankton-Detritus) ecosystem model of the seasonal nutrient cycle described in μmol/kg nitrogen in the mixed layer. The model differs from that of Fasham et al. (1990) in that it combines nitrate and ammonium to dissolved inorganic nitrogen; and bacteria and dissolved organic nitrogen are not resolved explicitly.

The model differs from some more commonly used *N-P-Z-D* model formulations (Fiechter et al., 2009; Fan and Lv, 2009; Denman and Pena, 1999; Oschlies and Garcon, 1999) in that it includes a temperature dependence on all remineralisation rates, a quadratic phytoplankton mortality term and a linear loss from phytoplankton back to the dissolved inorganic nitrogen (DIN) pool. This formulation draws on the quadratic mortality of phytoplankton to approximate the loss of phytoplankton due to the formation of aggregates. This loss enters the detritus compartment to then sink out of the system. The phytoplankton linear mortality term represents an implicit description of the bacterial loop without explicitly including bacteria and dissolved organic nitrogen as additional state variables in the model (Schartau and Oschlies, 2003,b). The model structure is shown in Figure 2.1.

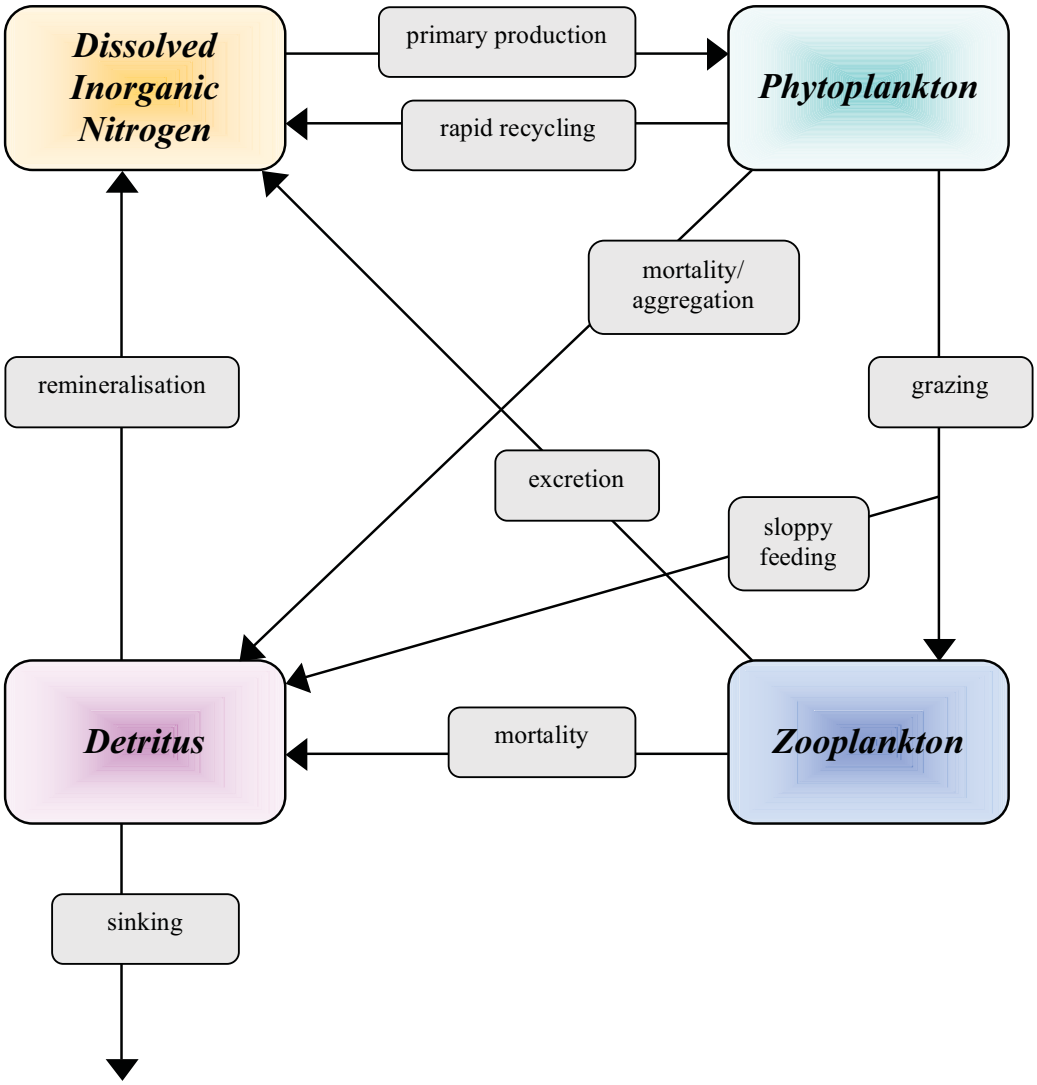

Figure 2.1: The biological model structure.

Mixed layer dynamics are not modelled explicitly. Instead following Evans and Parslow (1985); Fasham (1990); and Matear (1995), data are used to define the seasonal change in mixed layer depth (in metres), *M*, as a function of time (in days), t .

$$\frac{dM}{dt} = h(t) \tag{2,1}$$

In this simple zero-dimensional application the pelagic ecosystem is assumed to consist of a homogeneous mixed layer overlying a deeper abiotic layer. Phytoplankton and zooplankton are assumed to be homogeneously distributed in the upper mixed layer and horizontal advection and diffusion are ignored. An analytical solution for light limited growth introduced by Evans and Parslow (1985) is used that depends on photosynthetically available radiation (PAR) as a function of depth.

Following Evans and Parslow (1985) the concentrations of nonmotile entities like nitrate and phytoplankton remain constant in a shallowing of the mixed layer while the concentration of zooplankton increases since they are assumed able to actively maintain themselves within the mixed layer when its depth decreases. A deepening of the mixed layer dilutes the volumetric concentrations of nitrate, phytoplankton and zooplankton as the water mixes with the underlying water mass. Following Evans and Parslow (1985) we define the variable $h^+(t) = \max(h(t),0)$ and use $h^+(t)$ rather than $h(t)$ in equations representing nonmotile entities.

The biological source-minus-sink equations are:

Dissolved Inorganic Nitrogen (DIN)

$$\frac{dN}{dt} = \mu_D D + \gamma_2 Z + \mu_P P - \bar{J}(M,t,N)P + \frac{(m + h^+(t))}{M}(N_0 - N) \tag{2.2}$$

Phytoplankton Biomass

$$\frac{dP}{dt} = \bar{J}(M,t,N)P - G(P)Z - \mu_P P - \mu_P^2 P^2 - \frac{(m + h^+(t))P}{M} \tag{2.3}$$

Herbivorous zooplankton

$$\frac{dZ}{dt} = \gamma_1 G(P)Z - \gamma_2 Z - \mu_Z Z^2 - \frac{(h\ (t))Z}{M} \tag{2.4}$$

Detritus

$$\frac{dD}{dt} = (1-\gamma_1)G(P)Z + \mu_P^2 P^2 + \mu_Z Z^2 - \mu_D D - w_D \frac{\partial D}{\partial z} - \frac{(m + h^+(t))D}{M} \tag{2.5}$$

where *m* is a quantity that parameterises the diffusive mixing between the mixed layer and the deep ocean and N_0 is the DIN concentration below the mixed layer taken from climatological data.

Assuming light and nutrient limitation of growth to be independent effects, and following Hurtt and Armstrong (1996) and Oschlies and Garcon (1999) daily averaged growth is defined as the minimum of these two terms:

$$\bar{J}(M,t,\mathrm{N}) = \min\left(\bar{J}(M,t), J_{\max}\frac{\mathrm{N}}{K+\mathrm{N}}\right) \tag{2.6}$$

Where $\bar{J}(M,t)$ denotes the light limited growth rate and $J_{\max}$ the light saturated growth.

Since we do not model the diurnal cycle the actual light limited growth rate, $J(M,t)$, is averaged over $\tau_{24\mathrm{h}}$ = 1 day. Daily mean solar radiation is converted to peak values at noon assuming a triangular shape of daily incident radiation as described by Evans and Parslow (1985).

Assuming that the time a particular cell spends at depth is long compared to the photosynthesis reaction time, but short compared to the cell division time, then the daily growth rate, averaged over the mixed layer depth, *M*, can be written as:

$$\bar{J}(M,t) = \frac{1}{\tau_{24\mathrm{h}}}\int_0^{\tau_{24\mathrm{h}}} \frac{1}{M}\int_0^M J(I)dzdt \tag{2.7}$$

Where $J(I)$ is a function describing the phytoplankton photosynthesis-irradiance relationship. The function $J(I)$ was defined by the Smith function (Smith, 1936).

$$J(I) = \frac{J_{\max}(T)\alpha I(z,t)}{((J_{\max}(T))^2 + (\alpha I(z,t))^2)^{1/2}} \tag{2.8}$$

Where $J_{\max}$ is the growth rate as $I \to \infty$, and I is the photosynthetically active radiation as a function of depth below the surface of the water.

$$I(z,t) = PAR \cdot \tau(t) \cdot \frac{\tau_{24\text{h}}}{\tau_{\text{sun}}} I(0,t) \cdot \mathrm{e}^{(-k_w \bar{z})} \tag{2.9}$$

Where *I(0,t)* was the incident radiation observed immediately below the surface of the water, *PAR* was the photosynthetically active radiation at the surface, k_w was the light attenuation constant, $\bar{z} = z / \sqrt{1 - (\cos\theta / 1.33)^2}$ is the effective vertical coordinate with the angle θ of incidence at noon, z was depth in metres, $\tau(t)$ is a triangle function describing the evolution of the day, increasing linearly from 0 to 1 from daybreak to noon and decreasing linearly to 0 at nightfall over the variable day length, τ_{sun} ,calculated from standard trigonometric formula (Brock, 1981).

The maximum temperature-dependant growth was defined following the formula given by Eppley, 1972:

$$J_{\max} = ab^{cT} \tag{2.10}$$

Where T is temperature in degrees Celsius.

As well as growth the detritus remineralisation, zooplankton excretion and phytoplankton mortality parameters are temperature dependant as specified in Table 2.1 and as used in SO03.

For the loss of phytoplankton due to zooplankton grazing a Holling type III function is used:

$$G(\mathrm{P}) = \frac{g\varepsilon \mathrm{P}^2}{g + \varepsilon \mathrm{P}^2} \tag{2.11}$$

The model has 16 parameters, which are assigned the same values as those used by SO03, (shown in Table 2.1 and referred as the SO03 parameters here after). Following Matear (1995) the surface PAR and the light attenuation coefficient remain invariant in time. The remaining 14 parameters are 'free' parameters, used for the optimisation experiments.

2.2.2 Model numerics

The differential equations describing the ecosystem model were solved using a fourth order Runge-Kutta algorithm. The model simulations were run for three years with the annual output from the third year used for the optimisation process. Two years was the typical model spin up time, with a steady-state achieved by the third year. At steady state the concentrations of model components on the first day of the third year were the same as the concentrations on the first day of the fourth year and the annual cycle of the individual concentrations is not sensitive to their initial conditions, respectively.

2.2.3 Model forcing

The forcing fields of the ecosystem model are solar radiation, Sea Surface Temperature (SST), Mixed Layer Depth (MLD) and nitrate concentration below the mixed layer (Figure 2.2). The forcing data is taken from the GFDL global ocean circulation model MOM4 (Modular Ocean Model 4) with the OFAM (Ocean Forecasting Australian Model) configuration as described by Mongin et al. (in press). The global model restores SST to a monthly climatology of Reynolds SST (Reynolds and Smith, 1994) merged with the Levitus World Atlas 2001 (Levitus, 1982). Daily values of SST are obtained by interpolation. The daily MLD is taken as the depth of a 0.05 kg m^{-3} difference in density from the surface computed using the model output of temperature and salinity (Mongin et al., in press). Daily averaged values of solar radiation are from NCAR (National Centre for Atmospheric Research).

Parameter	Symbol	Value	Units
	Phytoplankton coefficients		
Maximum photosynthetic efficiency (initial slope of P-I curve)	α	0.256	$\text{day}^{-1}/(\text{W m}^{-2})$
Shortwave fraction of photosynthetically active radiation	PAR	0.43	
Light attenuation due to water	k_w	0.04	m^{-1}
Maximum growth rate parameters	a	0.27	day^{-1}
	b	1.066	
	c	1.0	$(^{\circ}C)^{-1}$
Half saturation constant for N uptake	K	0.7	mmol m^{-3}
Phytoplankton loss rate	μ_P	$0.04 \times b^{cT}$	day^{-1}
Quadratic mortality rate	μ_P^2	0.025	$(\text{mmol m}^{-3})^{-1}\,\text{day}^{-1}$
	Zooplankton coefficients		
Assimilation efficiency	γ_1	0.925	
Maximum grazing rate	g	1.575	day^{-1}
Prey capture rate	ε	1.6	$(\text{mmol m}^{-2})^{-1}\,\text{day}^{-1}$
Quadratic mortality	μ_Z	0.34	$(\text{mmol m}^{-3})^{-1}\,\text{day}^{-1}$
Excretion rate	γ_2	$0.01 \times b^{cT}$	day^{-1}
	Detrital coefficients		
Remineralisation rate	μ_D	$0.048 \times b^{cT}$	day^{-1}
Sinking velocity	w_D	18.0	m day^{-1}

Table 2.1: Parameters used to run the ecosystem model. The values are taken from Shartau and Oschilies, 2003a.

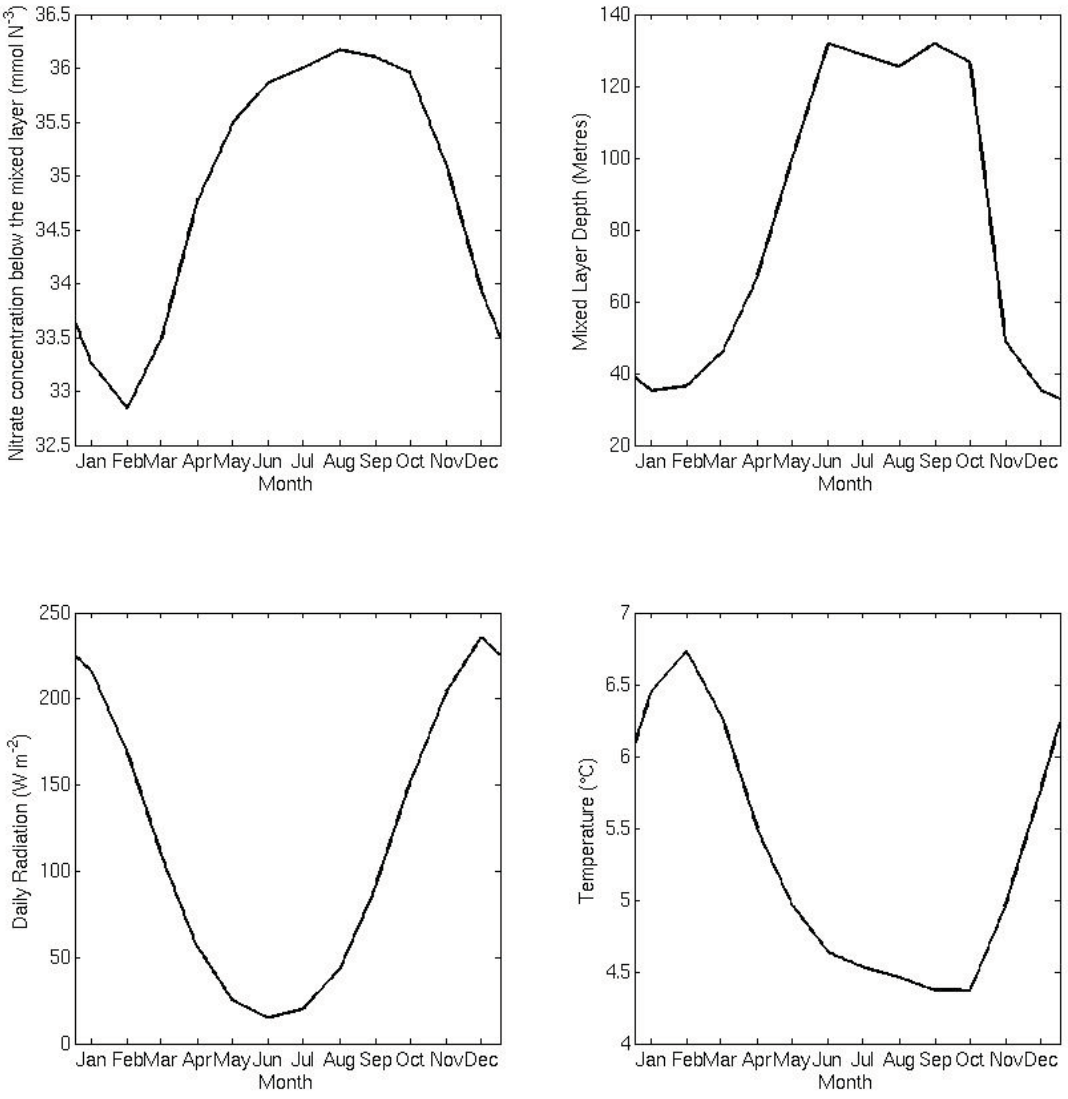

Figure 2.2 Forcing data used to run the model simulations. Panel A shows nitrogen concentration below the mixed layer (mmol N m^{-3}); panel B shows mixed layer depth (meters); panel C shows daily incident solar radiation (W/m^2); panel D shows temperature (degrees Celsius).

2.2.3 Data constraints

A simulated data set was created by running the model with the parameters defined in Table 2.1, thus providing a data set that is fully consistent with the model assumptions making systematic errors due to model formulation impossible. The biological parameters which generated the data are known, and are regarded as the true parameter values.

The model is run with a different parameter set to create a starting point or reference solution. This parameter set is optimised, i.e. data sets of N, P, Z and D are assimilated to the reference solution, generating a third time series of daily values for each state variable. The success of the data assimilation is determined by the agreement between the third time series and the data as well as the recovery of the true parameter values. This type of numerical experiment is called an identical twin experiment. The twin experiment procedure is summarised in Figure 2.3.

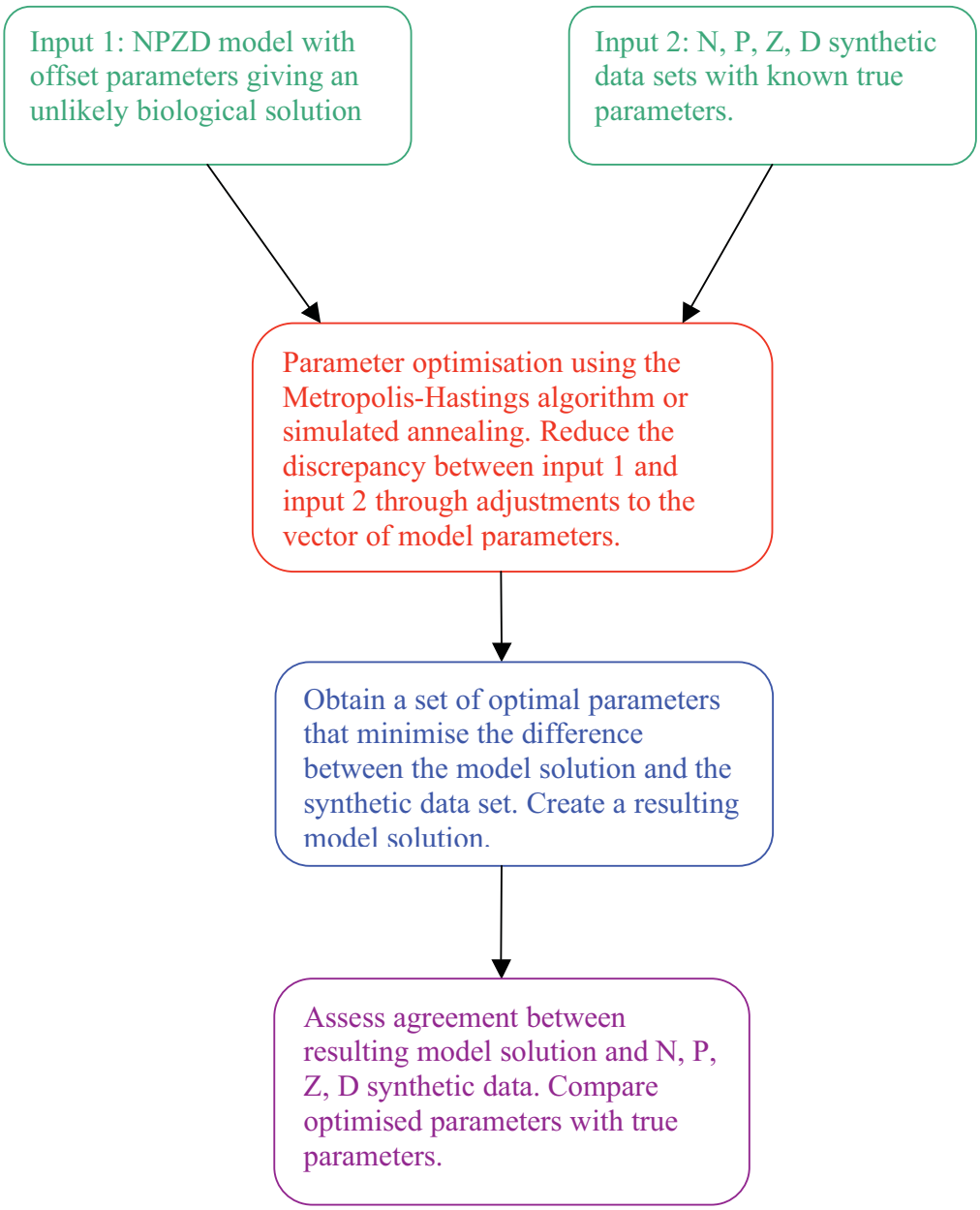

Figure 2.3: Process used for a running a twin experiment.

2.3 Parameter optimisation schemes

2.3.1 Bayesian inference

The parameter optimisation problem involves combining the best a priori estimate of a parameter with the available observations of the system, the synthesis of information is then used to make a (posterior) parameter estimate. The Bayesian perspective is one of a conjunction of different sources of information and is well suited to tackle this type of problem.

Bayesian methods enable us to make statistical inference about our uncertainty of parameters ϑ conditional on observed data y and the knowledge of the state. The probability that a parameter, ϑ, is correct given the information, y, is termed the posterior parameter distribution and denoted $f(\vartheta \mid y)$.

Using the rules of conditional probability known as Bayes' rule gives the posterior density:

$$f(\vartheta \mid y) = \frac{f(\vartheta) f(y \mid \vartheta)}{f(y)} \tag{2.12}$$

where $f(y) = \int f(y, \vartheta) d\vartheta = \int f(\vartheta) f(y \mid \vartheta) d\vartheta$

where $f(\vartheta)$ is the prior parameter distribution, $f(y)$ is the distribution of the observations y and $f(y \mid \vartheta)$ is the likelihood function through which the data y affect the posterior inference.

Evaluation of $f(y)$ is straightforward in the one-dimensional case but in practical applications high dimensionality and non-linearity prohibit direct numerical integration; hence historically implementation of Bayesian methods has been unfeasible. However now with the use of high-powered computing it is possible to use simulation methods to generate a distribution with identical statistical properties as the posterior distribution without actually solving the integration directly.

Markov Chain Monte Carlo techniques are used to generate a sample of parameter values having identical distribution to the real (intractable) parameter distribution. We can then compute summary statistics for the distribution such as the mean, variance and correlation between the estimates, which will be the same as for the distribution of interest. With the variance, error magnitude can be directly assessed which is key part of model evaluation. There is no consensus on the best method for error analysis in parameter optimisation experiments (e.g. Zhao and Lu, 2009; Schartau and Oschlies 2003a). This method provides a mathematically rigorous way of quantifying errors.

2.3.2 The Metropolis-Hastings algorithm

Monte Carlo methods are numerical processes that produce pseudo-random numbers within a parameter space and a Markov Chain is a sequence of random variables having the Markov property which means that given the present state of the sequence the future state is conditionally independent of the past. The idea of Markov chain simulation is to simulate a random walk in the space of ϑ which converges to a stationary distribution, (termed the target distribution), that is the posterior parameter distribution, $f(\vartheta|y)$.

Several techniques have been developed to make the long-term behaviour of the Markov chain tend towards a desired distribution. The most general and flexible of these is the Metropolis-Hastings algorithm in which an (arbitrary) initial parameter value is chosen as a first guess, the next estimate of the parameter is selected by perturbing the current value in some pre-defined way. The model is then run with the candidate parameter to assess whether the proposed parameter increases the posterior density. Based on this a decision of whether to accept the new choice for the parameter is made. If the new parameter increases the posterior density (improves the fit of the model to the data) it is kept and it becomes the next value in the chain. If it results in a decrease in posterior density it may be kept with a small probability, otherwise it is rejected and the previous parameter is maintained for next value in the chain. This is repeated thousands of times as it is important to make sure the entire range of possible parameter values are sampled and that the resulting distribution has reached the required target distribution.

More formally the Metropolis-Hastings algorithm is given by:

1. Set t=0. Choose a starting vector $\boldsymbol{\vartheta}^0$ from a starting distribution $f_0(\boldsymbol{\vartheta})$.

for t=1,2,…

2. Generate a proposal $\boldsymbol{\vartheta}'$ from a proposal distribution $q(\boldsymbol{\vartheta}' \mid \boldsymbol{\vartheta}^{t-1})$.

3. Generate a data set $\boldsymbol{y}'$ from $f(\boldsymbol{y} \mid \boldsymbol{\vartheta}')$.

4. Calculate acceptance probability $\alpha = \min\{1, r\}$ where $r = \dfrac{f(\boldsymbol{\vartheta}' \mid \boldsymbol{y}) / q(\boldsymbol{\vartheta}' \mid \boldsymbol{\vartheta}^{t-1})}{f(\boldsymbol{\vartheta}^{t-1} \mid \boldsymbol{y}) / q(\boldsymbol{\vartheta}^{t-1} \mid \boldsymbol{\vartheta}')}$.

5. With probability α set $\boldsymbol{\vartheta}^t = \boldsymbol{\vartheta}'$. Otherwise set $\boldsymbol{\vartheta}^t = \boldsymbol{\vartheta}^{t-1}$.

6. Return the values $\{\boldsymbol{\vartheta}^1, \boldsymbol{\vartheta}^2, ..., \boldsymbol{\vartheta}^N\}$.

The Metropolis-Hastings Algorithm is a generalisation of the basic Metropolis algorithm with the modification that the jumping rule q need not be symmetric – i.e. there is no requirement that $q(\boldsymbol{\vartheta}^a \left| \boldsymbol{\theta}^b \right.) \equiv q(\boldsymbol{\vartheta}^b \left| \boldsymbol{\vartheta}^a \right.)$ and to compensate for this asymmetry the ratio in step 4 is a ratio of importance ratios rather than the ratio of densities used in the Metropolis algorithm. This modification can be useful in increasing the convergence time. It can be proven that the sequence converges and to a unique stationary distribution (Gelman et al., 2004).

There are many ways to set the step size of the algorithm q. A general method, which has good results in a wide variety of problems, is a normal random walk jumping distribution, i.e. updates are chosen according to: $\boldsymbol{\vartheta}' = \boldsymbol{\vartheta}^{t-1} + \boldsymbol{\varepsilon}$ where the error structure $\boldsymbol{\varepsilon}$ has Gaussian distribution. When updating the algorithm with new parameter values it is important to choose a step length to give appropriate acceptance. If the step size is too large there will be too many rejections and the algorithm wastes time standing still. If the step size is too small the random walk moves too slowly and it will take an unacceptably long time to reach the target distribution. The most efficient multivariate normal random walk jumping distribution has the proportion of jumps accepted at about 25% (Gelman et al., 2004).

The first step in implementation is to formulate the prior and likelihood functions. Taking a formulation that assumes Gaussian uncertainty for both prior parameter values $\boldsymbol{\vartheta}^{obs}$ and the assimilated data $\boldsymbol{y}^{obs}$, and prescribed uncertainties for the priors $\boldsymbol{\delta\vartheta}$ and the data $\boldsymbol{\delta y}$, the likelihood function is expressed as the negative exponential of the misfit between model-derived values and measurements in relation to measurement error such that

$$f(\boldsymbol{y}|\boldsymbol{\vartheta}) = \exp\{-J(\boldsymbol{y}|\boldsymbol{\vartheta})\} \tag{2.13}$$

with J being equivalent to the cost function – a term used in many parameter optimisation studies for the model-data misfit function (e.g. Lawson et al., 1995; Friedrichs, 2002).

$$J(\boldsymbol{y}|\boldsymbol{\vartheta}) = \frac{1}{2}\sum_{i=1}^{n}(y_i^{prd} - y_i^{obs})^2 \frac{1}{\delta y_i^2} \tag{2.14}$$

where $\boldsymbol{y}^{prd}$ denotes the model predicted values and n is the number of observations.

Similarly the prior parameter distribution can be written as

$$f(\boldsymbol{\vartheta}) = \exp\{-J(\boldsymbol{\vartheta})\} \tag{2.15}$$

with

$$J(\boldsymbol{\vartheta}) = \frac{1}{2}\sum_{i=1}^{m}(\vartheta_i^{prd} - \vartheta_i^{obs})^2 \frac{1}{\delta\vartheta_i^2} \tag{2.16}$$

where $\boldsymbol{\vartheta}^{prd}$ denotes the algorithm predicted parameter values and m is the number of parameters. The prior parameter part of the cost function tries to force the model parameters to be within acceptable limits.

The posterior distribution for $\boldsymbol{\vartheta}$, calculated for the acceptance step of the Metropolis-Hastings algorithm is given by:

$$f(\boldsymbol{\vartheta}|\boldsymbol{y}) \propto \exp\left(-\frac{1}{2}\sum_{i=1}^{n}(y_i^{prd} - y_i^{obs})^2 \frac{1}{\delta y_i^2}\right)\exp\left(-\frac{1}{2}\sum_{i=1}^{n}(\vartheta_i^{prd} - \vartheta_i^{obs})^2 \frac{1}{\delta\vartheta_i^2}\right) \tag{2.17}$$

being weighted by an average of the data and the prior parameter distribution.

A point to note when running the Metropolis-Hastings algorithm is that if the iterations are not run for long enough the simulations may not accurately represent the target

distribution since proof of convergence is for the asymptotic behaviour of the chain. The early simulations will be influenced by the starting distribution rather than the target distribution; to ensure we are only using the converged parameter sequence in the analysis we discard the first section of the iterations of the simulation runs (termed the 'burn in' period).

To implement the algorithm the starting point or reference solution was created by offsetting the 'true' parameter values by adding Gaussian errors with standard deviation set to be equal to the expected parameter error specified in Table 2.2. Gaussian error was added to the observations with a standard deviation set to be 5% of the observation value for the biological observations and 1% of the observation value for the nitrate observations (since the nitrate observations are an order of magnitude larger than the biological observations). The step size on each parameter was set to be proportional to the prior standard deviation. The algorithm was run for 500,000 iterations. The first 300,000 iterations were discarded to ensure we were looking at the asymptotic distribution and not the prior distribution. The remaining 200,000 iterations were used to describe the posterior parameter distribution. The mean values of the posterior parameter distributions are used for the parameter estimate. Standard deviations were calculated directly from the posterior parameter distribution.

2.3.3 Simulated annealing

Simulated Annealing is a stochastic algorithm used for multivariate optimisation problems giving comparable results to the Metropolis-Hastings algorithm. As described by Kirkpatrick et al. (1983) and Kruger (1993) there is a strong connection between multivariate optimisation and statistical mechanics. An analogy with annealing in solids provides a basis for optimisation of large and complex systems.

Annealing is the term used to describe the thermodynamic process for growing crystals. It involves heating of a solid matter until it reaches a liquid state where the atoms are free to move randomly, it is then cooled slowly enough to permit thermal equilibrium at each

reduced temperature allowing the atoms to arrange themselves into the most stable position, eventually the system reaches a state closely resembling the structure of a perfect homogeneous crystal lattice at a global minimum of energy. If the substance is not cooled slowly enough, and allowed to get out of equilibrium, the resulting crystal will have many defects, or the substance may form a glass with no crystalline order and only metastable, locally optimal structures.

In this application each configuration, defined by the set of atomic positions of the system is weighted by its Boltzmann probability factor, $\exp(-E(y)/k_B T)$ where $E(y)$ is the energy of the configuration, k_B is Boltzmann's constant, and T is temperature. This results in a situation where each new configuration at a lower energy level than the previous one is unconditionally accepted but there is also a probability $\exp(-\Delta E / k_B T)$ that a configuration at a higher energy level may be accepted (where ΔE is the difference in energy between the two configurations) (Kirkpatrick et al., 1983).

Finding the low temperature state of a system when a formula for calculating its energy is given is an optimisation problem analogous to finding the parameterisation of a model with lowest model-data misfit where a known formula for calculating its cost is given. Iterative improvement of the model is much like the microscopic rearrangement process modelled by statistical mechanics, with a set of ecosystem parameters replacing configurations of atoms and the cost function playing the role of the energy. The temperature is replaced by a control parameter, which is still called T.

To simulate annealing first take a high initial value of T (T_0), imposing an arbitrary initial parameterisation, and start generating random models. They will be distributed following the prior probability density $f(\boldsymbol{\vartheta})$. In each iteration by slightly perturbing the current parameterisation $\boldsymbol{\vartheta}_i$, a new parameterisation $\boldsymbol{\vartheta}_j$ is generated. Very slowly make T tend to zero while continuing to generate random models. At each temperature the simulation must proceed long enough for the system to reach a steady state. If the reduction of T is too rapid, the system can be trapped in a metastable state – a local minimum of the cost

function (Tarantola, 1987). When T reaches zero the system is frozen in the state of lower energy at the point of the maximum likelihood estimate for $\boldsymbol{\vartheta}$ (minimum of the cost function).

Accepting only parameterisations that lower the cost function is comparable to extremely rapid cooling and results in metastable solutions. The Metropolis Algorithm, which allows incorporation of controlled uphill steps can be applied with the use of a Boltzmann acceptance criteria. The Metropolis Algorithm is the same as the Metropolis-Hastings algorithm with the additional constraints that the jumping distribution must be symmetric and the acceptance probability $\alpha = \min\{1, r\}$ is calculated by setting r to the ratio of densities

$$r = \frac{f(\boldsymbol{\vartheta}' | \boldsymbol{y})}{f(\boldsymbol{\vartheta}^{t-1} | \boldsymbol{y})} \tag{2.18}$$

The choice of a Boltzmann acceptance probability results in the system evolving into a Boltzmann distribution – the average of any property, such as the cost, is determined for some effective T, and as T is lowered the Boltzmann distribution collapses into the lowest energy state (minimum of the cost function).

Following Tarantola (1987) we define the energy function for T_0:

$$E(\boldsymbol{y}) = -T_0 \log\left(\frac{f(\boldsymbol{\vartheta}) f(\boldsymbol{\vartheta} \mid \boldsymbol{y})}{f(\boldsymbol{\vartheta})} \right) \tag{2.19}$$

where $f(\boldsymbol{\vartheta})$ is the prior probability distribution of the parameters and $f(\boldsymbol{\vartheta} \mid \boldsymbol{y})$ is the posterior probability distribution of the parameters.

This gives $f(\boldsymbol{\vartheta} \mid \boldsymbol{y}) = f(\boldsymbol{\vartheta}) \cdot \exp\{-E(\boldsymbol{y}) / T_0\}$ (2.20)

Defining for any T we have $f(\boldsymbol{\vartheta} \mid \boldsymbol{y}) = f(\boldsymbol{\vartheta}) \cdot \exp\{-E(\boldsymbol{y}) / T\}$ (2.21)

Using the Metropolis Algorithm we have a method that for any value of T can generate random models with probability density given by

$$f(\boldsymbol{\vartheta} \mid \boldsymbol{y}) = f(\boldsymbol{\vartheta}) f(\boldsymbol{y} \mid \boldsymbol{\vartheta}) \tag{2.22}$$

In nonlinear least squares usually $f(\boldsymbol{\vartheta})$ is taken to be a constant. We set the Boltzmann constant k_B to be equal to 1, and the energy function $E(\boldsymbol{y})$ is thus defined by the usual model-data misfit function J multiplied by T_0 (Tarantola, 1987):

$$E(\boldsymbol{y}) = T_0 \cdot J \tag{2.23}$$

In this case, following Matear (1995), we define the model-data misfit function J as the sum of the terms $J(\boldsymbol{y} \mid \boldsymbol{\vartheta})$ and $J(\boldsymbol{\vartheta})$ defined in Section 2.3.2 . A third term is included to penalise large deviations from the steady-state cycle reached after spin up (Matear, 1995; Schartau and Oschlies, 2003a). The steady state penalty requires the model components at the start of the third year to be approximately equal to the values at the start of the second year.

$$J = \frac{1}{2}\sum_{i=1}^{n}(y_i^{prd} - y_i^{obs})^2 \frac{1}{\delta y_i^2} + \frac{1}{2}\sum_{i=1}^{m}(\vartheta_i^{prd} - \vartheta_i^{obs})^2 \frac{1}{\delta \vartheta_i^2} + \frac{1}{2}\sum_{j=1}^{nc}(t_1^j - t_{365}^j)\frac{1}{\delta t^4} \tag{2.24}$$

As in Section 2.3.2 we assume Gaussian uncertainty for both prior parameter values $\boldsymbol{\vartheta}^{obs}$ and the assimilated data $\boldsymbol{y}^{obs}$, and prescribed uncertainties for the priors $\boldsymbol{\delta\vartheta}$ and the data $\boldsymbol{\delta y}$. The algorithm predicted parameter values are $\boldsymbol{\vartheta}^{prd}$ and m is the number of parameters. The model predicted values are denoted $\boldsymbol{y}^{prd}$ and n is the number of measurements. The steady state penalty, which penalises large deviations from the total nitrogen inventory reached after spin up, is denoted t, the number of data sets in the optimisation (N, P, …) is denoted by nc and $\delta t = 0.01$.

The procedure is independent of the structure and analytical properties of the cost function as well as the initial guess since the starting value of T enforces a random state. Following Matear (1995) the simulated annealing required 6 parameters: the starting value of T, T_0; a vector representing the standard deviations of Gaussian error to be

added to the model parameters $\boldsymbol{\sigma}_0$; the reduction factors for T_0 and $\boldsymbol{\sigma}_0$ after each annealing step dT and $d\sigma$ respectively; the maximum number of perturbations per annealing step $N_{\max}$; the maximum number of acceptable perturbations required before exiting from an annealing step N_g.

To calculate T_0 1000 simulations simulations were performed by perturbing the initial parameter set by $\boldsymbol{\sigma}_0$ and calculating the mean change in the cost function (ΔJ). T_0 is then given by

$$T_0 = -\frac{\Delta J}{\mathrm{In}\chi} \tag{2.25}$$

where χ is the probability of parameter sets with higher costs to be accepted, which was set to 0.9 (Kruger, 1993; Matear, 1995; Athias et al., 2000).

The vector $\boldsymbol{\sigma}_0$ was set to the standard deviation of the model parameters given in Table 2.2. The parameters of the simulated annealing were set to dT = 0.95, $d\sigma$ = 0.95, $N_{\max}$ = 5500 and N_g = 2500. These parameter values were chosen to ensure the algorithm converged to the same value independent of the initial guess of the parameter values. The initial guess was determined by adding or subtracting the prescribed Gaussian errors from the true parameter values (addition or subtraction was imposed randomly by the algorithm). Gaussian error was added to the observations with a standard deviation set to be 5% of the observation value for the biological observations and 1% of the observation value for the nitrate observations (since the nitrate observations are an order of magnitude larger than the biological observations).

Following Matear (1995), Vallino (2000), Fennel et al. (2001) and Friedrichs et al. (2006), the uncertainty of the parameter estimates is assessed by calculating their standard errors from the Hessian matrix (**H**) - the matrix of second partial derivatives of the likelihood function with respect to parameters evaluated at their maximum likelihood estimates $\boldsymbol{\vartheta}^*$.

$$\mathbf{H} = \left. \frac{\partial^2 J}{\partial \boldsymbol{\vartheta}^2} \right|_{\boldsymbol{\vartheta}=\boldsymbol{\vartheta}^*} \tag{2.26}$$

The Hessian provides a measure of how steeply likelihood drops off as you move away from the optimum solution. We wish to calculate the Hessian at the point of the global minimum. Near the global minimum the inverse of the Hessian matrix provides the matrix of approximate parameter variance and covariance's with the square roots of the diagonals being the standard errors (Thacker, 1987). The advantage of a twin experiment is that the 'true' parameters are known and one can determine if the global minimum has been found by assessing the optimised parameters.

The estimated standard errors may not recover the full information on the parameter uncertainties. Following Fennel et al. (2001) the singular vectors of the Hessian matrix are calculated to determine the parameter correlations as well as the sensitivities of the model solution to each parameter. The matrix **H** is expanded as

$$\mathbf{H} = \mathbf{U}\Lambda\mathbf{V}^T \tag{2.27}$$

where the diagonal matrix Λ contains the singular values of **H** and the matrices **U** and **V** contain the singular vectors. Following Matear (1995) the Hessian matrix was evaluated using a 3-point centered finite differencing scheme. The Hessian matrix was inverted using a Singular Value Decomposition algorithm.

The parameters associated with the largest singular values are determined from the ordered singular vectors; these parameters have the greatest influence on the model solution. The parameters associated with the smallest singular values have little influence on the model output but are responsible for explaining the largest degree of error. This provides quantitative information regarding the extent to which the model parameters are resolved by the observations (Matear, 1995).

2.4 Experimental design

The first experiments applying the Metropolis-Hastings algorithm (experiments M-H1) optimised all 14 free parameters of the model (Table 2.1). The posterior parameter distributions were used to obtain summary statistics on each parameter, with the mean value taken as the parameter estimate and the standard deviation used as a measure of the expected error. The results from experiments M-H1 dictated further experiments (experiments M-H2) in which the Metropolis-Hastings algorithm was used to optimise only a subset of parameters in order to improve the estimates.

Similarly the first experiment using simulated annealing (experiment SA1) optimised all 14 free parameters of the model. An analysis of the posterior errors of the estimated parameters was calculated from the Hessian matrix. The results from experiment SA1 encouraged a second experiment (experiment SA2) in which the only data constraint was the concentration of phytoplankton.

2.5 Metropolis-Hastings algorithm results and discussion

2.5.1 Experiments M-H1

The Metropolis-Hasting algorithm failed to recover the parameters in the first optimisation experiments, which allowed all 14 free parameters to vary (Table 2.2). Inspection of the parameter traces showed that after 500,000 iterations the parameters had not reached a stationary distribution. A number of experiments were run and extensive time was spent adjusting the step size and number of iterations. After 10 million iterations the parameters still did not reach a stationary distribution.

The highly non-linear nature of the problem makes the posterior probability in the model space extremely difficult to define. Correlations between parameters mean it is likely to be multi-modal preventing the algorithm from stabilising to a unique solution. If two or more parameters are correlated with each other a change in one can be accompanied by a corresponding change in the other without much affect on the model solution. Therefore, while optimising all the model parameters at once, there exists the possibility of

accurately reproducing the phytoplankton data with more that one combination of parameter values.

Using the Metropolis-Hastings algorithm our parameter estimates are defined as the mean of the posterior distribution. Since the algorithm did not result in a stable posterior distribution, the mean values are very different from the true parameters with large standard deviations (Table 2.2).

Parameter	True Parameter value	Experiment M-H1 estimate	Experiment M-H2 estimate
α	0.256 ± 0.1	0.770 ± 0.49	-
a	0.27 ± 0.1	0.18 ± 0.14	-
b	1.066 ± 0.01	1.426 ± 0.28	1.060 ± 0.028
c	1.0 ± 0.01	0.9 ± 0.57	-
K	0.7 ± 0.2	0.49 ± 0.28	-
μ_P	0.04 ± 0.01	0.02 ± 0.006	0.04 ± 0.002
γ_1	0.925 ± 0.01	0.920 ± 0.01	-
g	1.57 ± 0.1	6.13 ± 2.78	-
ε	1.6 ± 0.1	2.83 ± 1.06	-
μ_Z	0.34 ± 0.05	0.69 ± 0.30	-
γ_2	0.01 ± 0.01	0.005 ± 0.004	0.01 ± 0.008
μ_D	0.048 ± 0.01	0.043 ± 0.009	-
w_D	18.0 ± 2	33.0 ± 18.70	-
μ_P^2	0.025 ± 0.01	0.074 ± 0.004	-

Table 2.2: The mean and standard deviation of the posterior parameter distributions obtained by running the Metropolis-Hastings algorithm. A dash indicated the parameter was kept fixed at the 'true parameter value' in the optimisation.

2.5.2 Experiments M-H2

Through trial and error (optimising each parameter individually followed by two parameters at once, three parameters at once, etc., in many combinations) the well resolved parameters were found to be the maximum growth rate parameter *b*, mortality of phytoplankton μ_P, and zooplankton excretion rate, γ_2. Running the Metropolis-Hastings algorithm allowing only these three parameters to vary results in a stable posterior distribution for each parameter (Figure 2.4). The parameter values estimated from the mean of the posterior distributions are shown in Table 2.2, the accuracy of the estimates are reflected in the model solution, which is very close to the annual cycle of the data constraints (Figure 2.5).

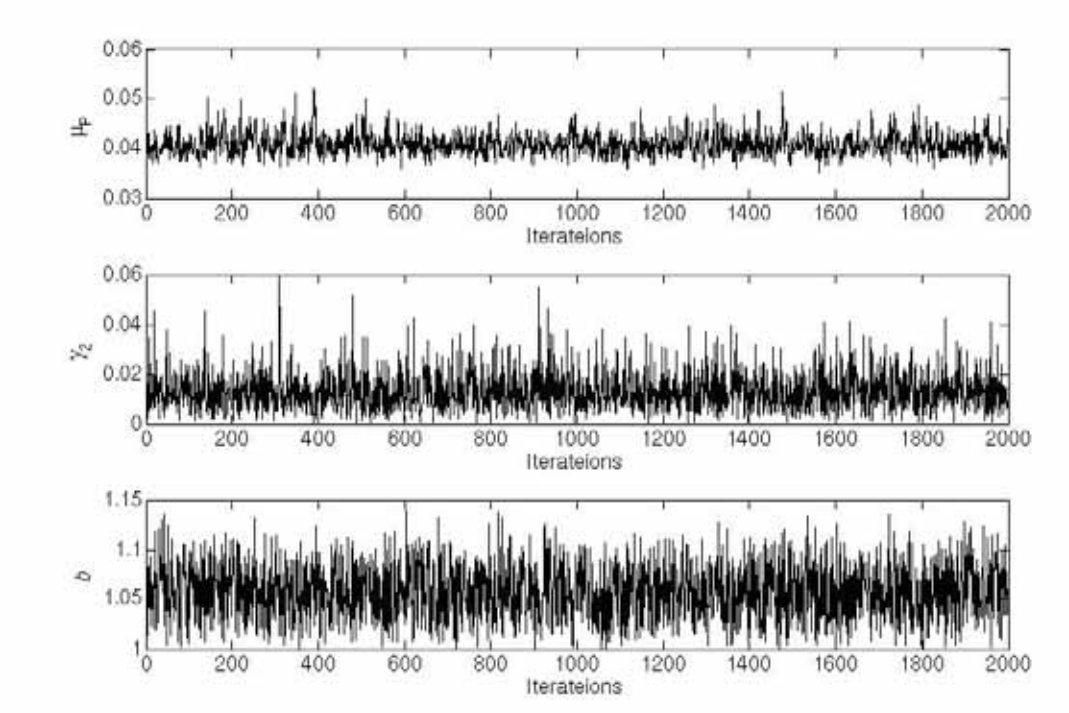

Figure 2.4: A subset of the iterations that occurred while running the Metropolis-Hasings algorithm in experiment M-H2. The last 20,000 iterations of the algorithm run is sampled at every 10^{th} point and shown for each parameter.

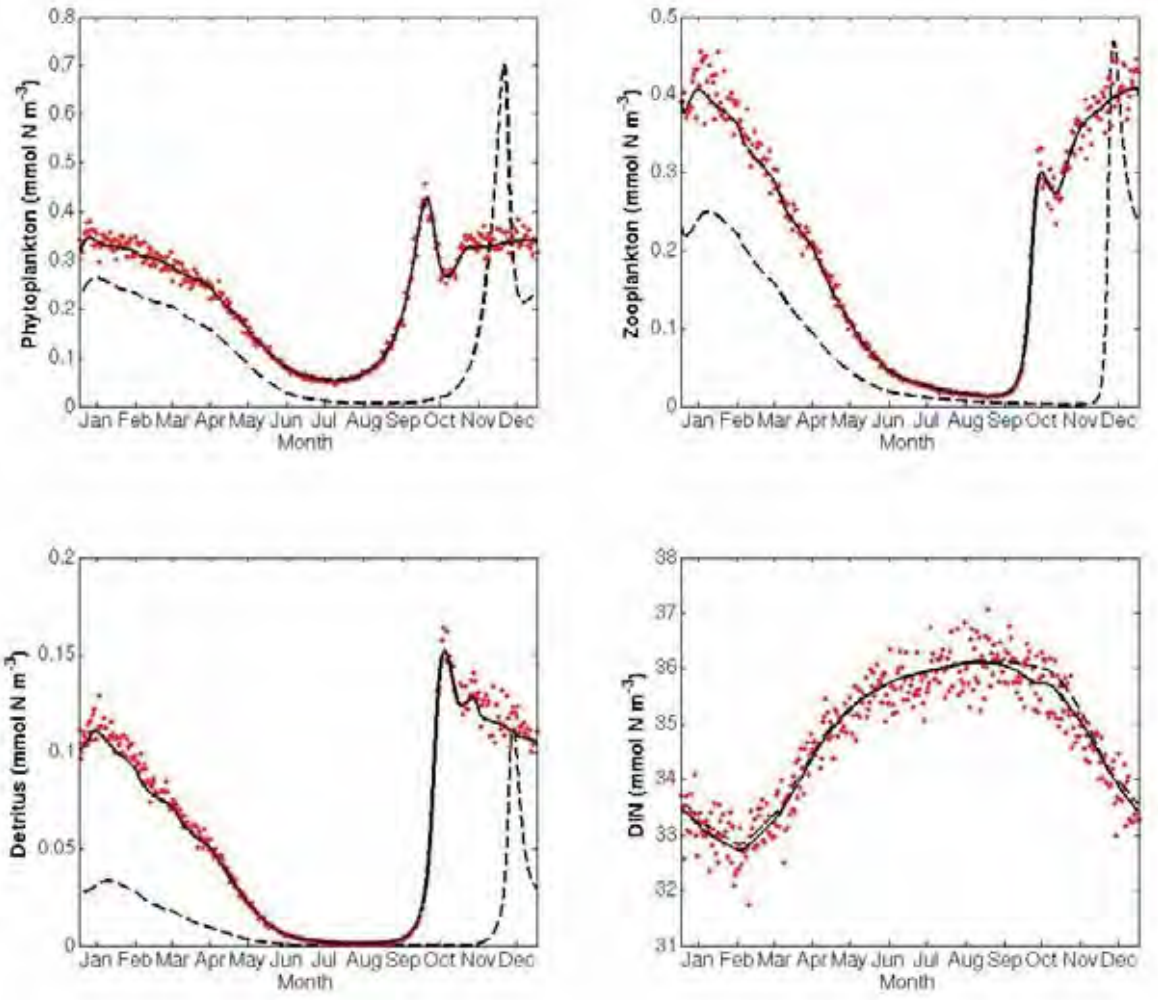

Figure 2.5: Annual model cycles of phytoplankton, zooplankton, detritus and DIN after optimising three parameters using the Metropolis-Hastings algorithm (black line). The annual model trajectories using the starting parameters are plotted in a dashed line. The simulated data are shown in red.

The inclusion of additional parameters in the optimisation impedes the algorithm from reaching a steady state and results in erratic parameter distributions. This is due to correlation between the parameters. For example the inclusion of the parameter for maximum photosynthetic efficiency (the initial slope of the P-I curve), α, in the optimisation with these three parameters results in neither α nor μ_P reaching a steady state. Figure 2.6 shows a subset of the iterations, demonstrating how changes to the choice of α are matched by changes to the choice of μ_P. A change in the value of α results in modification to phytoplankton growth; when trying to reproduce a particular value for the concentration of phytoplankton this modification to growth will need to be compensated for, such as by a complimentary adjustment to mortality of phytoplankton.

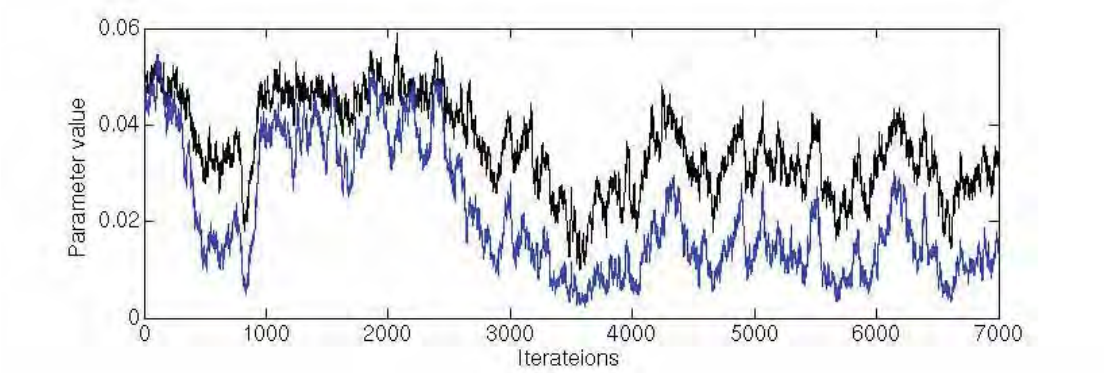

Figure 2.6: A subset of iterations that occurred while optimising four parameters using the Metropolis-Hastings algorithm. The parameter trace for the phytoplankton loss term μ_P is shown in black. The parameter trace for the maximum photosynthetic efficiency α in shown in blue. The values of α are divided by 10 to assist comparison between the two.

The correlation between parameters can be clearly seen by plotting the posterior distributions for each parameter against one another (Figure 2.7). The posterior distributions of the three well resolved parameters (maximum growth rate parameter *b*, mortality of phytoplankton μ_P, and zooplankton excretion rate, γ_2) are independent of one another, however the connection between between mortality of phytoplankton (μ_P) and maximum photosynthetic efficiency (α) is evident.

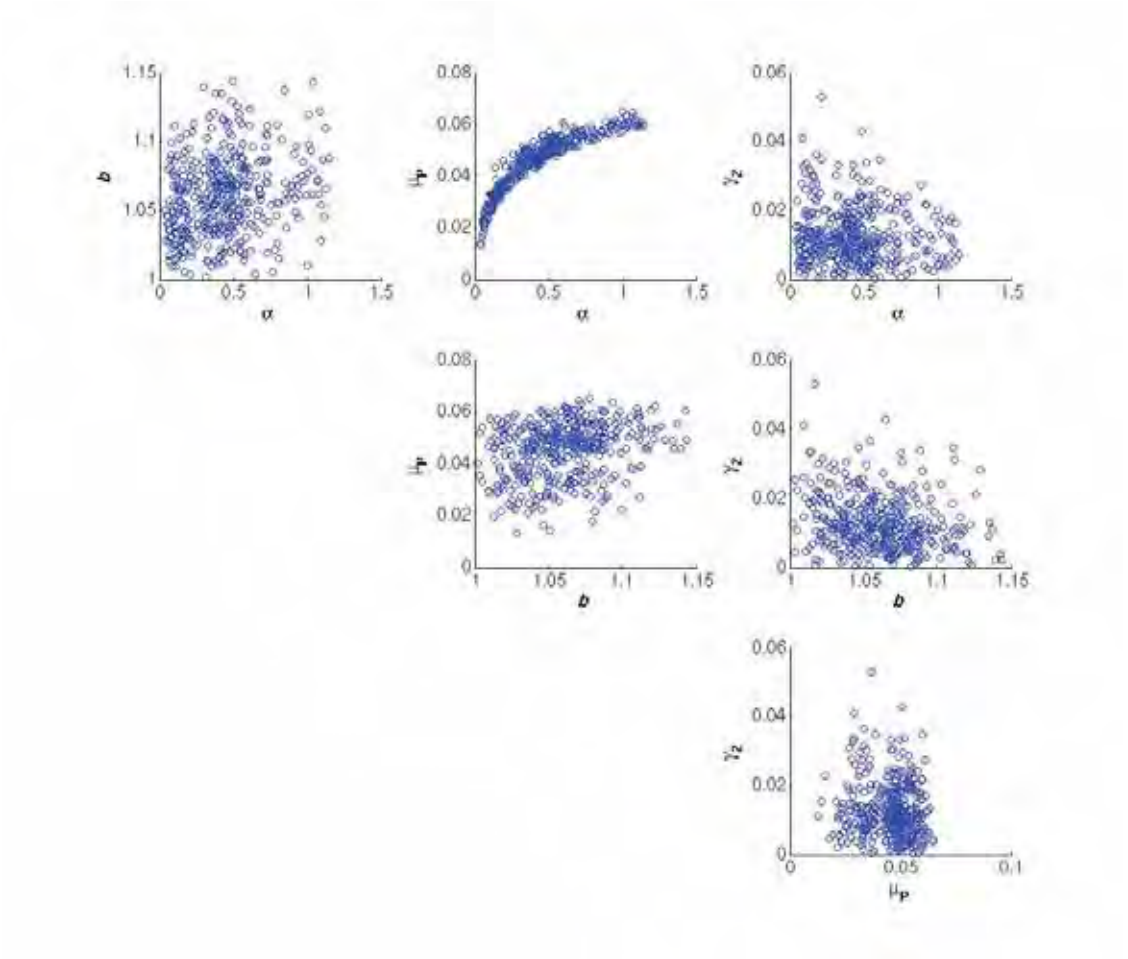

Figure 2.7: Correlation between the posterior parameter distributions after optimising the maximum growth rate, *b*, maximum photosynthetic efficiency, α, zooplankton excretion, γ_2, and phytoplankton loss rate, μ_P, using the Metropolis-Hastings algorithm.

Thus the Metropolis-Hastings algorithm is effective in optimising well resolved, un-correlated parameters. Based on the algorithm performance the three best resolved parameters of this model are maximum growth rate parameter *b*, mortality of phytoplankton μ_P, and zooplankton excretion rate, γ_2.

The estimation of only three parameters after extensive manual tuning of the algorithm and trial and error to find the uncorrelated parameters to optimise is a rather unsatisfactory result. The algorithm running time makes such numerous trial experiments rather time consuming. I coded a tridiagonal solver with the aim of finding a more computationally efficient method to solve the differential equations while performing the Metropolis-Hastings algorithm, however the alteration did not greatly improve the algorithm running time.

2.6 Simulated annealing results and discussion

2.6.1 Experiment SA1

The 14 free parameters were optimised using simulated annealing. The optimised parameters are very close to the true parameter values (Table 2.3), this is reflected in the model solution which accurately characterises the annual cycles of all four model components (Figure 2.8).

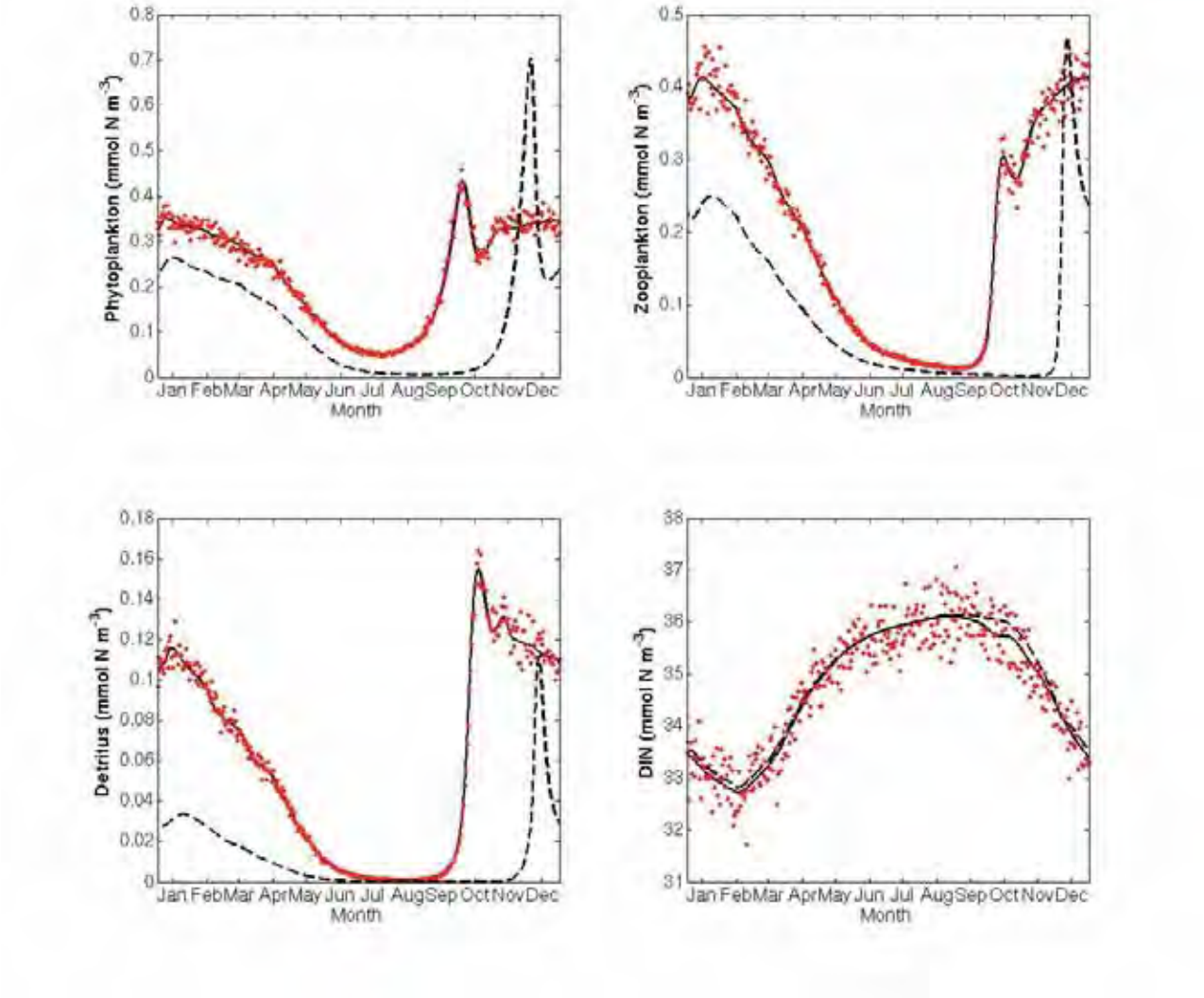

Figure 2.8: Annual model cycles of phytoplankton, zooplankton, detritus and DIN after optimising all fourteen parameters using simulated annealing (black line). The annual model trajectories using the starting parameters are plotted in a dashed line. The simulated data are shown in red.

Parameter	True Parameter value	Experiment SA1 estimate	Experiment SA2 estimate
α	0.256 ± 0.1	0.258 ± 0.07	0.263 ± 0.02
a	0.27 ± 0.1	0.27 ± 0.03	0.27 ± 0.003
b	1.066 ± 0.01	1.068 ± 0.004	1.068 ± 0.001
c	1.0 ± 0.01	1.0 ± 0.003	1.0 ± 0.001
K	0.7 ± 0.2	0.7 ± 1.3	0.7 ± 0.34
μ_P	0.04 ± 0.01	0.04 ± 0.004	0.04 ± 0.0004
γ_1	0.925 ± 0.01	0.924 ± 0.02	0.925 ± 0.001
g	1.57 ± 0.1	1.57 ± 0.30	1.58 ± 0.08
ε	1.6 ± 0.1	1.61 ± 0.16	1.6 ± 0.05
μ_Z	0.34 ± 0.05	0.34 ± 0.06	0.33 ± 0.02
γ_2	0.01 ± 0.01	0.01 ± 0.001	0.01 ± 0.0007
μ_D	0.048 ± 0.01	0.048 ± 0.06	0.048 ± 0.0008
w_D	18.0 ± 2	17.9 ± 10.7	18.0 ± 34.0
μ_P^2	0.025 ± 0.01	0.025 ± 0.003	0.027 ± 0.002

Table 2.3: Parameter estimates obtained from the simulated annealing optimisation experiments.

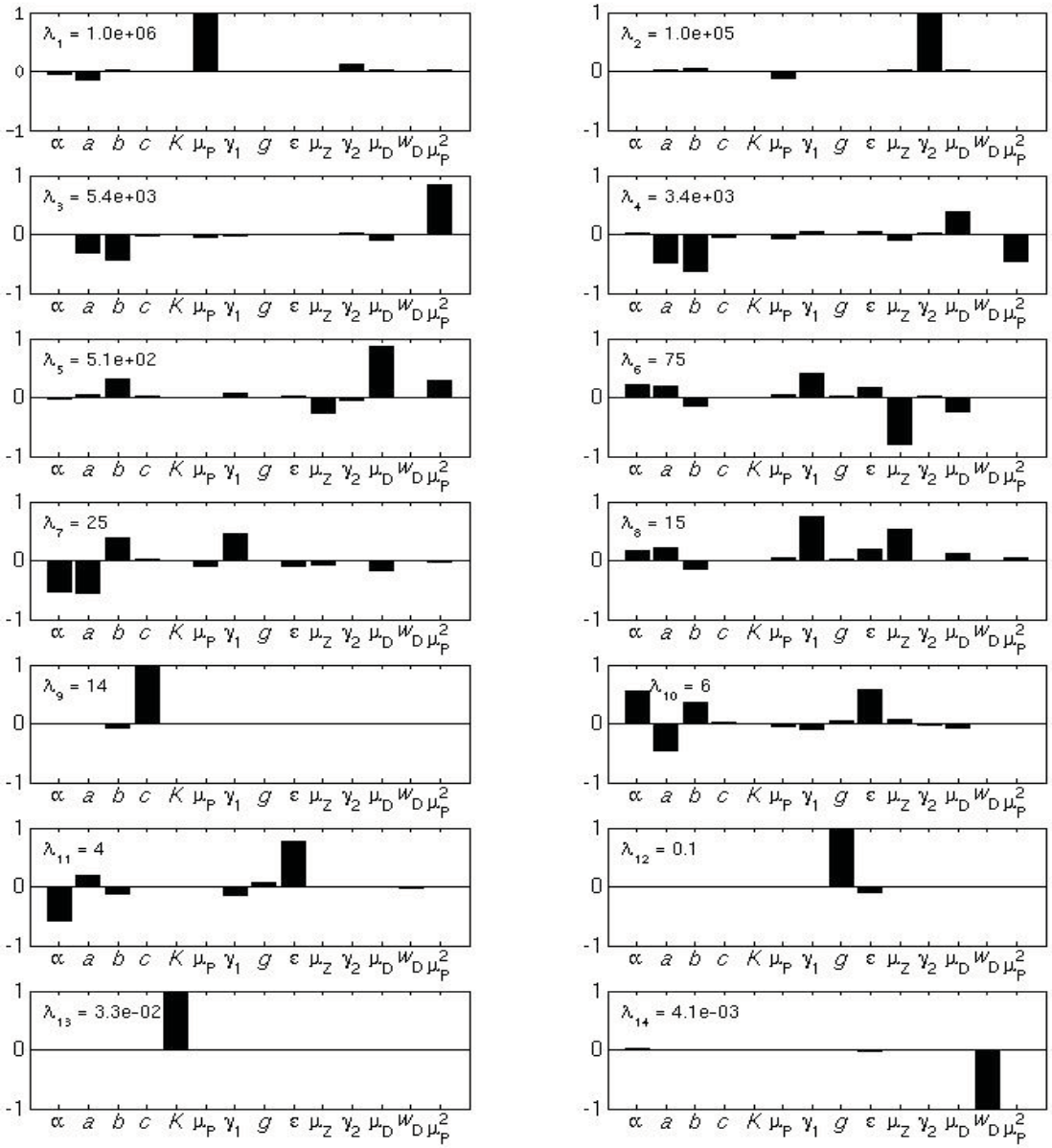

Figure 2.9 Parameter resolution for the 14 parameter simulated annealing optimisation experiment. The singular vectors, λ_i, i =1:14, are shown in decreasing order of the magnitude of their associated singular values. As the magnitude of the singular values decreases so the parameters contributing to the associated singular vector decrease in their impact upon the model solution.

The parameters best resolved by the data are the phytoplankton loss term μ_P and zooplankton excretion γ_2 (λ_1 and λ_2 in Figure 2.9, and smallest error in Table 3). The combination of the phytoplankton maximum growth rate parameters *a* and *b*, the mortality of phytoplankton, μ_P^2, and the remineralisation rate, μ_D, is also well resolved; however the values of these parameters cannot be estimated independently of one another (λ_3 and λ_4 in Figure 2.9). The correlation between the maximum phytoplankton growth rate parameters *a* and *b* is evident since they appear in combination in several of the singular vectors, and these maximum growth rate parameters are also correlated to the poorly determined parameter for maximum photosynthetic efficiency α (λ_7, λ_{10} and λ_{11}, Figure 2.9).

The maximum temperature dependent growth is dependent upon the multiplicative combination of *a* and *b*, this multiplicative formulation makes it highly unlikely that the data would be able to constrain the two terms independently, however in combination they are well determined. The phytoplankton photosynthesis-irradiance relationship is calculated as a function of the maximum temperature dependant growth, the photosynthetically available radiation and maximum photosynthetic efficiency (the initial slope of the P-I curve). This formulation results in an estimate of α which is not well resolved (Figure 2.9) and somewhat dependent on the maximum growth rate. Similarly the parameter optimisation experiments of SO03, which these parameter values are based on, showed phytoplankton growth and loss parameters (*a*, *b*, μ_P, μ_P^2) to be well constrained with maximum photosynthetic efficiency only poorly constrained.

Even in this idealised case of daily observations on all the model components of nitrogen, phytoplankton, zooplankton and detritus many of the parameters are only poorly resolved by the data. The estimates of the half saturation constant of DIN uptake rate, *K*, and the detrital sinking velocity, w_D, have large posterior errors (Table 2.3). The smallest singular values of the Hessian, which are effectively zero, correspond to singular vectors containing information on *K* and w_D only. There is no information on these parameters in

any of the other singular vectors, thus K and w_D are virtually unconstrained and independent of the other parameters (λ_{13} and λ_{14} in Figure 2.9).

The half saturation constant of DIN uptake rate, *K,* will only be used by the model equations in a case of nitrogen limited growth. Since there are high levels of DIN in the surface mixed layer annually, at this location, *K* is a redundant parameter. This result could be different if the optimisation was applied in a nutrient deficient region of the ocean. For example SO03 found the half saturation constant of DIN uptake rate to be a relatively well constrained parameter in their optimisations at 3 sites in the North Atlantic. Similarly Fennel et al. (2001) found the half saturation constant of DIN uptake rate to be among the well constrained parameters at the oligotrophic BATS site.

The sinking rate of detritus is quantified as a constant velocity. Using the same parameterisation SO03 also found the detrital sinking rate to be a very poorly resolved parameter in their vertically resolved model optimisation at three distinct locations in the North Atlantic. Likewise Xu et al (2008) found only very small model sensitivities to the detrital sinking rate parameter in their coupled physical-biological model optimisation for the Yellow Sea. The posterior error on the sinking rate indicates its value could lie somewhere between 7 and 27 d^{-1} without greatly changing the model solution (Table 3). This constant velocity representation of detrital sinking rate has been used in many modelling studies ranging from one dimensional studies (Mattern et al., 2010) to coupled physical-biological regional experiments (Fietcher et al., 2009; Xu et al., 2008) to fully coupled global modelling studies (Zahariev et al., 2008), and has been used in estimation of global export production (Cox et al., 2000; Palmer and Totterdell, 2001). Even if the model assumption of a constant sinking speed of detritus was certain, the daily rate cannot be estimated unambiguously using this model. This result highlights the need for thorough consideration of the parameter values assigned to an ecosystem model before making inference based on them.

SO03 found the sinking rate of detritus to be highly correlated to the remineralisation rate, with the fluxes out of the detrital compartment being dependent upon one another;

whereas in this experiment the remineralisation rate is correlated with the phytoplankton maximum growth rate parameters (Figure 2.9), with the fluxes into and out of the DIN compartment being dependent upon one another. This difference in dependencies is likely due to the different locations, with seasonal DIN gradients being more significant in the Southern Ocean. In the oligotrophic region considered in SO03 there is little seasonal variability in the DIN inventories of the euphotic zone.

The maximum grazing rate , *g*, is only poorly resolved by the data (Table 3 and Figure 2.9). The optimisation of SO03 set these grazing parameters at the maximum values imposed by their a priori assumptions, to avoid excessive grazing rates. They assumed the parameters to be unconstrained by the data due to lack of zooplankton observations. However this twin experiment shows that even in the case of daily zooplankton observations *g* and ε are only poorly resolved. Similar to the phytoplankton growth parameters, the zooplankton maximum grazing rate, *g,* and prey capture rate, ε , only enter the model equations through the grazing function *G(P)*; therefore it is unlikely that both may be accurately and independently determined due to the model formulation. A different formulation for zooplankton grazing was used in a four component *N-P-Z-D* model similar to this one by Zhao and Lu (2009) and Xu et al. (2008). Both studies found that the two parameters entering the grazing formula (maximum grazing rate and Ivlev grazing constant) could not be determined independently of one another.

The most accurately determined parameters are consistent with those found using the Metropolis-Hastings algorithm; however the process of determining them and optimising them is a great deal faster using simulated annealing. Additionally simulated annealing provides an estimate for the more poorly resolved parameters, and a straightforward way of assessing correlation between all parameters at once.

2.6.2 Experiment SA2

Experiment SA1 was repeated with the modification that only phytoplankton data was included in the assimilation process. The optimised parameters are again close to the true

values (Table 2.3). The model fit to the data is not compromised by including information on phytoplankton only (Figure 2.10). The singular vectors are very similar to those presented in Figure 2.9.

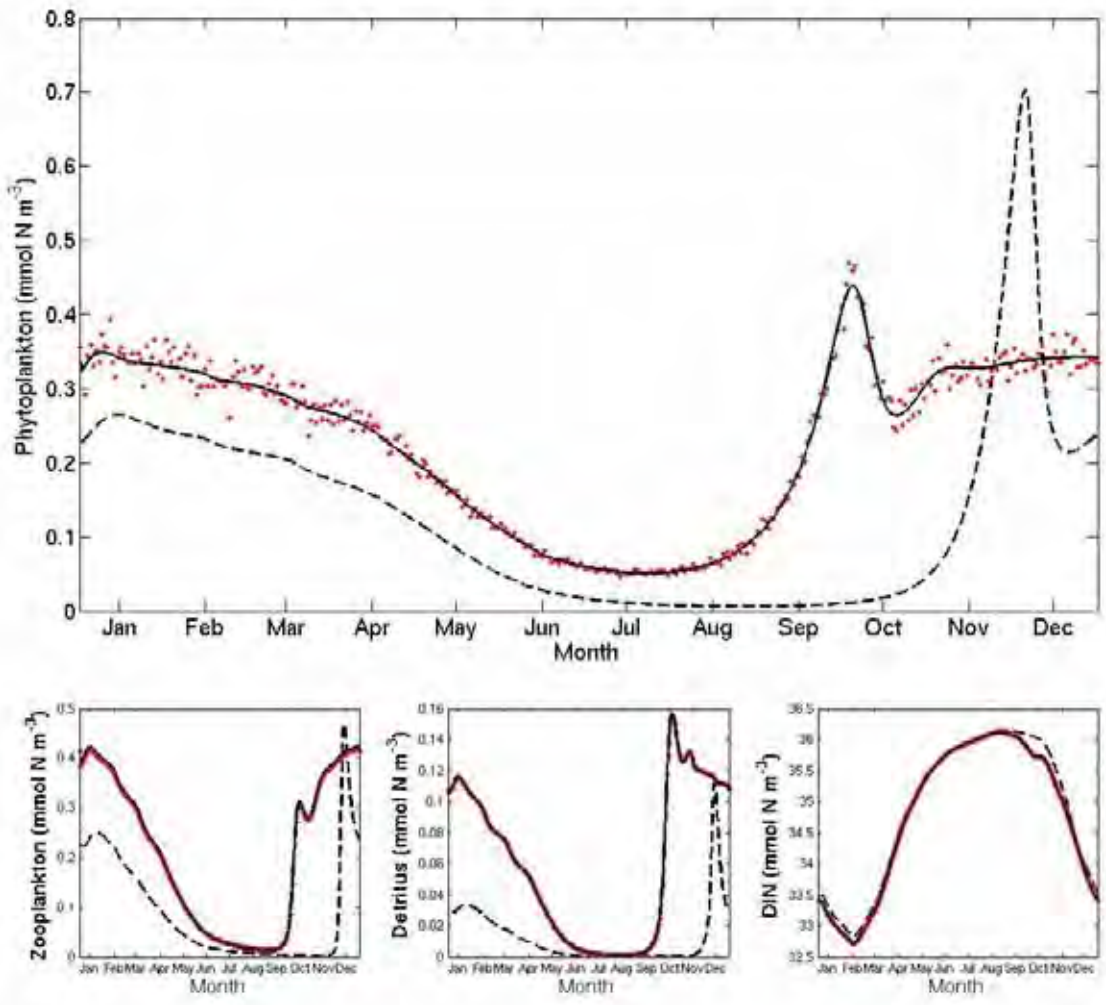

Figure 2.10: Annual model cycles of phytoplankton, zooplankton, detritus and DIN after optimising all fourteen parameters, assimilating simulated phytoplankton data using simulated annealing (black line). The annual model trajectories using the starting parameters are plotted in a dashed line. The simulated data are shown in red.

The exclusion of the nitrate and detritus data sets adversely affects the estimates of K and w_D. The errors on the estimates of these parameters are more than double that in experiment SA1 (Table 2.3). However they were virtually unconstrained in experiment SA1 so no inference could be based on their estimated values even with the additional data. The errors on all the other parameters are reduced by omitting the nitrate, zooplankton and detritus data sets. The use of only one data set means that the a priori parameter estimates take relatively more weight in the cost function.

Zhao and Lu (2009) conducted twin experiments to determine which of nutrient, phytoplankton and zooplankton data sets gave the best results in a parameter optimisation study with a model formulation very similar to this one. They found the best estimates were achieved when phytoplankton data were assimilated, and the addition of zooplankton data did not obviously improve their parameter estimates. The results presented here show that the parameter estimates are not compromised by assimilating only phytoplankton data, this gives confidence to the feasibility of using satellite ocean colour data to optimise the parameters of a marine ecosystem model such as this one.

2.7 Summary

Two methods of optimising the parameters of a marine ecosystem model have been applied in the Polar Frontal Zone of the Southern Ocean. The model had previously been optimised for the North Atlantic Ocean by Schartau and Oschlies (2003a).

The Metropolis-Hastings algorithm is proven to converge to a target parameter distribution, and allows sampling of the complete posterior distribution of the parameter estimates. While attractive in principle, for this application it required considerable computing time to run the optimisation, extensive time adjusting the step size for each parameter to ensure appropriate jumping, and substantial time performing individual optimisations to determine the well resolved parameters. Multiple experiments using this method would be impractical. Nonetheless the results from an initial twin experiment can

be used to estimate how well faster methods that derive uncertainties from the curvature of the cost function at its global minimum will work.

When using simulated annealing, as with other optimisation techniques such as the adjoint method, there is no guarantee that the minimum has been found since the cooling schedule may cause the system to become trapped in a local minimum of the objective function. This risk can be minimised if a very slow cooling schedule is implemented (Tarantola, 1987). The results presented here demonstrate that it is a practical and effective method and will find a near-optimal solution even in the presence of noisy data. The agreement of the model sensitivities derived from the Hessian with the model sensitivities derived from the Metropolis-Hastings experiments indicates that the Hessian was indeed analysed at the global minimum of the cost function. Optimisations assimilating only phytoplankton gave comparably good results, indicating that optimisations could be performed where remotely sensed ocean colour observations are the only comprehensive data source. For future optimisation experiments simulated annealing is the method we would use.

The optimisations show that several of the model parameters are correlated with one another. Error analysis must be an essential part of any parameter optimisation experiment, particularly when high correlations exist. When assimilating real data into this model parameter estimates should be compared with a variety of independent data sources that have not been used for the optimisation process to check that the estimates are a credible biological solution and not just a mathematical agreement to the data. Additionally model parameters or rates not directly optimised by the algorithm (such as *f*-ratio or primary production) should be compared with independent data sources to verify the solution.

To reduce errors arising from co-dependencies between the parameters it would be beneficial to remove the most poorly resolved parameters from the optimisation when assimilating real data (Fennel et al., 2001; Friedrichs, 2006; Zhao and Lu, 2009); however comparison of our results with the results from SO03 shows the model sensitivities may change depending on the region in which the model is applied. It would be beneficial to

perform supplementary twin experiments when applying this model to another location to assess model sensitivities before selecting which parameters to optimise in data experiments.

As well as sensitivities to the data sets, twin experiments can highlight potential improvements to model structure. The detrital sinking velocity cannot be unambiguously estimated in this model. More complex parameterisations of sinking particles exist (Kriest, 2002; Ruiz et al, 2002; Karakas et al., 2009); however we cannot validate all the parameters of this model so additional complexity without data support is not desirable for the parameter optimisation studies considered here. Rather we would suggest this model may be appropriate for modelling phytoplankton distributions and certain biogeochemical fluxes (primary production, phytoplankton mortality, zooplankton excretion) but not for estimation of carbon export through detrital sinking.

Chapter 3:

Parameter optimisation of a marine ecosystem model at two contrasting stations in the Sub-Antarctic Zone

(Paper submitted to Deep Sea Research Part II: Topical Studies in Oceanography, Special Issue: Biogeochemistry of the Australian Sector of the Southern Ocean.)

Abstract

SeaWiFS surface chlorophyll estimates in the Sub-Antarctic Zone show low concentrations south west of Tasmania and high concentrations south east of Tasmania. Data assimilation experiments were performed using simulated annealing to obtain parameter estimates of a simple nitrogen based mixed-layer marine ecosystem model at two locations in this region (station P1 at 140°E, 46.5°S and station P3 at 152°E, 45.5°S). The assimilation methods and parameter sensitivities are assessed in a twin experiment. This assessment determines the design of an optimisation experiment utilizing SeaWiFS chlorophyll observations. Model parameter estimates are compared to in situ parameter estimates from the SAZ-Sense (Sub-Antarctic Zone Sensitivity to environmental change) project stations P1 and P3 in the austral summer of 2007.

The parameter estimates suggest that different ecosystems are present within the Sub-Antarctic Zone. The optimisation reduces the model-data misfit dramatically compared with the original parameterisation, which assumed the same ecosystem dynamics at both stations. Different biological processes rather than different physical conditions between the two sites are responsible for the difference in ecosystem function in our experiments.

An analysis of parameter uncertainties shows at both stations accurate parameterisations of phytoplankton growth, zooplankton mortality and the biological recycling processes are required to realistically model chlorophyll.

The most significant differences in parameters between the two stations are the parameters relating to phytoplankton growth and zooplankton mortality. The difference in growth parameters results in spring time productivity estimates of 659 mg C $m^{-2} d^{-1}$ at P1 and 203 mg C $m^{-2} d^{-1}$ at P3. In situ estimates from the SAZ-Sense cruise do not support such dramatic differences in primary production between the two stations. We conclude that the same ecosystem model structure is not applicable at both stations and we need additional processes at P3 to reproduce the observed seasonality of phytoplankton and the observed primary productivity. We hypothesize that the missing

processes in the ecosystem model at P3 are iron limitation of phytoplankton and the seasonal variations in atmospheric deposition of iron.

3.1 Introduction

Marine plankton dynamics are recognised as having considerable influence on global climate (Riebesell et al., 2007; Le Quere et al., 2005; Matear et al., 1999; Sarmiento et al., 1998). The Southern Ocean plays a central role in global planktonic productivity (Marinov et al., 2006) and different regions within the Southern Ocean are likely to respond differently to climate variability (Kohfeld et al., 2005). Meridional asymmetries in Southern Ocean biogeochemistry were studied in the Sub-Antarctic Zone (SAZ) project (Trull et al., 2001) that focussed on the differences between the SAZ and the Polar Frontal Zone (PFZ); and the Antarctic Southern Ocean Environment Study (AESOPS) that focussed on the Ross Sea and Pacific Ocean (Anderson and Smith, 2001).

The region of the Sub-Antarctic Zone (SAZ) to the south of Tasmania is interesting in that it characterised by a large zonal gradient in the phytoplankton concentrations estimated from remotely sensed ocean colour (Figure 3.1). The region to the south east of Tasmania is characterised by much higher summer phytoplankton concentrations visible in surface waters during austral summer than the region to the south west (Griffiths et al., in press). Model simulations aid identification of the processes leading to the observed phytoplankton distribution. To the best of our knowledge no biological model simulations have been done to assess whether one set of biological model parameters can reproduce the observed phytoplankton seasonal cycle in these different regions of the Sub-Antarctic Zone or identify any important regional differences in model parameterisations.

The linking of models and data through data assimilation or inverse modelling is a developing field that can provide many insights into biogeochemical dynamics not possible by using data or models alone. Data assimilation for parameter estimation is a

systematic means of estimating model parameters in a way that is consistent with the available observations (Matear, 2004).

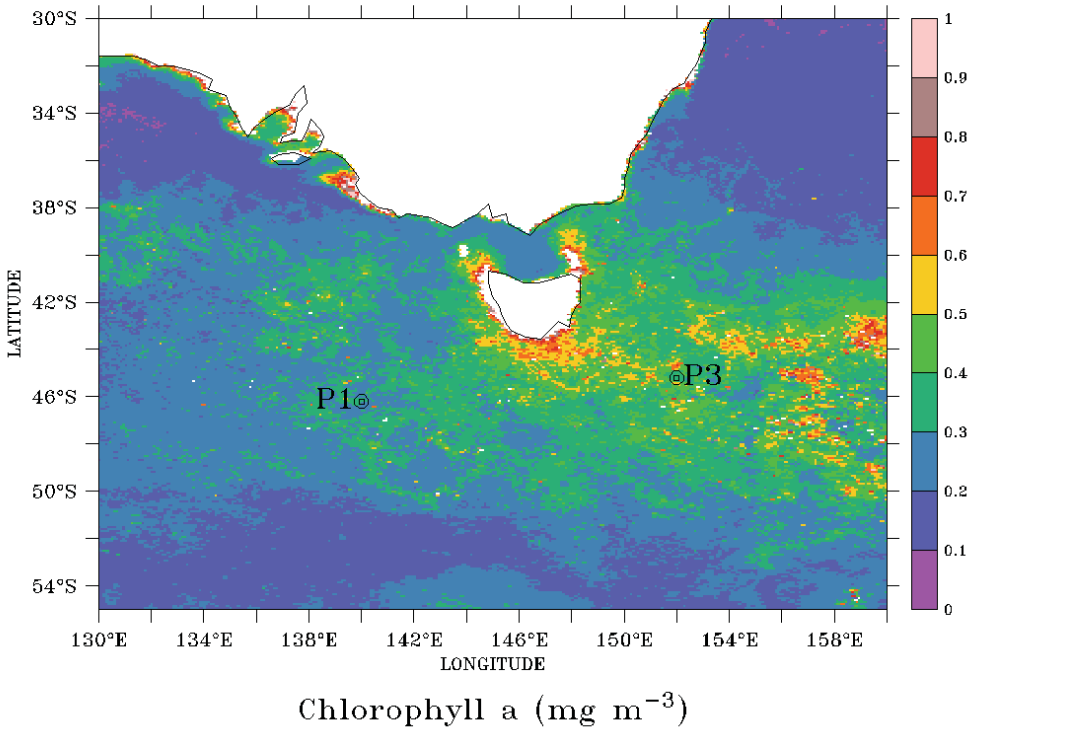

Figure 3.1: February SeaWiFS surface chlorophyll (mg m^{-3}) using a 1998 – 2008 climatology computed from 8-day composites.

There have been numerous studies concentrating on optimising ecosystem model parameters for various regions (e.g. Matear, 1995; Hurtt and Armstrong, 1999, Friedrichs, 2001, Schartau and Oschlies, 2003a) but thus far no one has applied this technique with a focus on the Sub-Antarctic Zone of the Southern Ocean. In this paper ecosystem model parameters are optimised and compared at the two Sub-Antarctic Zone process stations of

the SAZ-Sense project, station P1 south west of Tasmania at $140^{\circ}E, 46.5^{\circ}S$ and station P3 south east of Tasmania at $152^{\circ}E, 45.5^{\circ}S$ to examine possible reasons for the zonal gradient in phytoplankton concentrations. It is hypothesised the difference in the size of the summer bloom at the two sites (up to 1.7 times greater at P3 compared to P1) may be driven by either iron supply, phytoplankton growth rates, variations in zooplankton grazing, or other biogeochemical mechanisms (Griffiths et al., in press).

One of the models most commonly used in assimilation experiments is based on that of Fasham et al. (1990). Despite its simplicity this model can reproduce the main ecosystem features of the surface mixed layer at several locations and provide insight into the fundamental biological interactions in the ocean. Here a reduced four-component version of the Fasham et al. model as described by Schartau and Oschlies (2003a) is used. It is similar in formulation to the models used by Fennel et al. (2001); Oschlies and Garcon (1999) and Doney et al (1996). The study of nitrogen cycling in the surface ocean provides information to aid understanding of primary production and *f*-ratios (ratio of nitrate based production to total production), which are useful tools to characterize ecosystem functioning (Savoye et al., 2004). Here the nitrogen based model is used to explore the ecosystem characteristics, possible reasons for the regional variation in phytoplankton biomass, and determine whether a model that does not incorporate the role of iron can realistically simulate the surface chlorophyll observations.

The model sensitivities and assimilation procedure are first assessed with a twin experiment. We then apply the data assimilation methods to observational data from the two sites. Satellite derived data provides the only large-scale synoptic observations of the Southern Ocean and therefore SeaWiFS surface chlorophyll is used for our inversions. In situ measurements at P1 and P3 exist for only ~7 days at each station and are useful for assessment of parameter estimates rather than assimilation into the model. We examine whether one set of model parameters can describe the phytoplankton dynamics at the two contrasting sites, and whether a model that does not include the role of iron can simulate the surface chlorophyll concentrations observed at P1 and P3. We compare the biogeochemical characteristics of the two sites exploring whether the meridional

variation in phytoplankton biomass can be explained by either physical processes or ecosystem differences. Results are compared with in situ estimates of primary production and *f*-ratios from the SAZ-Sense (Sub-Antarctic Zone Sensitivity to environmental change) project; which took place from 18th January to 19th February 2007.

The rest of the paper is organised as follows: Section 2 describes the ecosystem model, the data sets and the assimilation methods used. Section 3 gives details of the experimental design of this study. In Section 4 the results of the twin experiment are presented and discussed. The results of the data experiments are presented and discussed in Section 5. The results are compared to results from the SAZ-Sense project in Section 6. Section 7 summarises this study.

3.2 Methods

In this Section a brief description of the biological model is presented and we review the forcing used in the model simulation, the key components of the data assimilation method are then described.

3.2.1 The biological model

Our four component *N-P-Z-D* (Nitrate-Phytoplankton-Zooplankton-Detritus) ecosystem model of the seasonal nutrient cycle follows Schartau and Oschlies (2003a). In this paper mixed layer dynamics are not modelled explicitly. Instead following Evans and Parslow (1985); Fasham (1990); and Matear (1995), model data is used to define the seasonal change in mixed layer depth (in metres), M, as a function of time (in days), t .

$$\frac{dM}{dt} = h(t) \tag{3.1}$$

In this simple zero-dimensional application the pelagic ecosystem is assumed to consist of a homogeneous mixed layer overlying a deeper abiotic layer. Phytoplankton and zooplankton are assumed to be homogeneously distributed in the upper mixed layer and

horizontal advection and diffusion are ignored. An analytical form for light limited growth introduced by Evans and Parslow (1985) is used that depends on photosynthetically available radiation (PAR) as a function of depth. The model equations are given in Chapter 2.

The model has 16 parameters, which are initially assigned the same values as those used by Schartau and Oschlies (2003a), (shown in Table 2.1 and referred as the SO03 parameters here after). Following Matear (1995) the surface PAR and light attenuation coefficient remain invariant in time. The remaining 14 parameters are used for the first optimisation experiment.

3.2.2 Model forcing

The forcing terms of the ecosystem model are solar radiation, Sea Surface Temperature (SST), Mixed Layer Depth (MLD) and nitrate concentration below the mixed layer (Figure 3.2). The forcing data is taken from the GFDL global ocean circulation model MOM4 (Modular Ocean Model 4) with the OFAM (Ocean Forecasting Australian Model) configuration as described by Mongin et al. (in press, a). The global model restores SST to a monthly climatology of Reynolds SST merged with the Levitus World Atlas 2001 (Levitus, 1982). Daily values of SST are obtained by interpolation. The daily MLD is taken as the depth of a 0.05 kg m^{-3} difference in density from the surface computed using the model output of temperature and salinity (Mongin et al., in press, a). Daily averaged values of solar radiation are from NCAR (National Centre for Atmospheric Research). The forcing data for nitrate concentration below the mixed layer shows a larger seasonal pattern than is seen in in-situ measurements (Brian Griffiths, personal communication). However these differences do not affect the model behaviour as both stations are nitrate replete; running the model with a constant value for the nitrate concentration below the mixed layer does not change the model solution.

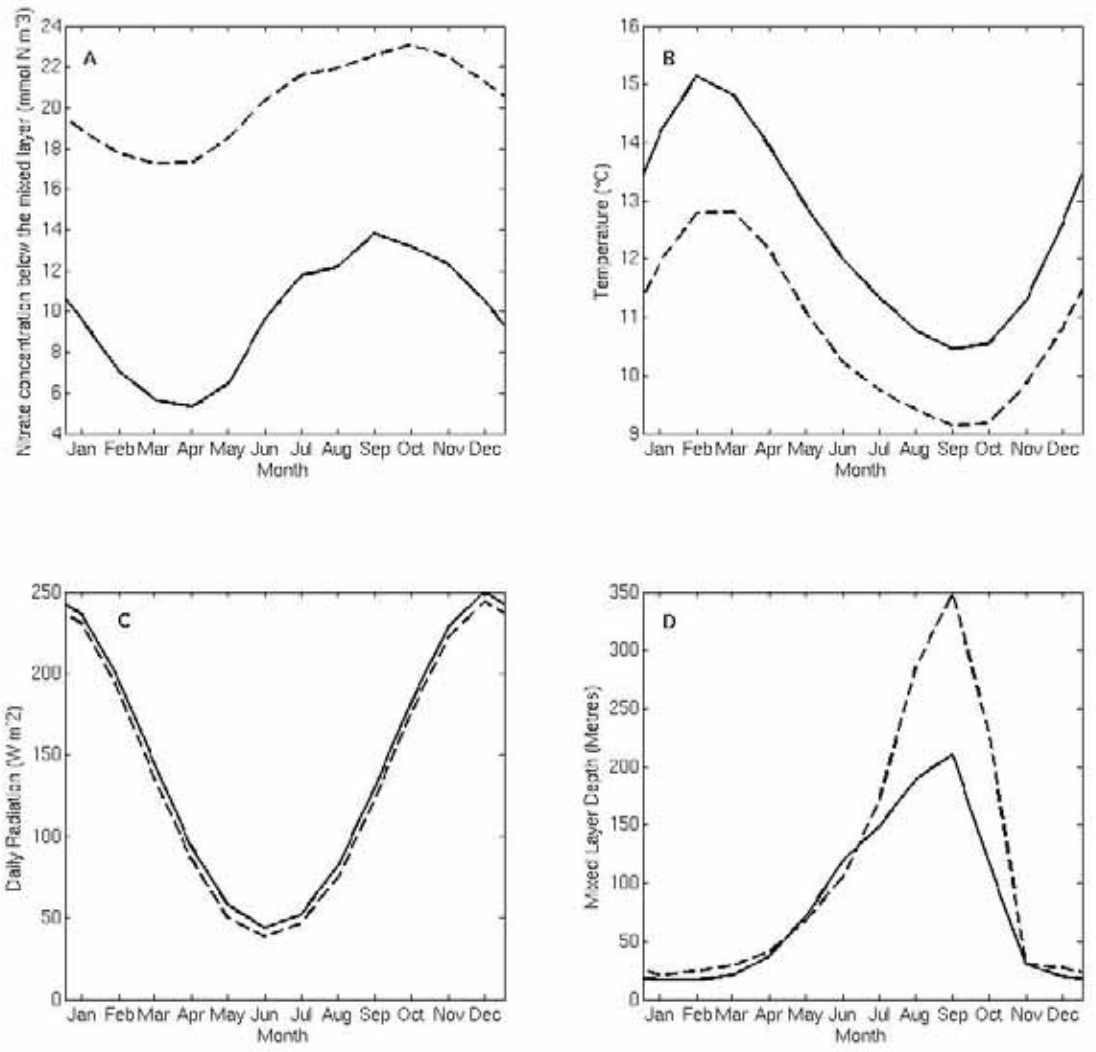

Figure 3.2: Forcing used for the model. Panel A shows nitrate concentration below the mixed layer (mmol N m^{-3}); panel B shows temperature ($^{\circ}$C); panel C shows daily incident solar radiation ($W\ m^{-2}$); panel D shows mixed layer depth (meters). Station P1 is shown in a dashed line. Station P3 is shown in a solid line.

3.2.3 Data constraints

We used surface chlorophyll concentration data taken from SeaWiFS (Sea-viewing Wide Field-of-view Sensor) 8-day composites (9km) generated by the NASA Goddard Space Flight Centre. Since the data is sparse in this regions a climatology was computed for the years 1998 – 2008 averaging the chlorophyll over a 1° square region centred on each process station (Mongin et al., in press, b). Daily values of chlorophyll are obtained by interpolation. A conversion factor of 1.59 mg Chl $(\text{mmolN})^{-1}$ was used to convert modelled phytoplankton nitrogen to chlorophyll (Fasham et al., 1990; Sarmiento et al., 1993). To obtain a measure of uncertainty in the observed chlorophyll, the standard deviation of the observations within the 1° square was calculated and is shown with the data in Figure 3.3. The main feature differentiating the two stations is the size of the phytoplankton bloom. At station P1 the bloom persists from December to February, while at station P3 the maximum is not observed until February and can be as large as twice the magnitude of the bloom at P1 (Figure 3.3).

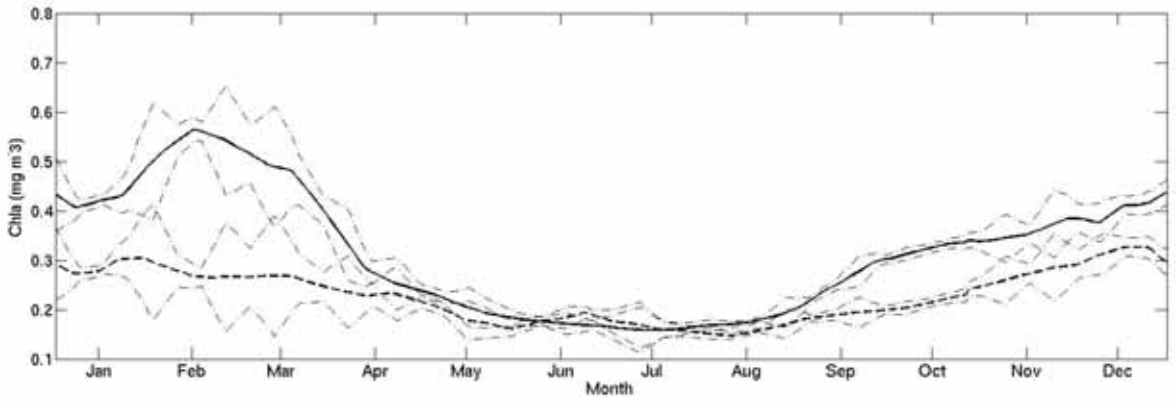

Figure 3.3: Chlorophyll climatology for the period 1998 – 2008 taken from Sea-WiFS. Station P1 is shown in a dashed line. Station P3 is shown in solid line. The standard deviation of the observations is plotted in a dot-dash line.

3.2.4 Cost function

For the optimisation we introduce a cost function *C*, defined to measure the misfit between model output and observations at each time step of the model run. Our cost function includes a term representing model-data misfit for different components of the model ($y = N, P, Z, D$ in the twin experiment; or y =Chl*a* in the data experiments) and a term representing parameter misfit from its *a priori* expected value. This is included to penalise parameter values that are outside acceptable limits. These acceptable limits are based on literature values (Schartau and Oschlies, 2003a; Matear, 1995) and set to be broad to represent our uncertainty on the parameter, but do not allow biologically unfeasable choices such as negative values. A third term is included to penalise large deviations from the steady-state cycle reached after spin up (Matear, 1995; Schartau and Oschlies, 2003a). The model is run for three years, two of which are spin up time, after which quasi steady state was achieved, thus the steady state penalty requires the model components at the start of the third year to be approximately equal to the values at the start of the second year.

Taking a formulation that assumes Gaussian errors for both prior parameter values ϑ^{obs} and the assimilated data y^{obs}, and prescribed uncertainties $\delta\vartheta$ for the parameters and δy for the data it is defined as

$$C = \frac{1}{2}\sum_{i=1}^{n}(y_i^{prd} - y_i^{obs})^2 \frac{1}{\delta y_i^2} + \frac{1}{2}\sum_{i=1}^{m}(\vartheta_i^{prd} - \vartheta_i^{obs})^2 \frac{1}{\delta\vartheta_i^2} + \frac{1}{2}\sum_{j=1}^{nc}(t_1^j - t_{365}^j)\frac{1}{\delta t^4} \tag{3.2}$$

where the superscripts *prd*, *obs* and *prior* denote the model predicted values, observations and prior values respectively and *t* is the steady state penalty; *n* refers to the number of data observations (*n*=365), *m* refers to the number of model parameters, *nc* refers to the number of data sets in the optimisation (*N*, *P*, …) and $\delta t = 0.01$ (following Matear, 1995). An algorithm is applied to find the minimum of the cost function.

The standard deviation on the observation error was set to be 20% of the data value, for consistency Gaussian noise of the same magnitude was added to the generated observations in the twin experiment.

This cost function follows a χ^2 (chi-squared) distribution. On successful minimisation it should have a value of order unity, indicating that the model-data misfit is of the order of the observational error (Tarantola, 1987).

3.2.5 Optimisation

Estimates of optimal parameter values are obtained using a simulated annealing algorithm, a stochastic process used to find unbiased estimates. It is a practical and effective method that will find a near-optimal solution even in the presence of noisy data. The method is described in detail by Kirkpatrick *et al* (1983) and Kruger (1993) and has been demonstrated in the context of marine ecosystem models by Matear (1995) and Hurtt and Armstrong (1996, 1999).

The simulated annealing algorithm was run for 400 iterations, as after 400 iterations the algorithm converged to the same value of the cost function independent of the initial guess of model parameters (i.e. several trial optimisations starting from different parameter guesses were performed). The SO03 parameters were offset from their value by $\pm 2\times$ their prescribed standard deviation and these offset parameters were used as an initial guess for running the algorithm. Following Matear (1995) the uncertainty of the parameter estimates is assessed from the Hessian matrix of the cost function (which is the same as the Jacobian matrix of the gradient of the cost function).

3.3 Experimental design

The experimental design is summarised in Figure 3.4.

Initially a twin experiment in which an idealised data set generated from the simulated annual model trajectories of N, P, Z and D (using the SO03 parameters as defined in Table 2.1) was conducted, optimising the 14 free parameters at station P1 and P3. With the twin experiment the "true" model parameter values are known and we can investigate the ability of the data assimilation to recover the model parameters without the added complexity due to inconsistencies between the applied biological model and reality. The results from this twin experiment were used to assess the feasibility of the problem and the parameters with the most influence on the model results.

The first data experiment optimised twelve model parameters (twelve parameter optimisation), which were chosen on the basis of the error analysis of the twin experiment, while assimilating chlorophyll data. This experiment establishes the best fit that the simulated annealing could give to the chlorophyll data set at each process station. A second data experiment is performed (reduced parameter optimisation), designed in light of the error analysis of the twelve parameter optimisation, in order to obtain better constrained estimates of the model parameters.

The results of the reduced parameter optimisation are used for a further experiment to assess the effect of the physical forcing compared to the biological parameterisation on the model. The optimal parameters from P1 were used to run the model at P3, and vice versa, to examine how the resulting parameterisations transfer across the region. The primary difference between the stations in physical forcing is the mixed layer depth (incoming radiation is almost identical due to the similarity in latitude of the stations, temperature varies by less than 2°C between the stations, and both stations are nitrate replete). In this Chapter the differences in mixed layer depth are taken to be indicative of the differences in physical forcing. The optimised model for station P1 was run using the mixed layer depth data from station P3, and vice versa, to examine how the mixed layer dynamics influence the biological response.

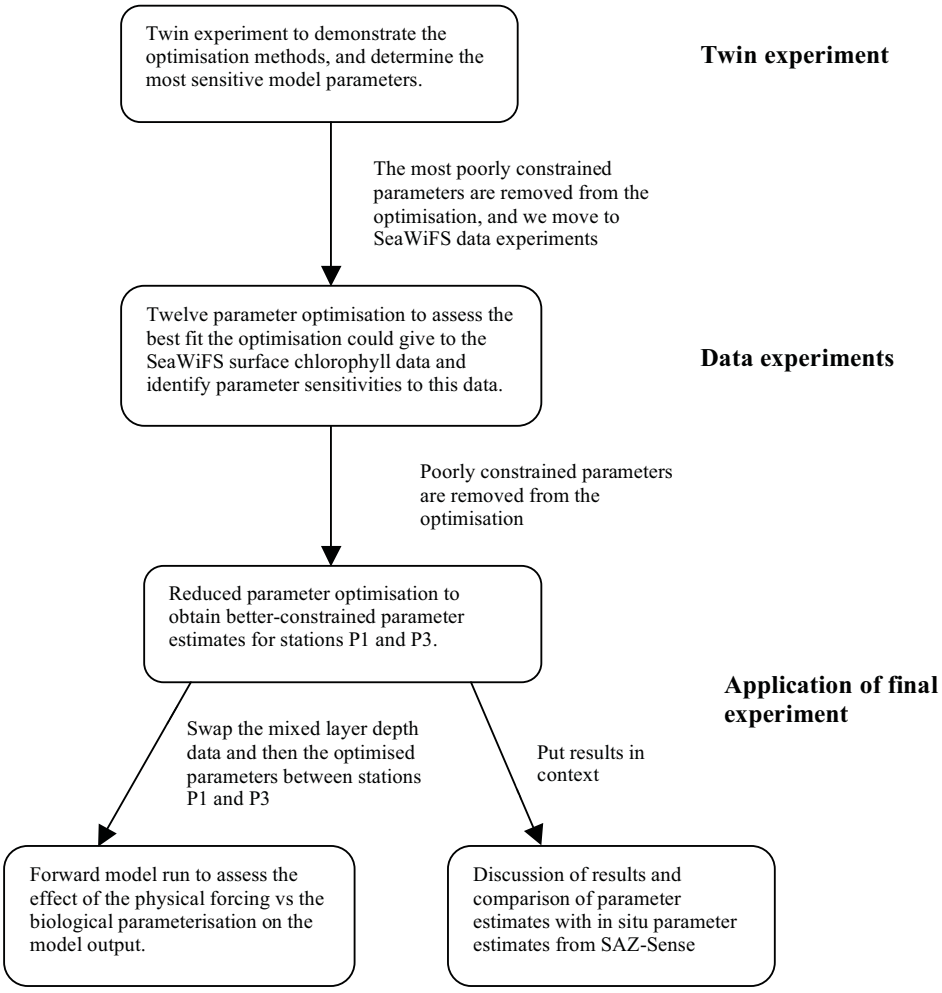

Figure 3.4: Summary of the experimental design of this study.

3.4 Twin Experiment

3.4.1 Twin experiment optimisation

At both stations the optimised parameter values are successful at reproducing the data (Figure 3.5) and recovering the SO03 parameters (Table 3.2). Many of the optimised parameter estimates have large standard deviations; particularly the sinking rate of detritus, w_D , and the half saturation constant for Dissolved Inorganic Nitrogen (DIN) uptake rate, K (Table 3.2).

Figure 3.6 shows parameter estimates that occurred during a simulated annealing optimisation of each parameter. All parameters other than the one being optimised were fixed at the values given in Table 2.1. The parameter values are plotted against the corresponding model cost function value; this shows the sensitivity of the cost function to variations in each parameter. The phytoplankton loss rate, μ_P, is the most sensitive parameter with small changes to its value resulting in a large increase in the cost function. The sinking rate of detritus, w_D, and the half saturation constant for Dissolved Inorganic Nitrogen (DIN) uptake rate, K, are the least sensitive parameters with very large changes in their values hardly affecting the cost function.

The response of the cost function to changes in the initial slope of the PI curve, α and the phytoplankton growth rate parameter, a, is notably different between P1 and P3. A possible reason for this is the difference in the magnitude of the chlorophyll bloom between the stations. The growth rates that correspond to the data at station P1 change more significantly as the bloom is larger at P1 in this twin experiment.

Even in this twin experiment case of daily N, P, Z and D observations the half saturation constant of DIN uptake rate and the detrital sinking rate cannot be accurately estimated for this model at stations P1 and P3.

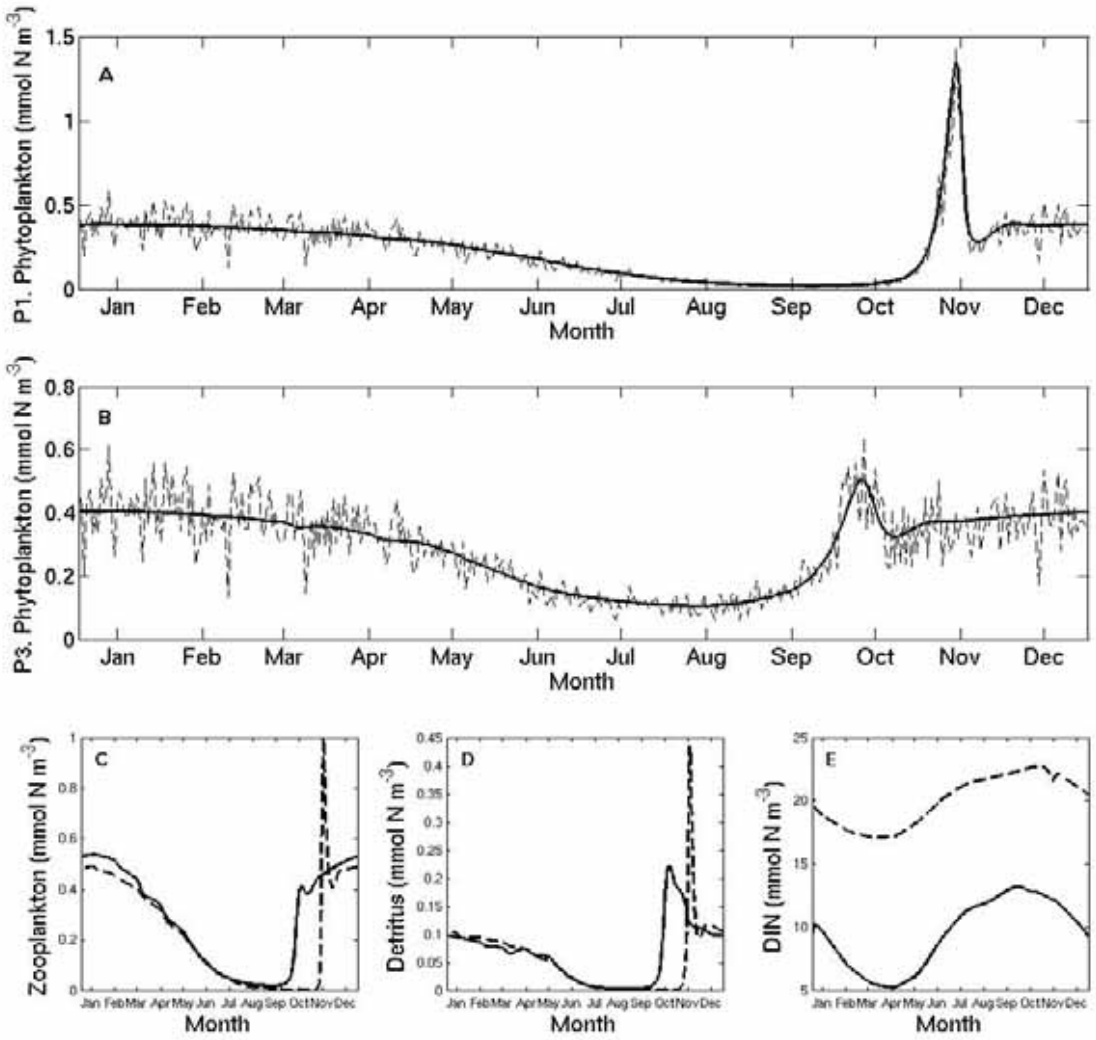

Figure 3.5: Annual model trajectories after optimising the model parameters using simulated annealing. Panels A and B show the model output for stations P1 and P3 respectively. The modelled phytoplankton is plotted in a solid line with the data created using the SO03 parameters with 20% Gaussian noise added plotted in a dashed line. Panels C – E show the modelled zooplankton, detritus and DIN at station P1 (dashed line) and station P3 (solid line).

Parameter	True Parameter value	P1 twin experiment optimisation estimate	P3 twin experiment optimisation estimate
α	0.256 ± 0.1	0.270 ± 0.0875	0.253 ± 0.0748
a	0.27 ± 0.1	0.28 ± 0.0193	0.28 ± 0.0289
b	1.066 ± 0.01	1.062 ± 0.0118	1.064 ± 0.0017
c	1.0 ± 0.01	1.0 ± 0.0034	1.0 ± 0.0033
K	0.7 ± 0.2	0.7 ± 1.3220	0.7 ± 1.3220
μ_P	0.04 ± 0.01	0.076 ± 0.0032	0.087 ± 0.0007
γ_1	0.925 ± 0.01	0.925 ± 0.0195	0.925 ± 0.0115
g	1.57 ± 0.1	1.58 ± 0.3581	1.57 ± 0.2926
ε	1.6 ± 0.1	1.57 ± 0.0572	1.60 ± 0.1236
μ_Z	0.34 ± 0.05	0.33 ± 0.0759	0.34 ± 0.0605
γ_2	0.01 ± 0.01	0.020 ± 0.0021	0.022 ± 0.0018
μ_D	0.048 ± 0.01	0.091 ± 0.0327	0.106 ± 0.0209
w_D	18.0 ± 2	17.8 ± 11.7412	18.0 ± 6.9362
μ_P^2	0.025 ± 0.01	0.024 ± 0.0024	0.025 ± 0.0005

Table 3.2: Parameter values and standard deviations before and after optimisation in the twin experiment using simulated annealing at stations P1 and P3. Parameter names and units are given in Table 2.1. The values listed for the remineralisation rates account for the mean temperature at the two stations.

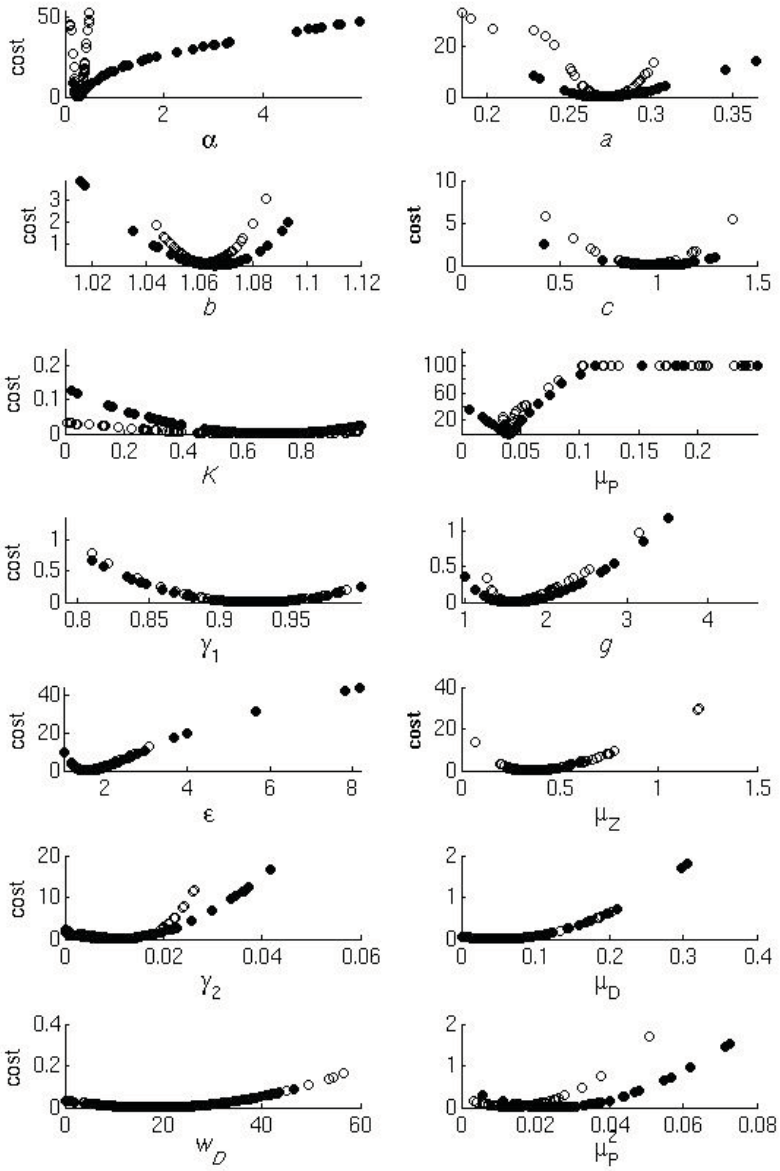

Figure 3.6: Model parameters plotted against the costs that occurred during a simulated annealing parameter optimisation of each parameter at station P1 (circles) and station P3 (filled circles).

3.4.2 Twin experiment summary

Simulated annealing is an effective algorithm for data assimilation. The optimal parameters are found and the model correctly reproduces the data. Our data assimilation analysis shows that the detrital sinking rate, w_D, and the half saturation constant of DIN uptake rate, *K*, cannot be estimated from the data constraints (Table 3.2) and they have very little influence on the cost function (Figure 3.6).

3.5 Data Experiment

3.5.1 Twelve parameter optimisation

Simulated annealing was used to find the optimal model parameters at SAZ-Sense stations P1 and P3 using observations of seasonal chlorophyll a from SeaWiFS. The analysis performed in Section 4 revealed that not all of the parameters can be determined by the optimisation in this region. Fennel et al. (2001) demonstrated how the errors of parameter estimates are improved by removing the most poorly constrained parameters from the optimisation. Frierichs et al. (2006) demonstrated that optimising too many parameters decreases the predictive ability of a model. To help reduce errors in our parameter estimates the detrital sinking rate, w_D and the half saturation constant of DIN uptake rate, *K* are held constant while the remaining twelve parameters are optimised.

The S003 parameter values are taken as the initial parameters (Table 2.1). The model solution using these parameters is very different to the observations (compare Figure 3.5 with Figure 3.3). Using the initial parameter set, the phytoplankton bloom occurs between September and November and is larger at station P1 than P3, in contrast to the observations which show the phytoplankton biomass is elevated between November and March with the bloom at P3 reaching as much as 1.7 times the magnitude of that at P1.

The optimisation greatly improves the model fit to the SeaWiFS surface chlorophyll data. The model output now captures the timing and magnitude of the annual cycle of

chlorophyll observations. The cost function is 0.79 at station P1 and 3.61 at station P3 (Figure 3.7).

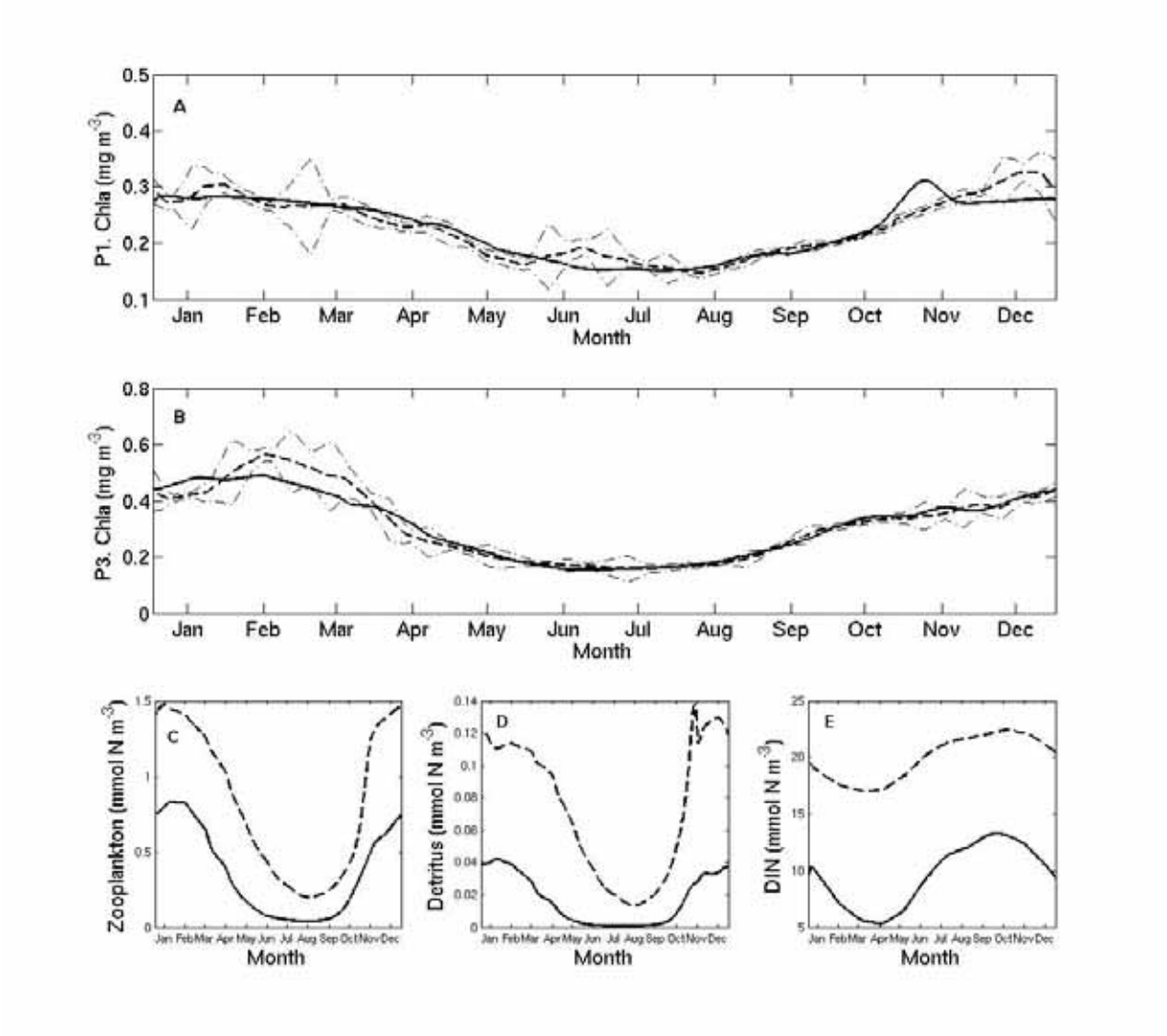

Figure 3.7: Annual model trajectories after optimising twelve parameters using simulated annealing. Panels A and B show the modelled chlorophyll (solid line) and the chlorophyll data using 8-day SeaWiFS climatology (bold dashed line) with error margins calculated as the standard deviation of all observations within a 1x1 degree square (dot-dashed line) around the process stations P1 and P3 respectively. Panels C – E show the modelled zooplankton, detritus and DIN at station P1 (dashed line) and station P3 (solid line).

3.5.1.1 Parameter uncertainty

The parameter estimates and their *a-posteriori* error is shown in Table 3.3. The singular values and associated singular vectors of the Hessian matrix were calculated for a thorough uncertainty analysis. The interested reader can refer to Section 3.8.

The singular vectors of the Hessian show that the parameters best resolved by the chlorophyll data are zooplankton excretion, γ_2; phytoplankton loss rate, μ_P; mortality of zooplankton, μ_Z; and phytoplankton maximum growth rate, *b* at station P1; and zooplankton excretion, γ_2; and phytoplankton loss rate, μ_P at station P3. The estimates of these parameter values are not independent of one another. The differences in the estimates of these parameters between P1 and P3 are discussed in Section 6.

The well resolved parameters for the phytoplankton loss rate, μ_P, and excretion by zooplankton, γ_2, control the flow of nitrogen from the phytoplankton and zooplankton pools back to the dissolved inorganic nitrogen pool. The rapid recycling of nitrogen from the P to the N compartments (as a function of μ_P) can be regarded as an implicit description of the bacterial loop without explicitly including bacteria and dissolved organic nitrogen as additional state variables in the model (Schartau and Oschlies, 2003b). The direct path of nitrogen from *Z* to *N* (as a function of γ_2) is a simplified parameterisation of remineralisation via zooplankton representing the production of ammonium.

The initial slope of the PI curve α and the phytoplankton growth rate parameter *a* are reasonably well resolved at station P3 compared to station P1 where both are poorly resolved. As discussed in Section 4.1 this may be due to the difference in the magnitude of the chlorophyll bloom between the stations, which is up to 1.7 times greater at P3 than P1. The mortality of zooplankton, μ_Z is well constrained by the data at station P1

compared to station P3. The zooplankton parameters for prey capture rate, ε, and maximum grazing rate, *g*, are poorly resolved at both stations (Figure 3.11).

Parameter	SO03 Parameter value	P1 twelve parameter optimisation estimate	P3 twelve parameter optimisation estimate	P1 reduced parameter optimisation estimate	P3 reduced parameter optimisation estimate
α	0.256 ± 0.1	0.118 ± 0.4977	0.014 ± 0.0001	-	0.015 ± 0.0002
a	0.27 ± 0.1	0.50 ± 1.4056	0.05 ± 0.0004	-	0.09 ± 0.0012
b	1.066 ± 0.01	1.075 ± 0.0087	1.209 ± 0.0012	1.073 ± 0.0005	1.141 ± 0.0007
c	1.0 ± 0.01	1.0 ± 0.0011	1.0 ± 0.0009	1.0 ± 0.0008	1.0 ± 0.0008
μ_P	0.04 ± 0.01	0.00 ± 0.0641	0.00 ± 0.0000	7.9×10^{-8} ± 0.0001	0.0002 ± 0.00003
γ_1	0.925 ± 0.01	0.935 ± 0.0111	0.952 ± 0.0011	0.936 ± 0.0008	0.938 ± 0.0008
g	1.57 ± 0.1	1.76 ± 0.2757	0.30 ± 0.0022	-	-
ε	1.6 ± 0.1	2.85 ± 0.8807	2.72 ± 0.0406	-	-
μ_Z	0.34 ± 0.05	0.05 ± 0.1193	0.11 ± 0.0027	0.047 ± 0.0003	0.13 ± 0.0131
γ_2	0.01 ± 0.01	0.004 ± 0.0086	0.002 ± 0.00007	0.009 ± 0.00001	0.021 ± 0.00002
μ_D	0.048 ± 0.01	0.048 ± 0.0008	0.048 ± 0.0008	0.102 ± 0.0008	0.248 ± 0.0008
μ_P^2	0.025 ± 0.01	0.018 ± 0.0018	0.014 ± 0.0011	0.018 ± 0.0008	0.019 ± 0.0009

Table 3.3: Initial parameter values from Schartau and Oschlies (2003a) with their prescribed uncertainties, and the optimised parameter estimates for stations P1 and P3 resulting from the twelve parameter optimisation experiment and reduced parameter optimisation experiment utilizing chlorophyll data from Sea-WIFS. Parameter names and units are given in Table 2.1. A dash indicates the parameter was not optimised in the reduced parameter experiment and was kept fixed at the optimised value from the twelve parameter experiment. The values listed for the remineralisation rates account for the mean temperature at the two stations.

The *a posteriori* errors and the parameter resolution, determined from the singular vectors, indicate that the experimental design of the twelve parameter optimisation needs revising particularly for station P1.

3.5.2 Reduced parameter optimisation

Several parameters are very poorly resolved in the twelve parameter optimisation. Following Fennel et al. (2001) we suppose that the most poorly constrained parameters, as indicated by the singular vectors, are known and fix them at the optimal values. The zooplankton grazing parameters, g and ε, become invariant parameters at both stations, and α and a are held constant at station P1. Removing poorly constrained parameters does not compromise the model solution since the parameter estimates (Table 3.3) and model dynamics (Figure 3.8) remain close to the previous twelve parameter results, with costs of 0.74 at P1 and 1.04 at P3 (compared to costs of 0.79 and 3.61 at P1 and P3 respectively in the Twelve parameter optimisation) the model solution looks nearly identical to Figure 3.7. The *a-posteriori* errors on the estimates are notably smaller for most parameters (Table 3.3); hence we now use these estimates for further experiments and comparison with in situ studies.

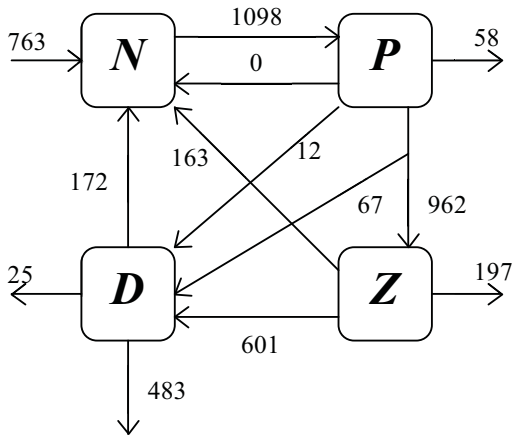

Station P1

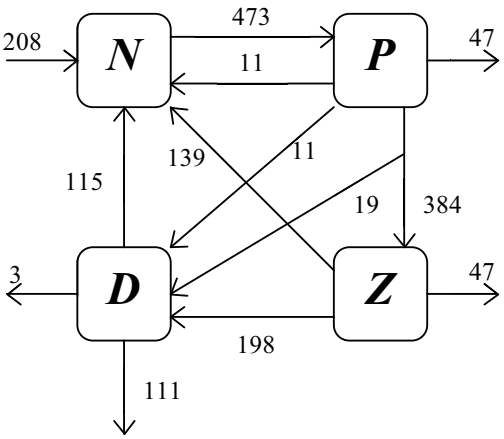

Station P3

Figure 3.8a: Annual flow of nitrogen between compartments of the model at stations P1 and P3 using the parameters from the twelve-parameter optimisation experiment in which Sea-WiFS chlorophyll data was used. Units are mmol $m^{-2}yr^{-1}$. The external arrows represent the entrainment and detrainment of the various components in and from the mixed layer.

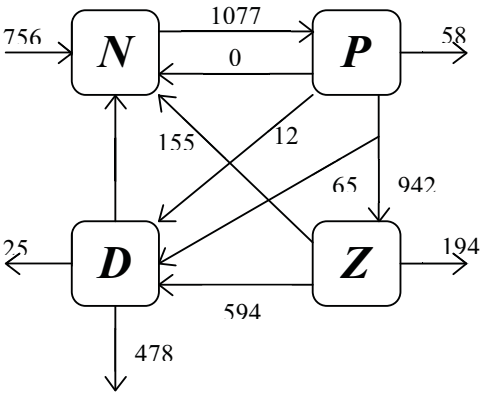

Station P1

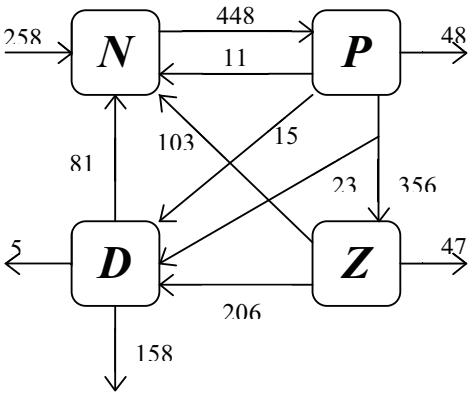

Station P3

Figure 3.8b: Annul flow of nitrogen between compartments of the model at stations P1 and P3 using the parameters from the reduced parameter optimisation experiment in which Sea-WiFS chlorophyll data was used. Units are mmol $m^{-2}yr^{-1}$ .3.5.3 Performance of parameter optimisations across the region.

It is unknown whether differing biological systems or differing physical environments dominate the variation in plankton between stations P1 and P3. To explore this question two experiments were performed. Firstly the optimised parameter estimates for station P1 from Section 5.2 (Table 3.3) were used to run the model at station P3, and vice-versa. Secondly the optimised model was run at station P1 using the mixed layer depth data from station P3, and vice-versa (the mixed layer depth data is shown in Figure 3.2d).

Running the model at P1 with the optimal parameters for P3 results in substantial changes in the biological dynamics, and similarly running the model at P3 with the optimal parameters for P1 also produces substantial changes. The nitrogen fluxes at P1 become very similar to the optimised solution for P3 from Section 5.2, and vice versa (Figure 3.9a). Thus the optimal parameters are distinctive to each station, and represent the ecosystem from that station even when utilized in a different physical setting.

Changing the mixed layer depth data does not make a considerable difference to the biological model dynamics (Figure 3.9b). The optimal parameters found are not dependent on the correct mixed layer depth data. The difference in magnitude of the mixed layer data between stations P1 and P3 (up to 140m deeper at station P1 in the winter) does not produce a considerable difference in biological response between the stations.

Experiments were performed swapping the temperature data and the light data between the stations. These changes did not have much impact on the biological model dynamics. The average temperature is less than 2°C different between stations and the solar radiation is almost identical at both stations (Figure 3.2).

These experiments show that the biological parameterisation has a greater impact on the modelled response in nitrogen fluxes than the physical forcing.

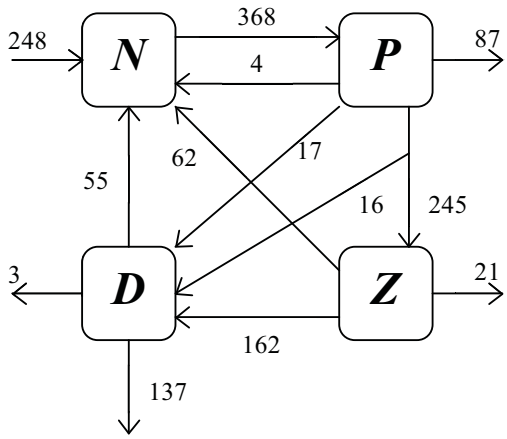

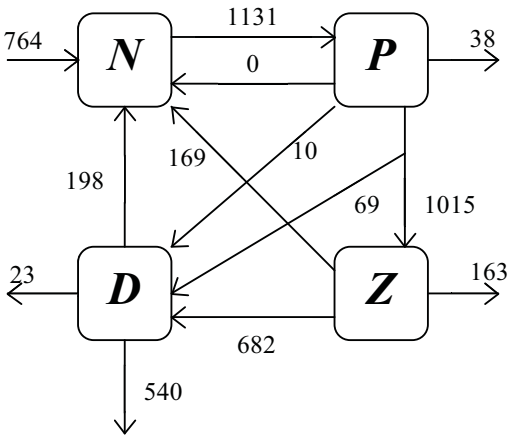

Station P1 Station P3

Figure 3.9a: Annual flow of nitrogen between compartments of the model at stations P1 and P3 using the parameters optimised for the opposite station. Units are $\mathrm{mmol\,m^{-2}yr^{-1}}$.

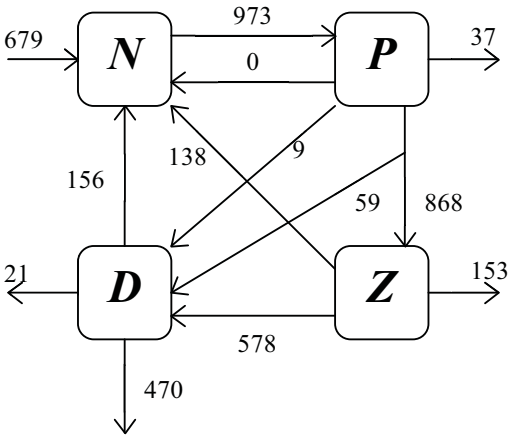

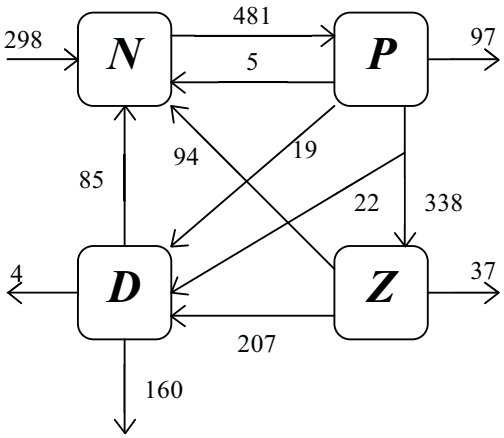

Station P1 Station P3

Figure 3.9b: Annual flow of nitrogen between compartments of the model at stations P1 and P3 using the the swapped mixed layer depth data. Units are $\mathrm{mmol\,m^{-2}yr^{-1}}$

3.6 Reduced parameter optimisation results in the context of other studies

The SAZ-Sense voyage measured rates of primary productivity and *f*-ratios over ~7 days at each process station in February 2007. This Section makes a comparison of the reduced parameter optimisation results with these measurements as well as with the initial parameters SO03 used by Schartau and Oschlies (2003a).

The reduced parameter optimisation changes the model behaviour significantly compared with using the SO03 parameters, which were optimised for an oligotrophic region in the North Atlantic (Schartau and Oschlies, 2003a). Our results produce a solution that has more production driven by nutrient supply from below the mixed layer at both stations compared to the SO03 parameters. The estimate of the phytoplankton loss rate term, μ_P is close to zero at both stations whereas the Schartau and Oschlies (2003) found a large flux of nitrogen from phytoplankton to the inorganic nutrient pool at all their stations. Accordingly the *f*-ratio (ratio of nitrate based production to total production) is higher at both stations P1 (0.70) and P3 (0.57) compared to the SO03 results of 0.09, 0.31 and 0.42 for the locations of BATS, NABE and OWS-INDIA respectively (Schartau and Oschlies, 2003b).

The optimised *f*-ratios vary seasonally between 0.47 and 0.81 at P1, and 0.14 and 0.69 at P3 (Figure 3.10) with the annual average being 0.70 at station P1 and 0.57 at P3. This is high when compared with findings by Cavagna et al. (in press) who found February *f*-ratios of 0.14 – 0.51 at station P1 and 0.17 – 0.26 at station P3. The results give a solution in which more of the production is driven by nitrogen recycled within the upper mixed layer at station P3 compared to P1. The recycling flux, $\gamma_2 Z$, representing a simplified parameterisation of ammonium production, makes up 16% of all zooplankton losses at P1 compared to 29% at P3. This is consistent with the results from Cavagna et al. (in press), who found that the higher *f*-ratio values observed at P1 could have been induced by very low ammonium concentrations; and that low *f*-ratios at P3 may result from a shallow subsurface ammonium maximum (30m) rendering it easily accessible to mixed layer phytoplankton. The recycling flux, $\mu_P P$, representing a simplified parameterisation of bacterial activity, is slightly greater at P3 than P1. Pearce *et al*. (in press) found rates of

bacterivory to be higher at P3 compared to P1. The recycling flux, $\mu_D D$, representing detritus remineralisation makes up 24% of the nitrogen flux from detritus at P1 and 33% at P3.

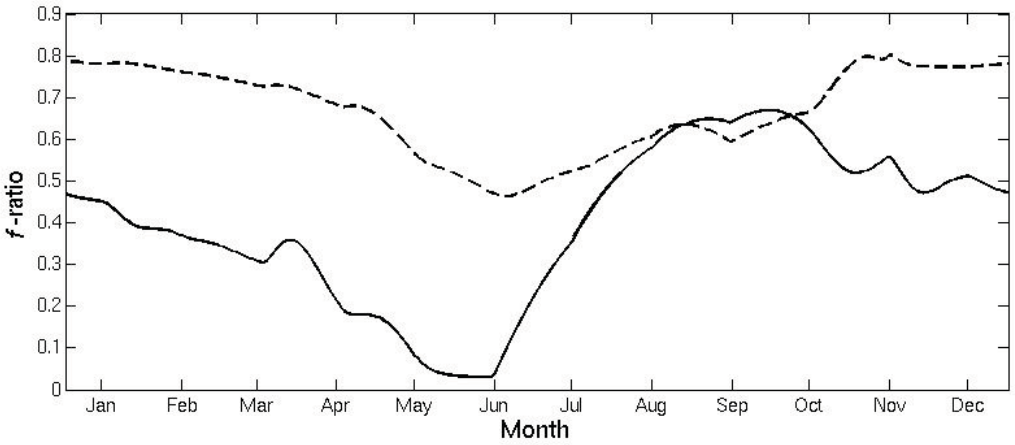

Figure 3.10: Model predicted annual *f*-ratio for station P1 (dashed line) and station P3 (solid line)

The difference in optimised values of the recycling rates implies the presence of different ecosystems between the two stations, with larger organisms at P1 and smaller organisms at P3. This is consistent with the in situ findings of Pearce *et al.* (in press). Their size fractioned Chl *a* analysis showed that station P1 had particularly high concentrations of large (20 -200 μm) phytoplankton which comprised 35% of total Chl *a*, whereas at P3 <3% of total Chl *a* was from the 20 -200 μm size phytoplankton and 77% of the total concentrations were from small (<2 μm) phytoplankton. The species composition study of de Salas et al., (in press) found dominance of diatoms at P1, while smaller flagellates dominated at P3; they found the average particle size category within the carbon biomass at P1 was almost two orders of magnitude larger than that at P3. Similarly the phytoplankton pigment results and analysis of Wright *et al.* (in press) found dominance of small dinoflagellates and cyanobacteria at P3 and virtually no cyanobacteria at P1.

The estimated parameters give an annual averaged productivity of 238.5 and 103.4 mg C m^{-2} d^{-1} at stations P1 and P3 respectively (3.0 and 1.3 mmol N m^{-2} d^{-1}); with maximum values of 659 mg C m^{-2} d^{-1} at P1 and 203.5 mg C m^{-2} d^{-1} at P3. This is much lower than the values observed during the SAZ-Sense cruise of 1304 ± 300.1 mg C m^{-2} d^{-1} and 986 ± 500.4 mg C m^{-2} d^{-1} at P1 and P3 respectively (Westwood et al., in press). As discussed by Westwood et al., their productivity measurements were high due to the method used and other studies in the SAZ found lower summer productivity values ranging between 158.7 to 730.0 mg C m^{-2} d^{-1} (Leblanc *et al*., 2002; Hiscock *et al*., 2003; Vaillancourt *et al*., 2003). The spring maximum of modelled primary productivity is of a similar magnitude to the various spring time in-situ estimates.

Although there is significant variability in summer time primary productivity in the SAZ it is evident from the observations that there is no large difference in primary production between stations P1 and P3. Our model estimates show nearly three times lower production at station P3 than P1. The estimates from Westwood et al. (in press) do not support dramatically lower primary production at P3 than P1.

Since the phytoplankton are growing slower at station P3 than P1 there is less grazing and lower zooplankton biomass. The mortality of zooplankton (μ_z), one of the well-constrained parameters, is considerably higher at station P3 than P1 (0.13 $(\text{mmol m}^{-3})^{-1}\text{d}^{-1}$ and 0.047 $(\text{mmol m}^{-3})^{-1}\text{d}^{-1}$ respectively). This further lowers zooplankton biomass at P3 and results in less grazing pressure. In reality an ecosystem dominated by small phytoplankton with a high recycling rate should be mostly grazed by microzooplankton with a high grazing rate. The optimisation at P3 has produced a solution with low primary production and grazing to prevent the phytoplankton from blooming too early in the season. Our optimisation experiments show that out model formulation can only reproduce the seasonal cycle of surface chlorophyll at station P3 by forcing the growth rates so low that we underestimate primary production and zooplankton grazing. The optimised model at P3 is biological unfeasible. An alternative representation of the ecosystem is needed to simulate the seasonal cycle at P3.

It is thought that variation in iron supply is partially responsible for the elevated chlorophyll at station P3. Lannuzel et al. (in press) and Bowie et al. (2009) found that iron concentrations were higher at station P3 than P1. They found that iron recycling within surface waters was important in explaining the differences in chlorophyll-a between the two sites. Mongin et al. (in press, b) showed with ocean simulations that atmospheric deposition is an important source of iron to P3. We hypothesize that at P3 an ecosystem model that includes seasonal variations in atmospheric deposition of iron is necessary to simulate the seasonal cycle of phytoplankton with reasonable values for primary production, zooplankton biomass and zooplankton grazing.

3.7 Conclusion

The SAZ-Sense project took place in austral summer 2007 to investigate the zonal asymmetries in planktonic ecosystems within the Sub-Antarctic Zone. The parameters of a simple NPZD model have been optimised for SAZ-Sense process stations P1 and P3 using simulated annealing by fitting the model to the observed seasonal surface chlorophyll concentrations.

An analysis of parameter uncertainties shows at both stations P1 and P3 the recycling processes, representing simplified parameterisations of the production of ammonium and the bacterial loop, are well constrained by the optimisation. In addition phytoplankton growth at P3, and zooplankton mortality at P1, are well-constrained parameters. These parameters are crucial to obtaining a representative simulation of phytoplankton biomass.

The optimised parameters indicate that different processes control ecosystem functioning at P3 and P1. Our experiments suggest that the difference in observed surface chlorophyll between P1 and P3 results from different ecosystem functioning rather than different physical conditions. Based on the analysis of the environmental fields in the region the

most likely environmental explanation for the different ecosystems is the bio-availability of iron (Mongin et al, in press, a).

The optimised estimates result in a convincing solution at P1 with reasonable estimates of primary production and biological dynamics. At P3 the optimisation results in satisfactory estimates of recycling rates but underestimates primary production, zooplankton biomass and zooplankton grazing. Despite its simplicity the model can reproduce the main ecosystem features in the surface mixed layer at P1. However at P3 there is not enough flexibility with this simple model to reproduce the late seasonal phytoplankton maximum. The model is missing the processes necessary to reproduce the biological features at P3.

Based on other studies (Mongin et al., in press, a and b) we hypothesise that seasonal variability in atmospheric iron deposition plays an important role in the seasonal evolution of phytoplankton and produces the late summer maximum in phytoplankton. An ecosystem model that includes seasonal variations in atmospheric deposition of iron may improve our modelling results at P3.

This study highlights the importance of substantiating model results with independent validation data. The close agreement between the model and the SeaWifs surface chlorophyll at station P3 occurs for the wrong reason. It is important for modellers and observationalists to collaborate to ensure thorough model evaluation and identify key observations to constrain biogeochemical models.

3.8 Appendix

The singular values of the Hessian matrix are calculated to assess the number of parameters needed to capture the essential features of the data. The parameters associated with the largest singular values are determined from the ordered singular vectors (denoted λ_i); these parameters have the greatest influence on the model solution. The parameters

associated with the smallest singular values have little influence on the model output but are responsible for explaining the largest degree of error. By ignoring the parameters associated with the smallest singular values it is possible to reduce the amount of error in the results (Wall et al., 2002).

Figure 3.11 shows the ordered singular vectors calculated from the Hessian matrix from the twelve-parameter optimisation experiment utilising Sea-WiFS surface chlorophyll data. The singular vectors $\lambda_1 - \lambda_3$ in Figure 3.11a show that the parameters best resolved by the chlorophyll data are zooplankton excretion, γ_2; phytoplankton loss rate, μ_P; mortality of zooplankton, μ_Z; and phytoplankton maximum growth rate, *b* at station P1. The singular vectors λ_1 and λ_2 in Figure 3.11b show that the parameters best resolved by the chlorophyll data at P3 are zooplankton excretion, γ_2; and phytoplankton loss rate, μ_P.

The singular vectors λ_3 and λ_4 in Figure 3.11b show the initial slope of the PI curve, α and the phytoplankton growth rate parameter, *a* are reasonably well resolved at station P3 compared to station P1 where both are poorly resolved, as shown by λ_{10} and λ_{12} in Figure 3.11a.

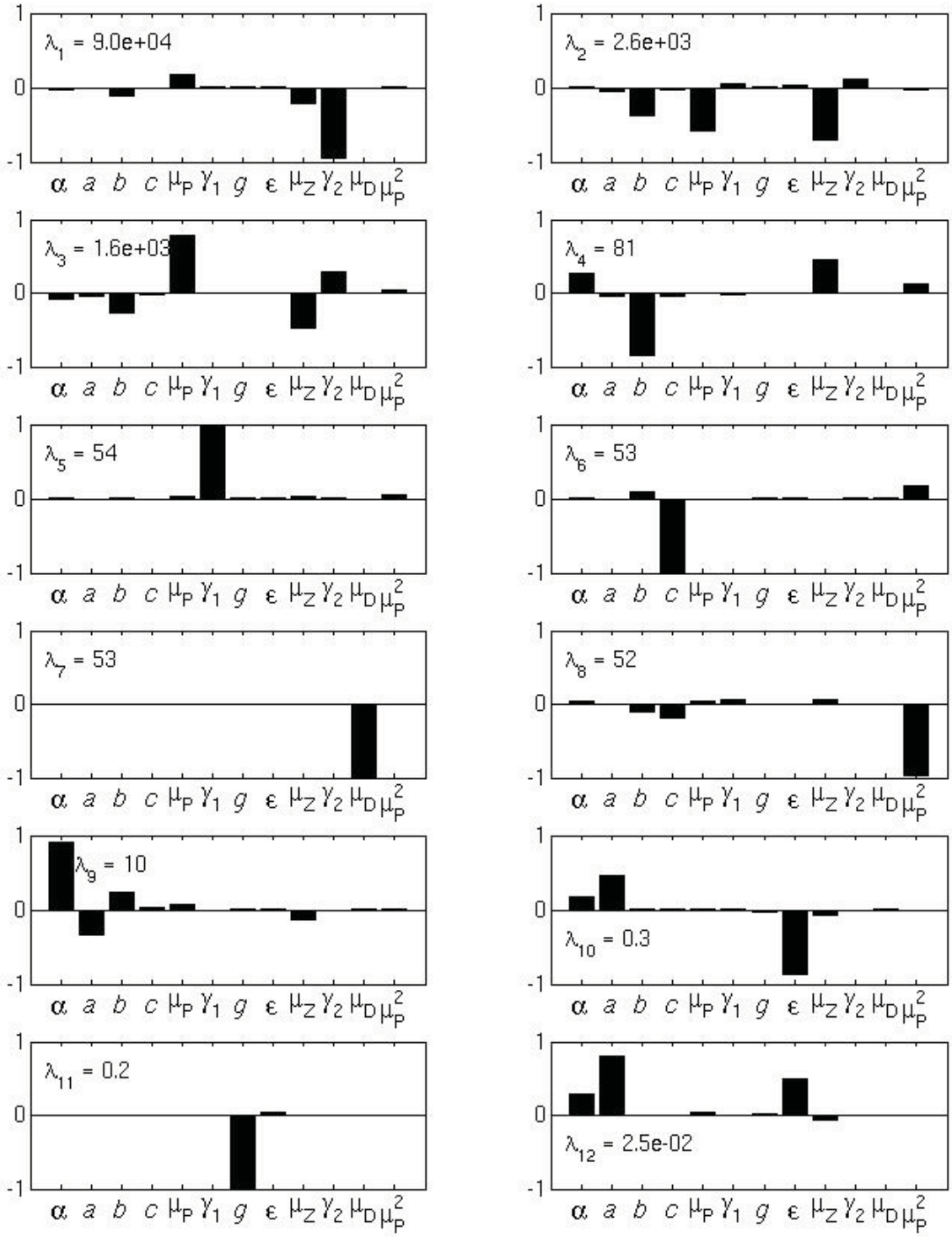

Figure 3.11a: Parameter resolution for the 12 parameter optimisation experiment utilising Sea-WiFS chlorophyll data at station P1. The singular vectors λ_i , i=1:12, are shown in decreasing order of the magnitude of their associated singular values. As the magnitude of the singular values decreases so the parameters contributing to the associated singular vector decrease in their impact upon the model solution.

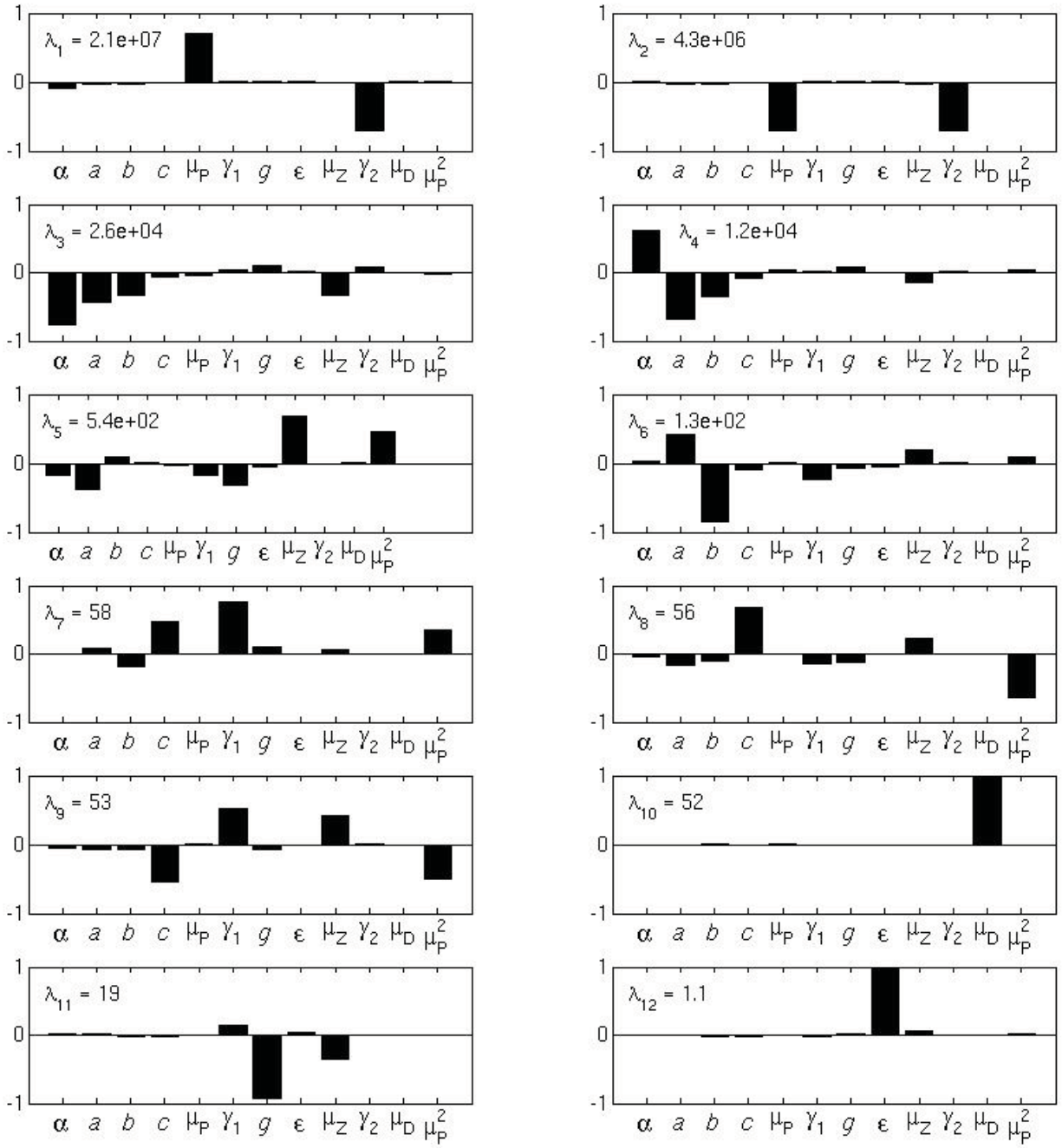

Figure 3.11b: Parameter resolution for the 12 parameter optimisation experiment utilising Sea-WiFS chlorophyll data at station P3.

Chapter 4:

Phytoplankton growth in the Australian sector of the Southern Ocean, examined by optimising ecosystem model parameters.

4.1 Introduction

In large areas of the worlds oceans there is an excess of nitrate and phosphate that remain unutilised in the surface waters where phytoplankton populations do not manage to bloom sufficiently to strip out the nutrients. There has been considerable debate about the principle factors causing anomalously low phytoplankton biomass in relation to nutrients in the Southern Ocean, the equatorial Pacific and the North Pacific. The Southern Ocean HNLC (high nutrient low chlorophyll) region is particularly important because it is one of the major regions of intermediate and deep water formation (Sarmiento and Orr, 1991) and Sub-Antarctic waters are an important sink for anthropogenic carbon dioxide (CO_2) (Metzl et al., 1999).

Growth limitation by micronutrients (Coale et al., 1991; Sedwick et al., 1999; Boyd et al 2000), limited light availability in the high latitudes (Holm-Hansen et al., 1977; Smith and Nelson, 1985; Mitchell and Holm-Hansen, 1991), suppression of phytoplankton populations by zooplankton grazing (Duce and Tindale, 1991; Miller et al., 1991; Minas and Minas, 1992; Tsuda et al., 2007), or some combination of these factors (Chavez et., 1991; Landry et al., 1997; Boyd et al., 2001) have been considered to explain HNLC regions.

The most likely micronutrient in limiting phytoplankton growth in HNLC regions is iron (Martin and Fitzwater, 1988; Kolber et al., 2002). Silica is also a contender (Ku et al., 1995; Laynaert et al., 2001). Iron is an essential nutrient for phytoplankton growth, required for the synthesis of chlorophyll and for the photosynthetic production of organic compounds (Street and Paytan, 2005).

The role of iron in limiting phytoplankton growth in HNLC regions has been given added importance since Martin et al. (1990) proposed the ‘Iron Hypothesis’ speculating that iron deficiency was alleviated in glacial periods due do aeolian dust deposition in a windier and dryer climate. They hypothesised that this allowed increased phytoplankton

productivity and export of CO_2, resulting in the reduced atmospheric CO_2 concentrations that characterise glacial periods. Iron fertilisation of HNLC regions of the ocean has been proposed as a geo-engineering approach to mitigate climate change, by stimulating a phytoplankton bloom large enough to remove substantial amounts of CO_2 from the atmosphere (Denman, 2008). Additionally, natural delivery of iron to the Southern Ocean by dust from land masses and advective sources from shelf sediments is projected be significantly altered under future climate change scenarios (Bowie et al. In press).

A number of iron enrichment experiments and incubation experiments (Martin et al., 1994; Coale et al., 1996; Boyd et al., 2000; Tsuda et al., 2003; Bakker et al., 2005; Timmermans et al., 1998; Franck et al., 2000; Blain et al., 2004) have demonstrated an increase in phytoplankton growth and primary productivity with iron enrichment of surface ocean waters. The Southern Ocean Iron Release Experiment (SOIREE), an in situ mesoscale iron fertilisation experiment, provided evidence of enhanced algal growth rates due to iron enrichment at $140^{\circ}E, 61^{\circ}S$ (Boyd et al., 2000); however many of the previous Southern Ocean studies provided ambiguous results, with increases in chlorophyll in both iron enriched treatments and control treatments (reviewed in de Baar and Boyd, 2000).

Although results support the importance of iron in regulating primary productivity, they do not imply that iron is the ultimate control (Fennel et al., 2003). Recent studies show the factors controlling phytoplankton biomass in the Southern Ocean are still open to debate. Boyd et al. (2001) studied the effect of iron supply and irradiance on phytoplankton growth in the SAZ (Sub-Antarctic Zone) and PFZ (Polar Frontal Zone) of the Australian sector of the Southern Ocean and found that in both regions iron was limiting algal growth rates while in the PFZ light was also limiting growth. In contrast Oijen et al. (2004) studied the effect of iron supply and irradiance on phytoplankton growth in the Atlantic sector of the Southern Ocean and found that low phytoplankton biomass was mainly caused by light limitation rather than iron. Conversely Banse (1996)

studied the effects of underwater irradiance, iron and grazing on SAZ chlorophyll and found that zooplankton grazing was controlling the phytoplankton populations.

Ecosystem models provide a useful tool to separate the factors indicated in the control of phytoplankton biomass and look at different processes individually. Complex models have been developed to simulate the role of iron on marine ecosystems. Fasham et al. (2006) developed a multi nutrient model incorporating iron cycling and performed a parameter optimisation to fit the model to iron replete and iron limited conditions. They showed that underwater light levels have a more limiting effect on phytoplankton growth than iron supply at their experiment site in the Indian Ocean sector of the Southern Ocean. Mongin et al. (2006) applied a flexible composition model incorporation iron cycling, phytoplankton iron/carbon ratios and iron limitation to the same region and found phytoplankton growth to be strongly limited by an interaction of iron and light, with grazing also being a significant factor.

There have been a number of iron modelling studies that do not explicitly include iron as a state variable (Fennel et al., 2003; Hense et al., 2000; Denman and Pena, 1999). Fennel et al. (2003) looked at the effect of iron on phytoplankton photosynthetic growth rates to investigate inter-glacial changes in CO_2 concentrations. Hense et al. (2000) used a 5-7 compartment model to investigate the role of iron limitation in the PFZ by using different Si:N uptake ratios and reduced phytoplankton growth rates. Denman and Pena (1999) used a 4 compartment NPZD model to simulate the planktonic ecosystem and examine iron limitation in the North Pacific by reducing growth rates of phytoplankton. They found that the annual cycle of surface layer nitrate concentrations in this region was best reproduced by reducing the maximum photosynthetic growth by a factor of 3.0 – 3.5.

Here we present a modelling study to explore the ecosystem functioning of the HNLC regime in the Australian sector of the Southern Ocean. The HNLC conditions in this region become more prominent moving south from the SAZ, with surface chlorophyll generally decreasing and nitrate increasing with latitude (Figures 4.4 and 4.5). We perform data assimilation experiments using simulated annealing to fit a nitrogen based

model to Sea-WiFS surface chlorophyll data in three distinct regions of the Southern Ocean in the Sub-Antarctic Zone, Polar Frontal Zone and Antarctic Zone. Possible reasons for the latitudinal variation in phytoplankton biomass in this region are discussed in light of what our parameter estimates indicate about the ecosystem functioning. We hypothesise that iron is limiting phytoplankton growth but other explanations such as light availability and temperature are also considered.

Current knowledge of iron in seawater, and the availability of iron to phytoplankton, shows that the cycling of iron is complex and qualitatively different from the cycling of macronutrients (Fennel et al., 2003). The processes relating to the cycling of iron are poorly quantified, particularly those that effect bio-availability and biological uptake (Johnson et al., 1997; Wells et al., 1995). The main physiological response of phytoplankton to iron deficiency is a reduction in light saturated photosynthetic growth and an increase in the initial slope of the P-I curve, the photosynthetic efficiency. Greene et al. (1991) found a 2-fold reduction in light saturated photosynthesis and a 1.3 fold increase in the initial slope of the P-I curve between iron replete and iron deficient cells. This, combined with the lack of observations of iron in the Southern Ocean to validate complex model parameterisations, governs the decision to use a simple NPZD model, which does not explicitly include iron as a state variable (Oschlies and Garcon, 1999), and optimise the parameters for maximum photosynthetic growth and photosynthetic efficiency.

This Chapter is organised as follows: Section 4.2 describes the oceanographic characteristics of the study region. Section 4.3 explains the experimental design of this study. Section 4.4 presents the results of our experiments. The results are discussed in Section 4.5. Section 4.6 summarises this study.

4.2 Oceanographic characteristics

In this Section the physical characteristics of the experiment locations are described and the forcing used to run the model is explained.

4.2.1 Physical setting

The Southern Ocean is separated from the warmer and saltier waters of the subtropical oceans by pronounced meridional gradients in surface properties - a hydrographic boundary termed the Subtropical Front (Orsi et al., 1995). South of the Subtropical Front is the continuous eastward flowing Antarctic Circumpolar Current (ACC), which is divided in the horizontal direction by several fronts, characterised by bands of enhanced lateral density gradients, which are associated with strong surface currents (Nowlin et al., 1977). Between the fronts lie zones of relatively uniform water mass properties which tend to be populated by distinct biological communities (Trull et al., 2001).

The fronts and zones of the Southern Ocean, from north to south, are: the Subtropical Front (STF), the Subantarctic Zone (SAZ), the Subantarctic Front (SAF) , the Polar Frontal Zone (PFZ), the Polar Front (PF), and the Antarctic Zone (AZ) (Whitworth, 1980). Additionally Orsi et al. (1995) identified the Southern ACC Front (SACCF) south of the AZ. The fronts are important boundaries for geographical variations of phytoplankton size composition and community structure in the Southern Ocean (Odate and Fukuchi, 1995), for example numbers of diatoms increase markedly south of the polar front south of Australia (Wright et al., 1996).

The SAZ is a region characterised by strong winds and deep mixed layers of up to 800 m (Rintoul and Trull, 2001) The surface waters are warmer and less dense than the higher latitude regions with SST generally above 9˚C and salinities generally above 34.2 psu (Morrow et al., 2008). Phytoplankton community consists of a high abundance of cyanobacteria (Odate and Fukuchi, 1995) and is dominated by coccolithophores (Sokolov and Rintoul, 2007).

In contrast to the SAZ, the PFZ is characterised by relatively shallow mixed layer depth's of ~150m and smaller seasonal changes in the mixed layer depth because of a lack of deep convection in winter (Rintoul and Bullister, 1999). Sea Surface Temperatures are generally < 4˚C (Sokolov and Rintoul, 2002). The PFZ phytoplankton community is dominated by diatoms (Sohrin et al., 2000).

The AZ is a region with fairly homogeneous surface properties characterised by a low salinity (~33.9 psu) due to sea ice melt (Chaigneau et al., 2004) and SST generally below 5˚C (Morrow et al., 2008). Phytoplankton composition shows typically very low cyanobacteria (Odate and Fukuchi, 1995), higher concentrations of diatoms, and dominance by pico-eukaryotes (Boyd et al., 2000).

The fronts separating these water masses do not extend simply in a zonal direction, they include meanders, convolutions and eddies. The regional variation in frontal structure in the Australian sector of the Southern Ocean is described in detail by Sokolov and Rintoul (2002), who use sea surface height (SSH) contours for the period between 1992 and 2000 to identify fronts between 130˚E and 160˚E. They identify two branches to the SAF and the PF. Each of the branches of both fronts correspond to maxima in horizontal gradients of temperature, salinity and density.

The three experiment sites were chosen to be in the SAZ, the PFZ and AZ at 140˚E based on the frontal locations described by Sokolov and Rintoul (2002). The SAF is the strongest front and main jet of the ACC south of Australia, corresponding to a temperature decrease from north to south by more than 5˚C. At 140˚E the northern SAF (SAF-N) is found at ~47˚S and 50˚S. The southern SAF (SAF-S) is at ~52˚S. The PF marks the northernmost extent of the AZ and of temperature minimum water cooler than 2˚C at 200m depth (Belkin and Gordon, 1996). At 140˚E the northern PF (PF-N) is seen at ~56˚S. The southern PF (PF-S) is at ~60˚S. The SACCF is the only Southern Ocean front that does not separate distinct surface water masses and usually coincides with the

southernmost extent of water warmer than 1.8 ˚C (Orsi et al., 1995). At 140˚E the SACCF-N is found at ~63˚S.

The SAZ experiment site is located at 140˚E, 46˚S; the PFZ site is located at 140˚E, 54˚S; and the AZ experiment site is at 140˚E, 61˚S (Figure 4.1).

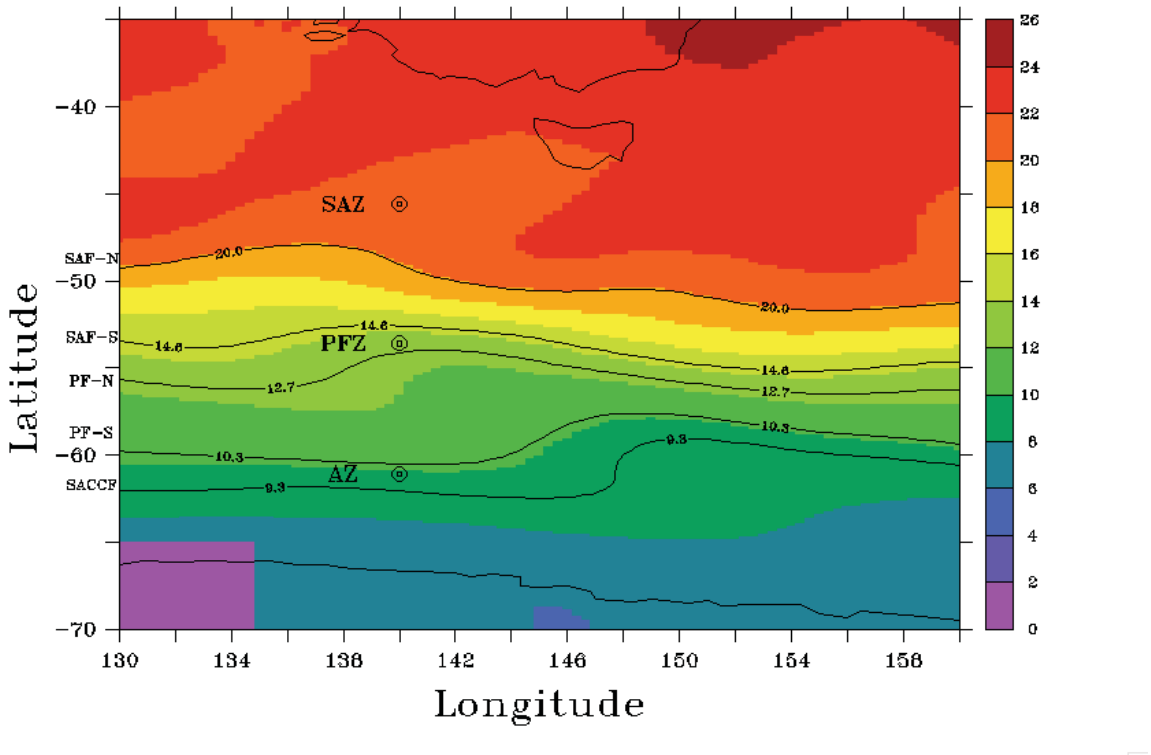

Figure 4.1: Sea Surface Height (dm). The contour lines indicate the frontal locations identified by Sokolov and Rintoul (2002).

4.2.2 Chlorophyll a

Satellite derived data provides the only large-scale synoptic observations of chlorophyll in the Southern Ocean. As in Chapter 3 we used surface chlorophyll concentration data

taken from SeaWiFS (Sea-viewing Wide Field-of-view Sensor) 8-day composites (9km) generated by the NASA Goddard Space Flight Centre for the assimilation procedure. A climatology was computed for the years 1998 – 2008 averaging the chlorophyll over a 1° square region centred on each process station (Mongin et al., in press). Interpolation was used to obtain daily values. A conversion factor of 1.59 mg Chl $(mmolN)^{-1}$ was used to convert modelled phytoplankton nitrogen to chlorophyll (Fasham et al., 1990; Sarmiento et al., 1993). To obtain a measure of uncertainty in the observed chlorophyll, the standard deviation of the observations within the 1° square was calculated and is shown with the data in Figure 4.2.

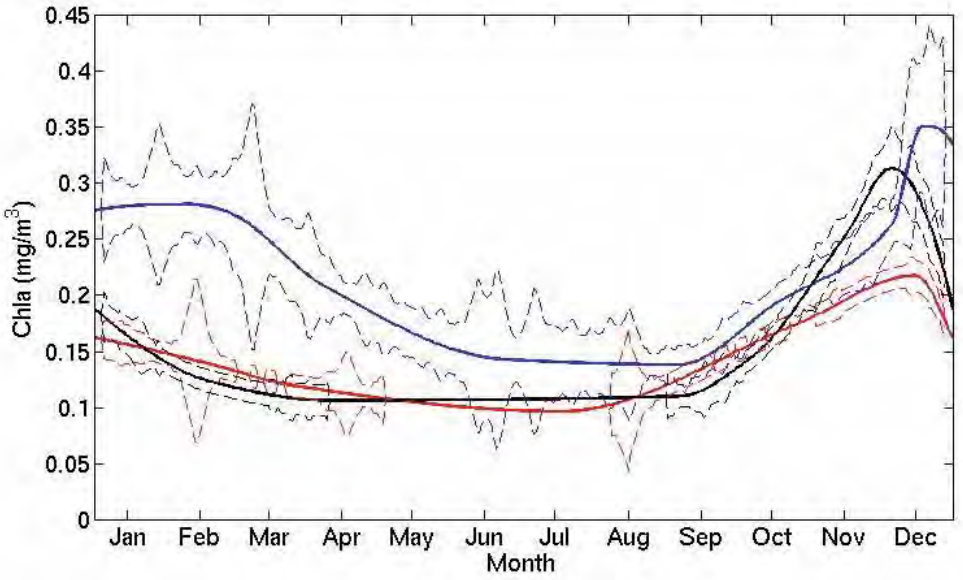

Figure 4.2: Chlorophyll climatology for the period 1998 – 2008 taken from Sea-WIFS. The SAZ site (140°E, 46°S) is shown in blue. The PFZ site (140°E, 54°S) is shown in red. The AZ site (140°E, 61°S) is shown in black. The standard deviation of the observations is plotted in a dashed line.

SeaWiFS chlorophyll data is not available for the higher latitude sites in the PFZ and AZ during mid-winter due to a high solar zenith angle. For the days where data was

unavailable the chlorophyll concentrations were interpolated between the last available observation from autumn and the first available observation in spring.

The SeaWiFS surface chlorophyll data (Figures 4.2 and 4.3) shows that the chlorophyll remains relatively low (<0.35 mg m^{-3}) at all three sites throughout the year in comparison to other regions of the ocean, such as Bermuda Station "S" where chlorophyll *a* values of up to 1 mg m^{-3} are typical in spring (Fasham et al., 1993).

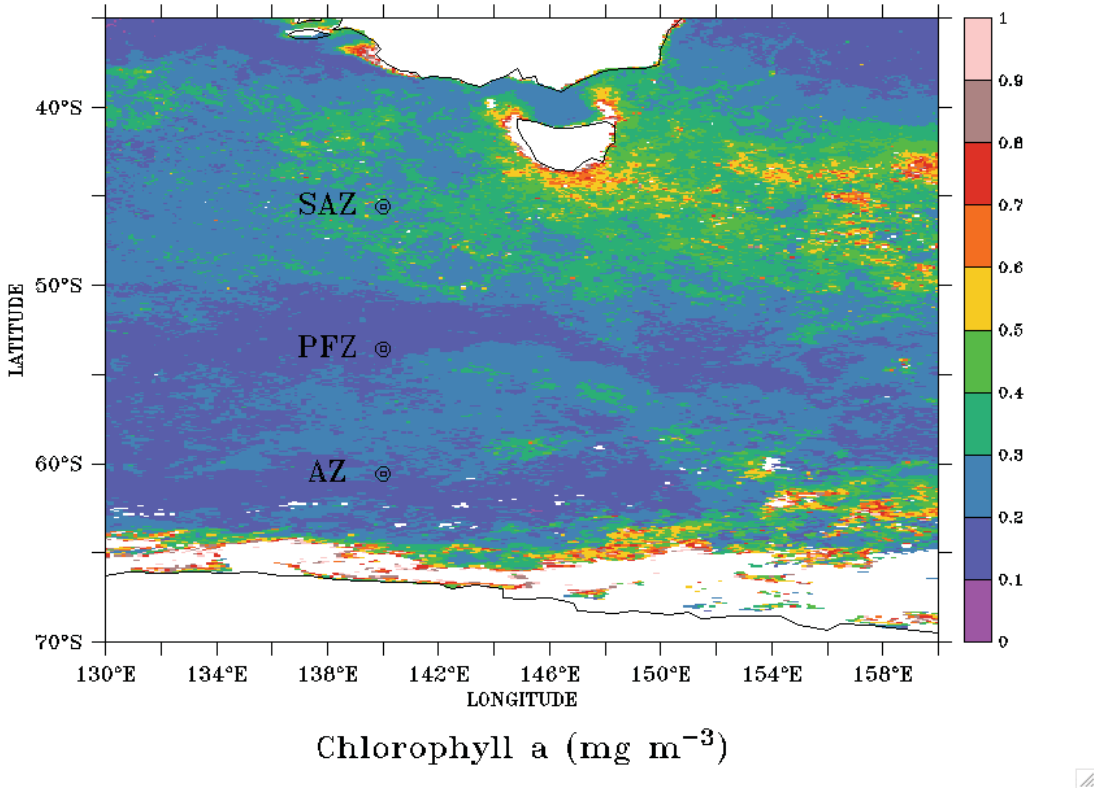

Figure 4.4: February SeaWiFS surface chlorophyll (mg m^{-3}) using a 1998 – 2008 climatology computed from 8-day composites.

The experiment locations differ in that the SAZ site has generally higher chlorophyll concentrations, with an annual mean of 0.21 mg m^{-3} compared with 0.14 mg m^{-3} at the PFZ site and 0.15 mg m^{-3} at the AZ site. The PFZ and AZ annual chlorophyll distribution

is quite similar, with the only notably distinction being the magnitude of the spring bloom, which reaches 0.31 $mg\,m^{-3}$ in the AZ compared to the PFZ where the chlorophyll reaches a maximum of 0.22 $mg\,m^{-3}$. The phytoplankton bloom in the SAZ reaches a maximum of 0.35 $mg\,m^{-3}$ in December, but unlike the higher latitude regions the bloom persists throughout the summer months with concentrations of ~0.275 $mg\,m^{-3}$ through January – March (Figure 4.2).

4.2.3 Nutrients

The SAZ, PFZ and AZ south of Australia all exhibit typical Southern Ocean HNLC conditions. The major nutrient concentrations increase with latitude and shipboard incubation experiments suggest that phytoplankton community growth is not limited by the availability of nitrate or phosphate (Lourey and Trull, 2001). Surface concentrations of nitrate in the summer are ~10.0 mmol N m^{-3} at the SAZ experiment site, ~22 mmol N m^{-3} at the PFZ experiment site, and ~24 mmol N m^{-3} at the AZ experiment site (Figure 4.4).

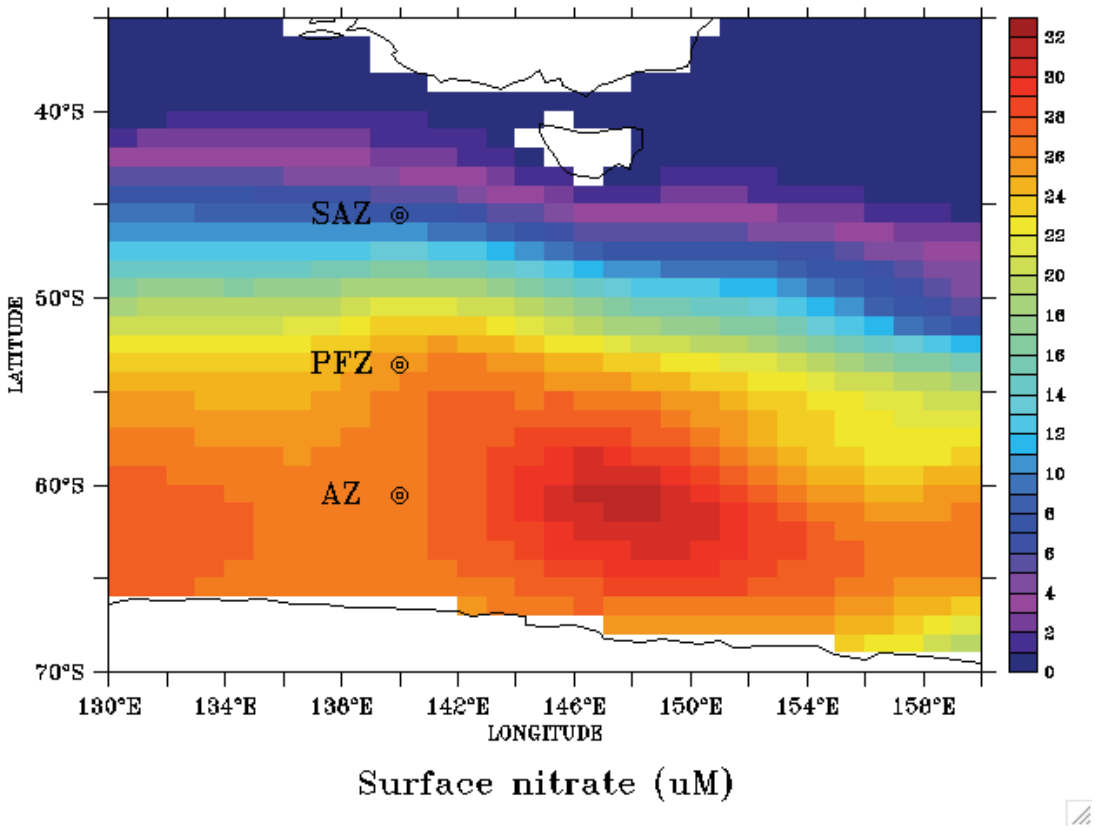

Figure 4.4: Surface nitrate concentration in February from Levitus World Ocean Atlas 2001.

Silicate, through its link to diatom structure and metabolism, may control phytoplankton processes in some regions of the ocean (Dugdale et al., 1995). The Sub-Antarctic Zone is the largest 'high-nitrate-low silic acid' region in the world ocean; surface waters are typically depleted to levels near or below measured half saturation constants for diatom uptake during summer and autumn (Hutchins et al., 2001). Silic acid depletion extends throughout the PFZ during the growth season (Kamykowski and Zentara, 1985), however in the AZ high concentrations of silic acid are introduced into surface waters by persistent upwelling (Hutchins et al., 2001).

Iron is an essential micro-nutrient for phytoplankton growth and may limit growth at low levels. The Southern Ocean receives relatively low air born iron supply from dust deposition due to distance from major land masses. In situ measurements of iron in the Australian sector of the Southern Ocean are sparse and disparate. Sedwick et al. (2008) took measurements along ~140E in autumn 1998 and spring 2001 and found mixed layer dissolved iron concentrations decrease with latitude, from values of ~0.22 nM in the SAZ to uniformly low concentrations of <0.1 nM in the AZ. Conversely Lai et al. (2008) found dissolved iron concentrations generally increased with latitude with values of 0.3nM in the SAZ, 0.4nM in the PFZ and 0.5nM in the AZ along 140E in summer 2001/02.

4.2.4 Model forcing

The forcing fields applied to the ecosystem model are incident solar radiation, Sea Surface Temperature (SST), Mixed Layer Depth (MLD) and concentration of nitrogen below the mixed layer (Figure 4.5). The SST and nitrogen data sets come from Levitus World Ocean Atlas 2001 monthly means (Levitus, 1982). The daily MLD is taken as the depth of a 0.05 kg m^{-3} difference in density from the surface computed using the model output of temperature and salinity (Mongin et al., in press). Daily averaged values of solar radiation are taken from NCAR (National Centre for Atmospheric Research).

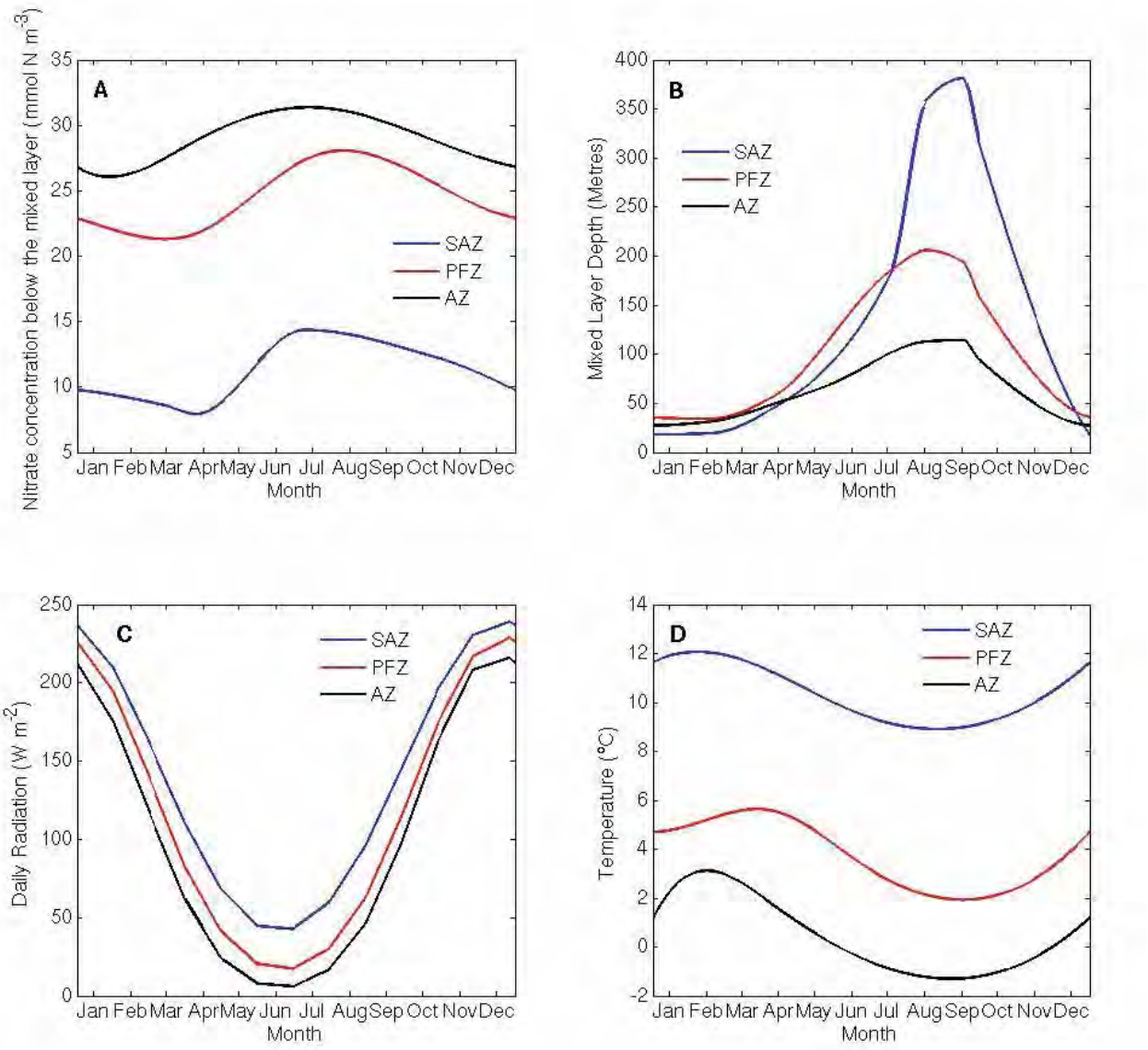

Figure 4.5: Forcing used for the model. Panel A shows nitrogen concentration below the mixed layer (mmol N m^{-3}); panel B shows mixed layer depth (meters); panel C shows daily incident solar radiation (W/m^2); panel D shows temperature (degrees Celsius). The SAZ site (140˚E, 46˚S) is shown in blue, the PFZ site (140˚E, 54˚S) is shown in red and the AZ site (140˚E, 61˚S) is shown in black.

4.3 Experimental design

In this Section the reasons for the experiments performed in this Chapter are outlined and the reasons for the model configuration and parameter values are explained. The experimental design is summarised in Figure 4.6. (The simulated annealing data assimilation methods have already been described in Chapter 2).

4.3.1 Experiments

The experiments in Chapter 3 demonstrated that simulated annealing is an effective method of optimising the parameters of a simple NPZD model assimilating remotely sensed surface chlorophyll data. Our estimates of mixed layer ecosystem behaviour at station P1 were generally consistent with in-situ estimates confirming that the model parameterisation for the chlorophyll data was a realistic biological solution. We showed that not all of the parameters could be optimised, and that the precision of parameter estimates increased when only a subset of parameters was optimised. Furthermore a good fit to the chlorophyll data was achieved without including iron in the model.

Previous NPZD modelling studies have shown that mixed layer ecosystem dynamics can be successfully reproduced in iron deficient regions without explicitly modelling iron by modifying phytoplankton photosynthetic growth parameters (Denman and Pena, 1999; Chai et al., 1996). In this Chapter the phytoplankton photosynthetic growth parameters were optimised, using simulated annealing, while all other model parameters were held constant.

The parameters optimised were maximum photosynthetic efficiency/the initial slope of the PI curve, α; and maximum light saturated growth, which is a combination of the two phytoplankton maximum growth rate parameters a and b ($P_{max} = a \cdot b^T$ (where T is temperature)). The optimisation was performed at three sites in the SAZ, PFZ and AZ in the Southern Ocean (Figure 2).

To investigate causes of differences in optimised parameter values between the sites three physical forcing interchange experiments were performed. The optimisation was repeated interchanging the light regimes between the SAZ and AZ, interchanging the temperature regimes between the SAZ and AZ and interchanging the MLD regimes between the SAZ and AZ. The optimised parameters were then inspected to determine to what degree the physical forcing influences the optimal model parameterisation.

4.3.2 Model configuration and parameter values

The results of the data experiments in Chapter 3 revealed that the initial parameterisation used, which was optimised for three sites in the North Atlantic by Schartau and Oschlies (2003a), was unsuitable for modelling the ecosystem in the Australian region of the SAZ. One of the most sensitive parameters, the phytoplankton loss rate, μ_P (one of two phytoplankton loss parameters), was optimised to effectively zero. Therefore the phytoplankton loss rate, μ_P, is a superfluous model process in this region. The un-optimised version of the model from the Schartau and Oschlies (2003a) study differed from their optimised model in parameter values as well as in the absence of this parameter μ_P. The parameter values of the un-optimised version of their model are more consistent with other modelling studies than the optimised version (Fasham et al., 1990; Sarmiento et al., 1993; Spitz et al., 1998). Therefore we use the un-optimised version of the model of that study as a starting point for this set of experiments. The model is described in Oschlies and Garcon (1999) and is referred to as OG99 hereafter. The model configuration is the same as that described in Chapter 2 (Section 2.2) with the exception that the biological source-minus-sink equations are:

Dissolved Inorganic Nitrogen (DIN)

$$\frac{dN}{dt} = \mu_D D + \gamma_2 Z - \bar{J}(M,t,N)P + \frac{(m + h^+(t))}{M}(N_0 - N) \qquad (4.1)$$

Phytoplankton Biomass

$$\frac{dP}{dt} = \bar{J}(M,t,N)P - G(P)Z - \mu_P^2 P^2 - \frac{(m + h^+(t))P}{M} \qquad (4.2)$$

Herbivorous zooplankton

$$\frac{dZ}{dt} = \gamma_1 G(P)Z - \gamma_2 Z - \mu_Z Z^2 - \frac{(h\ (t))Z}{M} \tag{4.3}$$

Detritus

$$\frac{dD}{dt} = (1-\gamma_1)G(P)Z + \mu_P^2 P^2 + \mu_Z Z^2 - \mu_D D - w_D \frac{\partial D}{\partial z} - \frac{(m + h^+(t))D}{M} \tag{4.4}$$

All other model equations are given in Section 2.2.

The only parameters from OG99 that deviate markedly from the afore-mentioned literature are the zooplankton grazing and mortality parameters which were subjectively tuned to fit the annual cycle of primary production and chlorophyll concentrations in the North Atlantic (Oschlies and Garcon, 1999). However using these parameters the annual cycle of chlorophyll is as much as double the magnitude of the observations at the SAZ site, and up to triple the magnitude of the observations at the PFZ and AZ sites. Using these parameters the grazing rate $G(P)$ is only 0.04 – 0.15 for phytoplankton concentrations between 0.2– 0.4 mmol N m^{-3}, allowing the phytoplankton populations to become too large. Therefore we set the maximum grazing rate, g, to 1.0 d^{-1} to be consistent with Fasham et al. (1990) and Evans and Parslow (1985); and set prey capture rate, ε, to 3.0 (mmol m^{-2})$^{-1}d^{-1}$ to make the overall grazing rate $G(P)$ = 0.12 – 0.32 for phytoplankton concentrations between 0.2– 0.4 mmol N m^{-3} to be closer to measurements of herbivory in the Australian sector of the Southern Ocean by Pearce et al. (in press) which ranged from 0.12 – 1.39 d^{-1} .

Therefore the parameter values used are more consistent with established literature and measured values whilst making our model output of phytoplankton closer to the observed annual cycle. Since we are only optimising three parameters it is helpful to have a reasonable starting point for our model solution since the parameter estimates found will be somewhat dependent on the fixed parameters, as shown in Chapter 3. The model parameters are shown in Table 4.1. Note that in contrast to the SO03 parameters, here the

remineralisation parameters (remineralisation of detritus, zooplankton excretion and phytoplankton loss rate) are not temperature dependent.

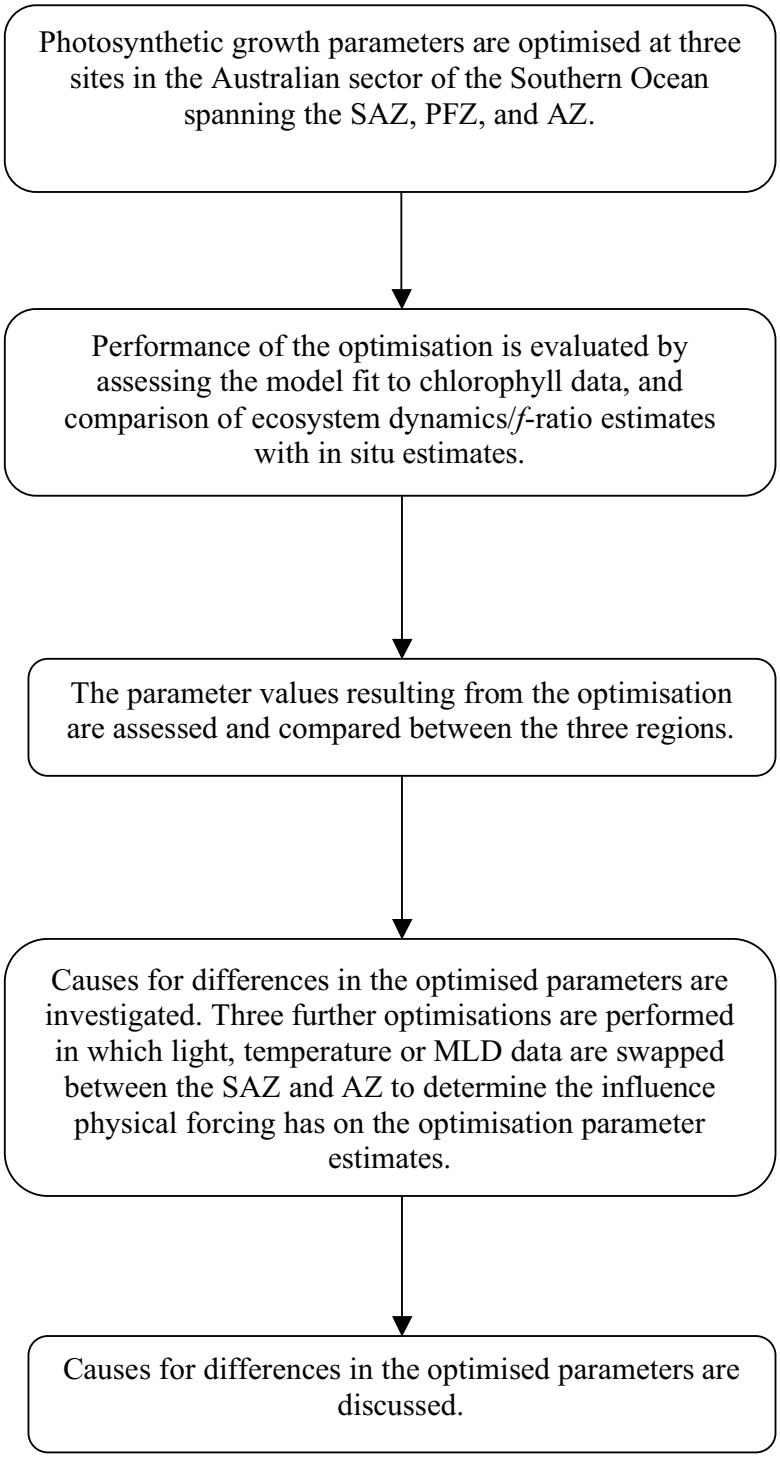

Figure 4.6: Experimental design of this Chapter.

Parameter	Symbol	Value	Units
	Phytoplankton coefficients		
Photosynthetic efficiency (initial slope of P-I curve)	α	0.025	$\text{day}^{-1}/(\text{W m}^{-2})$
Shortwave fraction of photosynthetically active radiation	PAR	0.43	
Light attenuation due to water	k_w	0.04	m^{-1}
Maximum growth rate parameters	a	0.6	day^{-1}
	b	1.066	
Half saturation constant for N uptake	K	0.5	mmol m^{-3}
Quadratic mortality rate	μ_P^2	0.03	$(\text{mmol m}^{-3})^{-1}\,\text{day}^{-1}$
	Zooplankton coefficients		
Assimilation efficiency	γ_1	0.75	
Maximum grazing rate	g	1.0	day^{-1}
Prey capture rate	ε	3.0	$(\text{mmol m}^{-2})^{-1}\,\text{day}^{-1}$
Quadratic mortality	μ_Z	0.20	$(\text{mmol m}^{-3})^{-1}\,\text{day}^{-1}$
Excretion	γ_2	0.03	day^{-1}
	Detrital coefficients		
Remineralisation rate	μ_D	0.05	day^{-1}
Sinking velocity	w_D	5.0	m day^{-1}

Table 4.1: Parameters used to run the ecosystem model. These values are used as a starting point in the optimisation experiments.

4.4 Results

4.4.1 Model performance, primary production, f-ratios and grazing

The parameter optimisation was performed at three locations in the Australian sector of the Southern Ocean, spanning the SAZ, the PFZ and the AZ at 140°E, 46°S; 140°E, 54°S and 140°E, 61°S. The model parameters for maximum photosynthetic efficiency, α and maximum light saturated photosynthetic rates, $P_{max} = a \cdot b^T$, were optimised while all other parameters remained invariant in time.

The optimisation results in a good fit of the model trajectory to the Sea-WiFS surface chlorophyll data in all three regions (Figure 4.7). The model now approximately reproduces the chlorophyll biomass and seasonality with cost function values of 1.7, 3.3 and 3.5 in the SAZ, PFZ and AZ respectively, compared with the initial parameterisation which gives cost functions of 2.9, 32.6 and 45.3 in the SAZ, PFZ and AZ respectively.

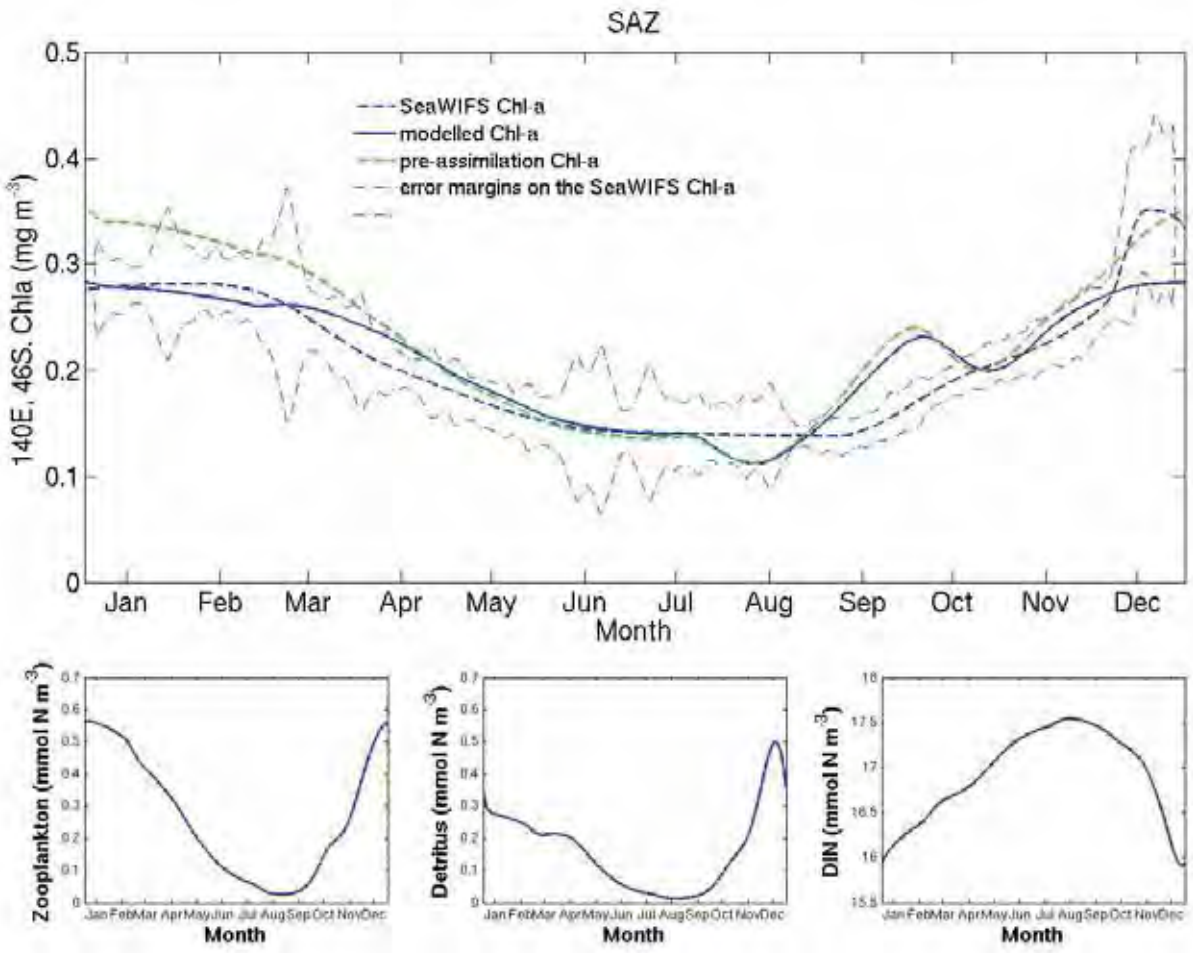

Figure 4.7a: Annual model trajectories at 140˚E, 46˚S after optimising phytoplankton maximum photosynthetic rate and photosynthetic efficiency parameters using simulated annealing. Panel A shows the modelled chlorophyll (solid line) and the chlorophyll data using 8-day SeaWIFS climatology (dashed line) with error margins calculated as the standard deviation of all observations within a 1x1 degree square around the optimisation site. The modelled chlorophyll using the original parameters is shown in a green dot-dash line. Panels B – D show the modelled zooplankton, detritus and DIN.

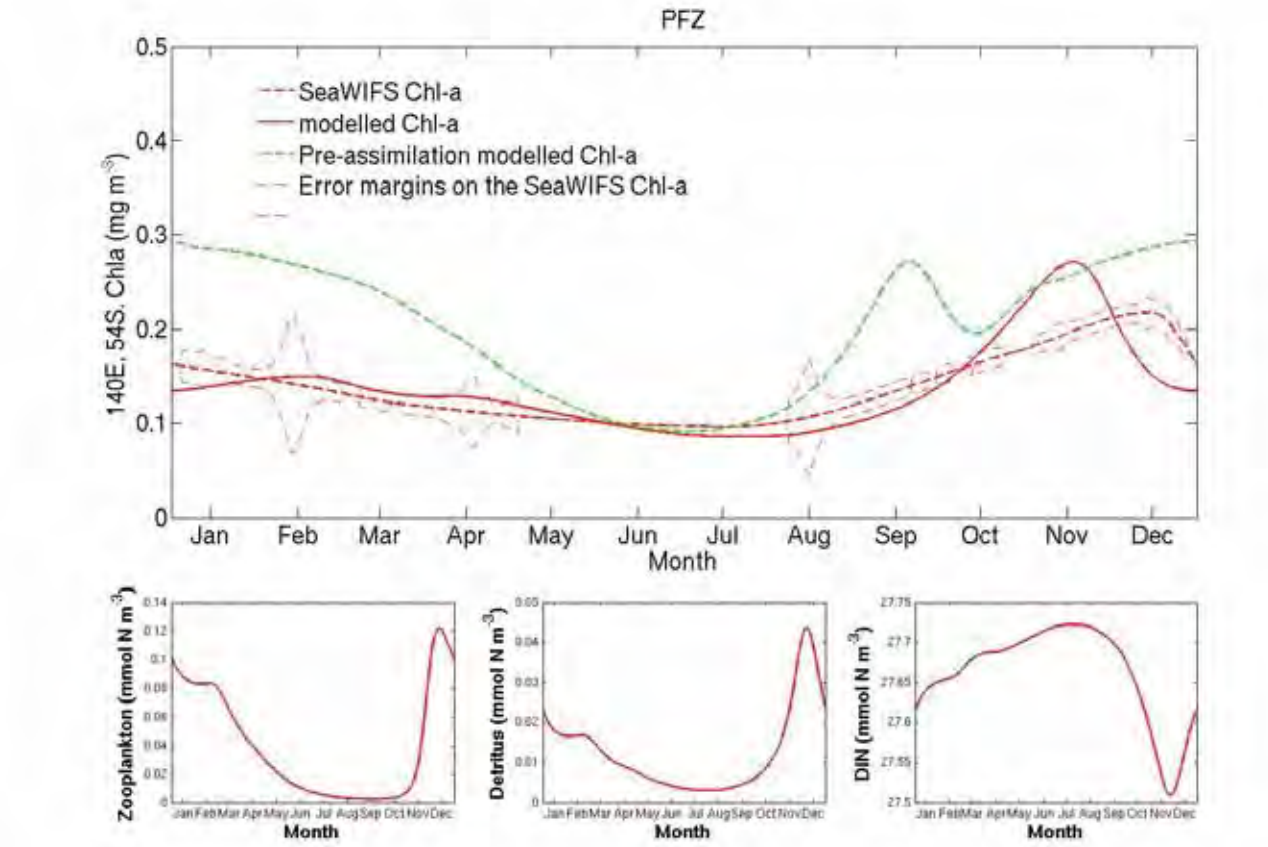

Figure 4.7b: Annual model trajectories as per Figure 7a for 140˚E, 54˚S.

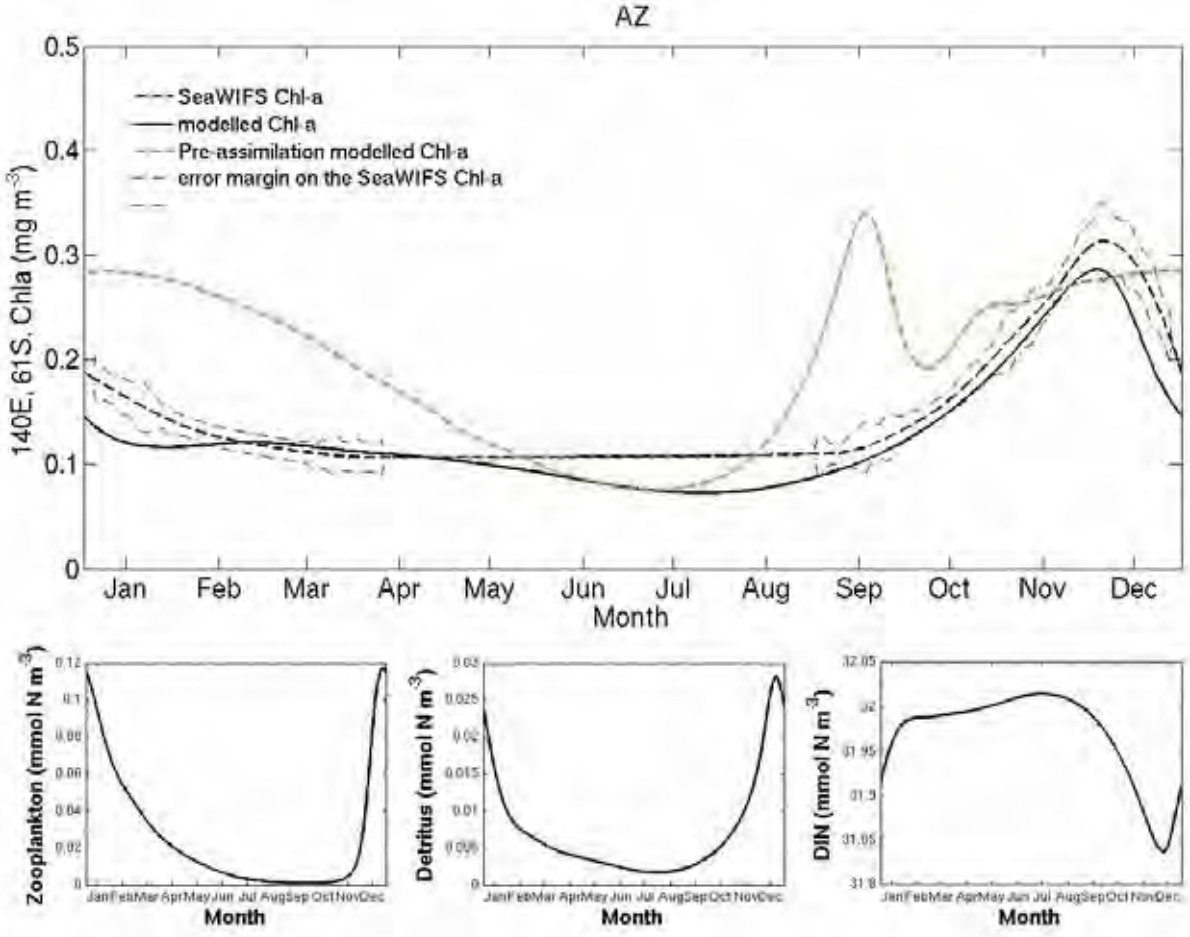

Figure 4.7c: Annual model trajectories as per Figure 7a for 140˚E, 61˚S.

The model predicted primary productivity (Figure 4.8) is considerably higher at 46˚S than at the higher latitude sites with maximum rates of 6.75 mmol N m^{-2} d^{-1} in austral spring (November), falling to near 1.0 mmol N m^{-2} d^{-1} through the winter months June – August. At 54˚S the maximum rates are on order of magnitude less, with spring production reaching only 0.69 mmol N m^{-2} d^{-1} and rates remaining very low throughout much of the year with a minimum of 0.14 mmol N m^{-2} d^{-1}. Productivity falls even further at 61˚S with a spring maximum of 0.34 mmol N m^{-2} d^{-1} and very low rates of 0.05 mmol N m^{-2} d^{-1} throughout most of the year.

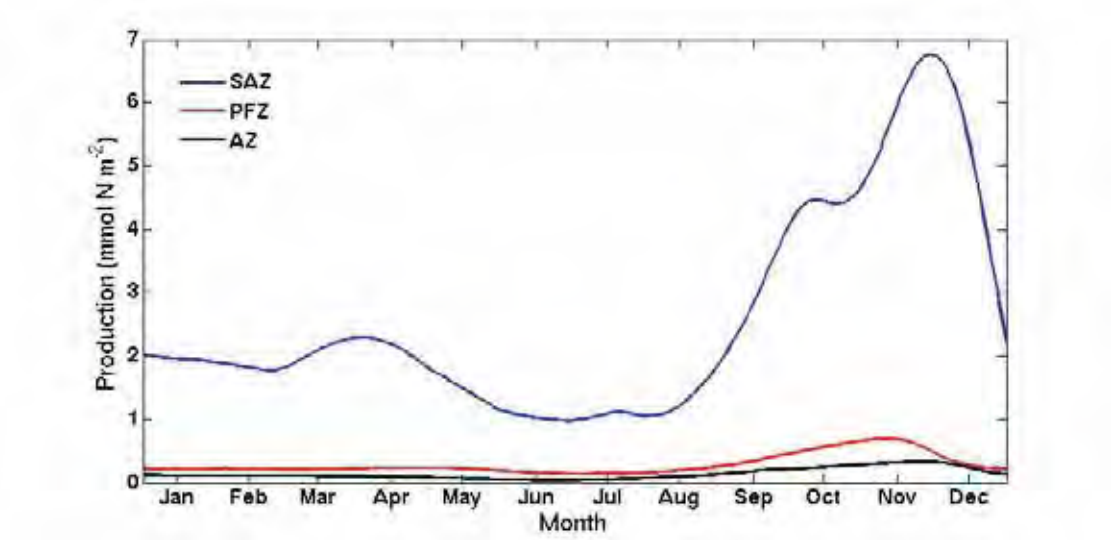

Figure 4.8: Model predicted annual primary productivity for the three sites. The annual mean production is 2.6 mmol N d^{-1} at the SAZ site (140˚E, 46˚S), shown in blue; 0.29 mmol N d^{-1} at the PFZ site (140˚E, 54˚S), shown in red; and 0.14 mmol N d^{-1} at the AZ site (140˚E, 61˚S), shown in black.

The model predicted *f*-ratios (Figure 4.9) indicate a system dominated by new production at all three sites with an annual mean of 0.57, 0.59 and 0.62 in the SAZ, PFZ and AZ respectively. The *f*-ratios vary seasonally with the maximum new production occurring in austral spring following the peak in MLD in September in both the PFZ and AZ (maximum *f*-ratios = 0.88 and 0.91 respectively), while seasonal *f*-ratios in the SAZ show a maximum in September as well as through the summer months January - March (maximum *f*-ratio = 0.90). The lowest *f*-ratios occur in May at the end of the summer period of shallow MLD's in the SAZ, compared with December in the PFZ and AZ at the start of a period of shallow MLD's indicating a peak in regenerated production occurs in different seasons each side of the SAF.

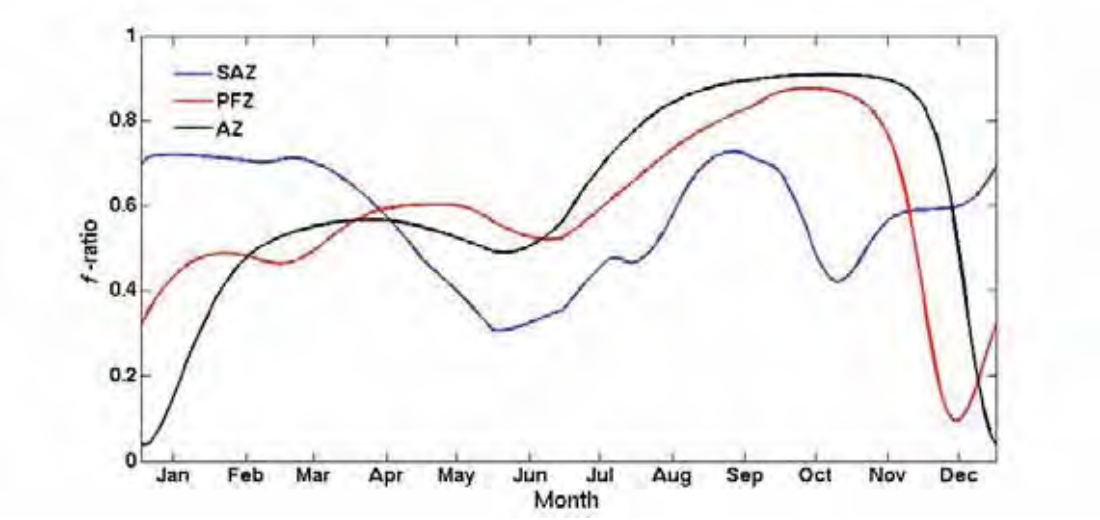

Figure 4.9: Model predicted annual *f*-ratio for the three sites. The annual mean *f*-ratio is 0.57 at the SAZ site (140E, 46˚S), shown in blue; 0.59 at the PFZ site (140˚E, 54˚S), shown in red; and 0.62 at the AZ site (140˚E, 61˚S), shown in black.

The fluxes of nitrogen between model compartments are shown in Figure 4.10. The optimisation results in highest zooplankton grazing in the SAZ, with 63% of phytoplankton primary production going to zooplankton biomass compared with the PFZ and AZ where 35% and 29% of the primary production is grazed by zooplankton

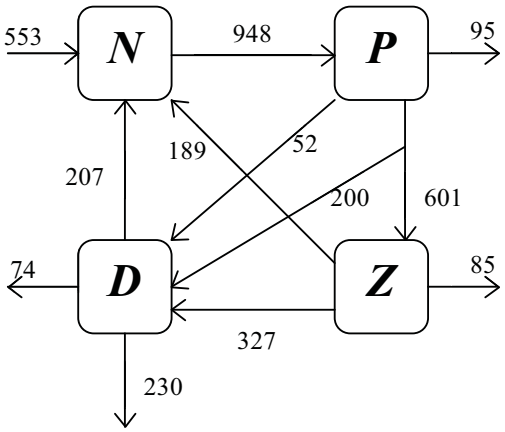

SAZ (140˚E, 46˚S)

Figure 4.10a: Annual flow of nitrogen between compartments of the model at the SAZ site (140˚E, 46˚S) using the optimised phytoplankton maximum photosynthetic rate and photosynthetic efficiency parameters. Units are mmol $m^{-2}yr^{-1}$. The external arrows represent the entrainment and detrainment of the various components in and from the mixed layer.

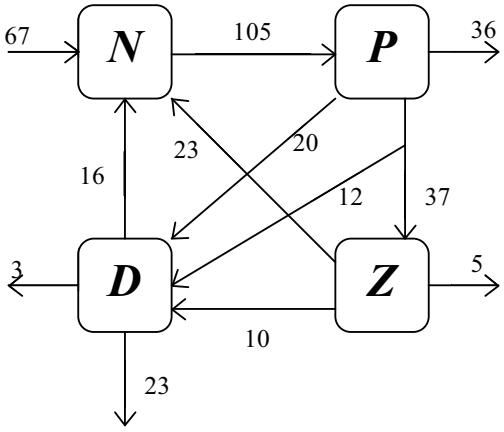

PFZ (140˚E, 54˚S)

Figure 4.10b: Annual flow of nitrogen between compartments of the model as per Figure 10a for 140˚E, 54˚S.

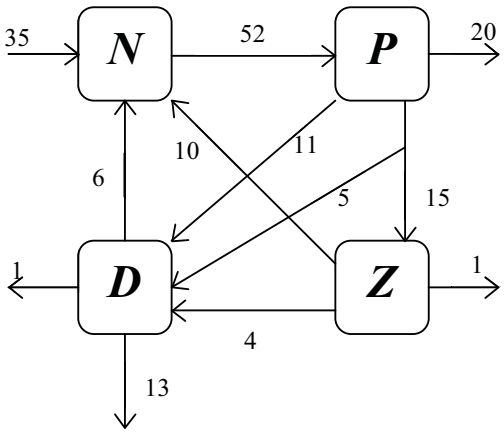

AZ (140˚E, 61˚S)

Figure 4.10c: Annual flow of nitrogen between compartments of the model as per Figure 10a for 140˚E, 61˚S.

4.4.2 Parameter estimates

The parameter estimates of maximum light saturated photosynthetic rate, P_{max}, and photosynthetic efficiency, α, are shown in Table 4.2. The optimisation results in a relatively low photosynthetic efficiency of 0.04 $(Wm^{-2}d)^{-1}$ in the SAZ, and much higher estimates in both the PFZ and AZ of 0.6 and 0.4 $(Wm^{-2}d)^{-1}$ respectively.

Parameter	OG99 Parameter value	140°E, 46°S	140°E, 54°S	140°E, 61°S
α	0.025 ± 0.1	0.044 ± 0.0004	0.60 ± 0.0082	0.35 ± 0.0073
a	0.6 ± 0.1	0.40 ± 0.0115	0.03 ± 0.00009	0.04 ± 0.00003
b	1.066 ± 0.01	1.043 ± 0.0023	1.176 ± 0.0004	1.089 ± 0.0003
P_{max}		0.63	0.06	0.04
f-ratio		0.57	0.59	0.62

Table 4.2: Parameter values after optimisation at the SAZ site (140°E, 46°S), the PFZ site (140°E, 54°S) and the AZ site (140°E, 61°S) in which photosynthetic efficiency, α, and maximum light saturated photosynthesis rate, $P_{max} = a \cdot b^T$ were optimised.

Despite lower photosynthetic efficiency the optimisation results in higher algal maximum growth rates in the SAZ with estimates of P_{max} being $0.63\,d^{-1}$, $0.06\,d^{-1}$ and $0.04\,d^{-1}$ in the SAZ, PFZ and AZ respectively.

4.4.3 Physical forcing interchange optimisations

- Light interchange optimisation

The average daily surface radiation varies between 43 and $239\,Wm^{-2}$ at 46°S compared with 6 to 216 Wm^{-2} at 61°S (Figure 4.5). The interchange in light fields results in a ten fold increase in the optimised value of α in the SAZ with a relatively high estimate of

0.42 $(Wm^{-2}d)^{-1}$ and a 50% reduction in the optimised value of α in the AZ with a relatively low estimate of 0.18 $(Wm^{-2}d)^{-1}$, showing the photosynthetic efficiency is partly determined by irradiance. The modified forcing does not result in a large change in the optimised values for P_{max}, which remain high in the SAZ (0.47) and low in the AZ (0.04) (Table 4.3).

- *MLD interchange optimisation*

The SAZ is a region characterised by deep mixed layers with the MLD forcing data ranging between 18 and 381 m compared to the AZ where the MLD data ranges between 65 and 114 m. The interchange of MLD forcing results in a 60% reduction in the optimised value of α in the SAZ resulting in an estimate of 0.018 $(Wm^{-2}d)^{-1}$, and a 260% increase of α in the AZ, giving an estimate of 0.92 $(Wm^{-2}d)^{-1}$. This indicates that the photosynthetic efficiency is partly determined by the MLD, an effect of deeper mixing waters reducing the effective light level to which the phytoplankton are exposed. The MLD forcing does not have a substantial effect on the optimised estimates of P_{max}, which remain high in the SAZ (0.56) and low in the AZ (0.09) (Table 4.3).

- *Temperature interchange optimisation*

The estimate of P_{max} is determined by the growth rate parameters *a* and *b*, with *b* being raised to the power of *T* ($P_{max} = a \cdot b^T$). The SST drops considerably with increasing latitude, with the SAZ SST data ranging between 9 and 12 °C while the AZ SST maximum is 3 °C and falls to a low of -1 °C (Figure 4.5). The optimisations in which the SST forcing is interchanged do not result in a considerable change to the optimised values of α or P_{max} (Table 4.3).

The differences in the optimised values of P_{max} giving higher maximum light saturated photosynthetic rates in the SAZ compared with the PFZ and AZ are not reversed in any of the experiments in which forcing is interchanged. The differences occur due to

processes not explicitly represented by the model or its forcing, such as macro/micronutrient availability.

Parameter	140° E, 46° S	140° E, 61°
light interchange optimisation		
α	0.42	0.18
P_{max}	0.47	0.04
temperature interchange optimisation		
α	0.05	0.34
P_{max}	0.57	0.04
MLD interchange optimisation		
α	0.02	0.92
P_{max}	0.56	0.09

Table 4.3: Parameter values after photosynthetic efficiency, α, and maximum light saturated photosynthesis rate, $P_{max} = a \cdot b^T$ were optimised with the forcing data for the SAZ site interchanged with the forcing data for the AZ site. None of these optimisations result in a high estimate of P_{max} at the AZ site or a low estimate of P_{max} at the SAZ site. Only the optimisation in which light is swapped results in both a high estimate of α at the SAZ site and a lower estimate of α at the AZ site.

4.4.4 Parameter resolution

The singular values and associated singular vectors of the Hessian matrix show that maximum photosynthetic growth is more important in fitting the model trajectory to the chlorophyll data than photosynthetic efficiency, particularly in the PFZ and AZ where photosynthetic efficiency has negligible effect on the model solution (Figure 4.11).

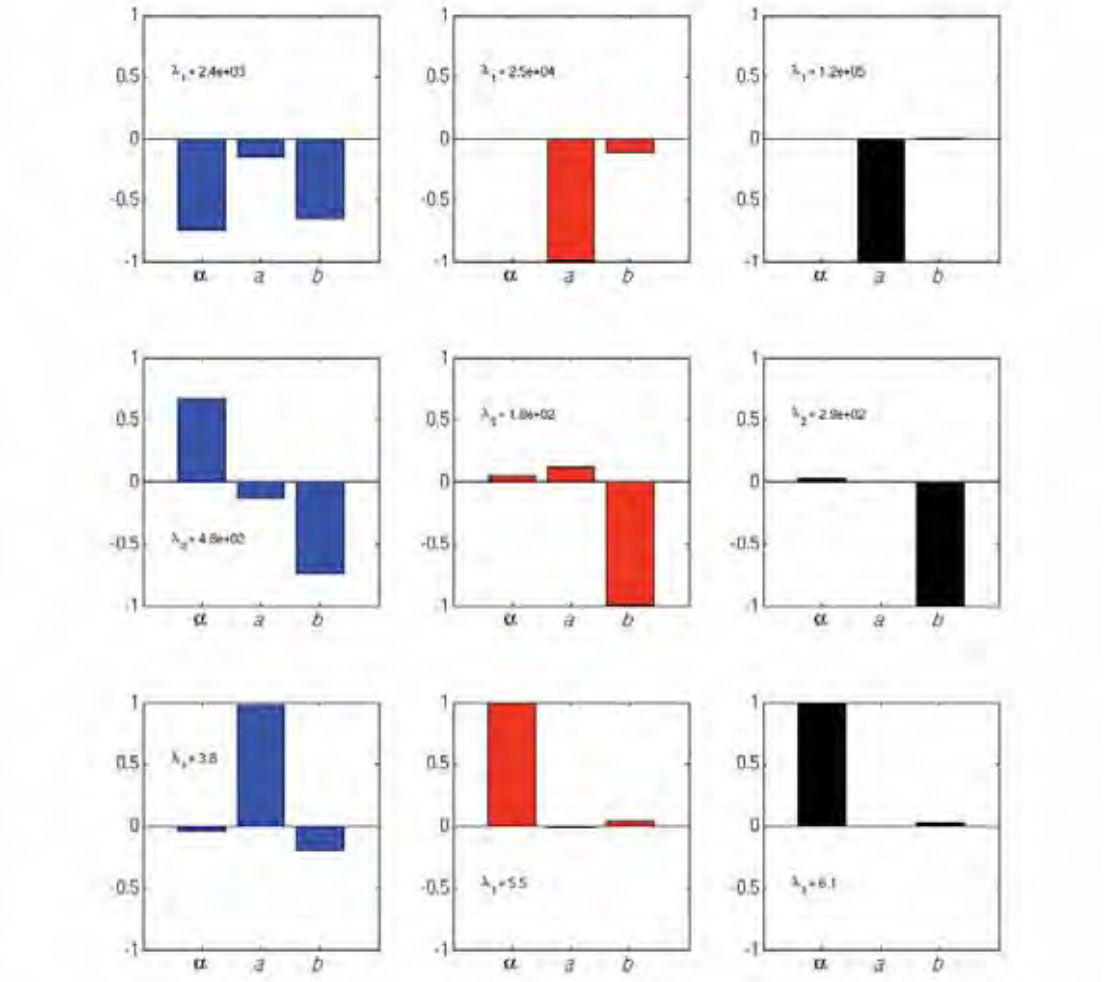

Figure 4.11: Parameter resolution for the optimisation experiment. The singular vectors λ_i , i=1:3, are shown in decreasing order of the magnitude of their associated singular values. As the magnitude of the singular values decreases so the parameters contributing to the associated singular vector decrease in their impact upon the model solution. The SAZ site (140° E, 46° S) is shown in blue, the PFZ site (140° E, 54° S) is shown in red and the AZ site (140° E, 61° S) is shown in black.

4.5 Discussion

4.5.1 Model performance: f-ratios, primary production and zooplankton grazing

The modelled *f*-ratios (ratio of nitrate based production to total production) from the optimisation in Section 4.4.1 are consistent with observational data from Savoye et al. (2004), who measured N-uptake and new production in the SAZ, PFZ and AZ in the Australian sector of the Southern Ocean in austral spring 2001. They found that new production decreased from SAZ (~49°S) to PFZ (~54°S) and then increased southward in the AZ (~61°S), where they measured the highest rates of new production on the transect. Equally in austral spring (November-December) our modelled *f*-ratios are high in the SAZ, lower in the PFZ and highest in the AZ. They found highly variable *f*-ratios in the SAZ shifting from 0.38 to 0.82 within one month, and *f*-ratios of 0.59 and 0.61 in the PFZ and AZ respectively, which are approximately the same as our modelled mean *f*-ratios of 0.57, 0.59 and 0.62 in the SAZ, PFZ and AZ respectively. Cavagna et al. (in press) measured regenerated production and new production in the SAZ and PFZ in the Australian sector of the Southern Ocean in mid-summer 2007 and found generally low *f*-ratios, mostly < 0.3 apart from one estimate of 0.5 in the SAZ. This is generally consistent with our summer *f*-ratio estimates of 0.1 – 0.4 in the PFZ and AZ and ~0.7 in the SAZ.

The modelled production is generally consistent with observational data which indicates decreasing primary production from the SAZ to the PFZ south of Australia (Lourey and Trull, 2001). Westwood et al., (in press) estimated gross primary productivity rates integrated over the euphotic layer in the Australian sector of the SAZ in austral summer 2007 using ^{14}C-incubations. They found higher production in the SAZ than the PFZ with measurements of 1304 ± 300 and 749 ± 543 mg C m^2 d^{-1} in the SAZ at 46°S and 47°S respectively, and 475 ± 168 mg C m^2 d^{-1} in the PFZ at 54°S. Over the same period Cavagna et al (in press) calculated daily gross primary production (integrated over the euphotic zone) from ^{13}C-incubations and found 66 ± 31 and 49 ± 14 mmol C m^2 d^{-1} in the SAZ and 35 ± 2 mmol C m^2 d^{-1} in the PFZ m^{-2} d^{-1} in the PFZ. Savoye et al (2004)

found much lower productivity rates in austral spring 2001 using ^{15}N and ^{13}C-incubations, with estimated production rates of 1.76 mmol N m^{-2} d^{-1} in the SAZ, 1.5 mmol N m^{-2} d^{-1} in the PFZ. Comparatively our model estimates of primary production in the SAZ are reasonable (496.1 mg C m^2 d^{-1} in austral spring) but the modelled production is rather low in the PFZ and AZ (spring values of 50.7 and 25.0 mg C m^2 d^{-1} respectively).

Pearce et al. (in press) measured the average percentage of primary production grazed by zooplankton in the Australian sector of the Southern Ocean in mid summer 2007. They found grazing rates were highest where concentrations of microzooplankton were also highest, with 82% (± 38%) and 67% (± 12%) of primary production being removed at two stations in the SAZ and 47% (± 10%) removed in the PFZ. Pakhomov and Froneman (2004) measured zooplankton grazing in the Atlantic sector of the Southern Ocean in austral summer 1997. They found 22-33% of daily primary production was grazed by zooplankton in the PFZ ~50°S and lower zooplankton grazing removing <10% of primary production further south ~60°S. The model solution of decreasing zooplankton grazing with increasing latitude is consistent with these observational studies and this result indicates that grazing is not the cause of low phytoplankton biomass and production in the PFZ and AZ compared with the SAZ.

The modelled *f*-ratios, primary production and grazing show that the parameter estimates give a biologically plausible solution as well as a good fit to the chlorophyll data. However there is an under-estimation of primary production in the PFZ and AZ suggesting there may be a limitation to phytoplankton growth south of the Sub-Antarctic Front which is not captured explicitly by the model.

4.5.2 Parameter estimates –photosynthetic efficiency

Typically photosynthetic efficiency increases as irradiance declines (Douglas et al., 2003). The parameter optimisation finds a ten fold higher photosynthetic efficiency, α, in the lower light environments of the PFZ and AZ compared with the SAZ (Table 4.2).

In the original parameterisation of the full model Fasham et al. (1990) set the photosynthetic efficiency parameter, α, to $0.025\,(\mathrm{Wm^{-2}d})^{-1}$ in order to fit the model output to annual cycles of physical and biological data for Bermuda Station "S" at ~32°N, using MLD and solar radiation forcing fields. Fasham and Evans (1995) subsequently optimised the model parameters for the JGOFS Station at 47°N and found higher estimates of, α, of 0.164 and $0.222\,(\mathrm{Wm^{-2}d})^{-1}$. Our SAZ (46°S) estimate of 0.04 $(\mathrm{Wm^{-2}d})^{-1}$ is similar to the estimate of $0.035\,(\mathrm{Wm^{-2}d})^{-1}$ found in the optimisation experiment by Evans (1999) for NABE site (North Atlantic Bloom Experiment) at 47°N. Parameter optimisations performed at the higher latitude station OWS-INDIA at 59°N by Hurt and Armstrong resulted in a very high estimate of α of $0.93\,(\mathrm{Wm^{-2}d})^{-1}$ which they attributed to the low light conditions.

These independently optimised estimates of α show an increase in photosynthetic efficiency when going from the SAZ to the PFZ. These findings are consistent with field analyses of natural marine phytoplankton assemblages which show an increase in photosynthetic efficiency with latitude (Harrison and Platt, 1986), and our results for α which are 0.044 $(\mathrm{Wm^{-2}d})^{-1}$ in the SAZ $0.60\,(\mathrm{Wm^{-2}d})^{-1}$ in the PFZ and $0.35\,(\mathrm{Wm^{-2}d})^{-1}$ in the AZ.

Limited information on in situ measurements of photosynthetic parameters of phytoplankton in the Southern Ocean has been published. Estimates of photosynthetic efficiency measured by Westwood et al. (in press) found $\alpha = 0.034 \pm 0.013$ to 0.057 ± 0.021 mg C mg chl a^{-1} $\mathrm{h^{-1}}$ $(\mu\mathrm{mol\ m^{-2}\ s^{-1}})^{-1}$ in the SAZ which results in a range between 0.05 and $0.17\,(\mathrm{Wm^{-2}d})^{-1}$ suggesting our estimates in the SAZ are reasonable, however our PFZ and AZ estimates for α are somewhat higher than generally found in in-situ studies in the region (Griffiths, F.B., personal communication).

The optimisations in which the forcing data was interchanged between the SAZ and AZ showed the estimate of α is highly dependent on available light, with the optimised value

being partly determined by the surface solar radiation data and partly determined by the MLD data. The photosynthetic efficiency term , α , enters the model equations in multiplicative combination with the term *I(z,t)* - the photosynthetically active radiation as a function of depth below the surface of the water, which is itself a function of the surface radiation forcing data, the MLD and the attenuation of sunlight by seawater.

The photosynthetically active radiation in the mixed layer is shown for the three sites in Figure 4.12. The surface radiation and mixed layer depth data are shown in Figure 4.5. In the summer months of January – March the SAZ has the shallowest MLD, combined with the highest surface sunlight, this results in considerably higher mean mixed layer light levels in summer, up to $73\,(\mathrm{Wm^{-2}d})^{-1}$, compared with the PFZ and AZ summer mean mixed layer light levels of up to 52 and $56\,(\mathrm{Wm^{-2}d})^{-1}$ respectively. In September when the SAZ MLD reaches its maximum the mean light in the mixed layer water column becomes lower than both the PFZ and AZ despite the higher surface sunlight. The AZ has a shallower MLD throughout the year than the PFZ. The shallow depths compensate for lower surface sunlight and the mean light intensity throughout spring and summer is actually higher than in the PFZ. The annual mean mixed layer light is 22, 18 and $19\,(\mathrm{Wm^{-2}d})^{-1}$ in the SAZ, PFZ and AZ respectively.

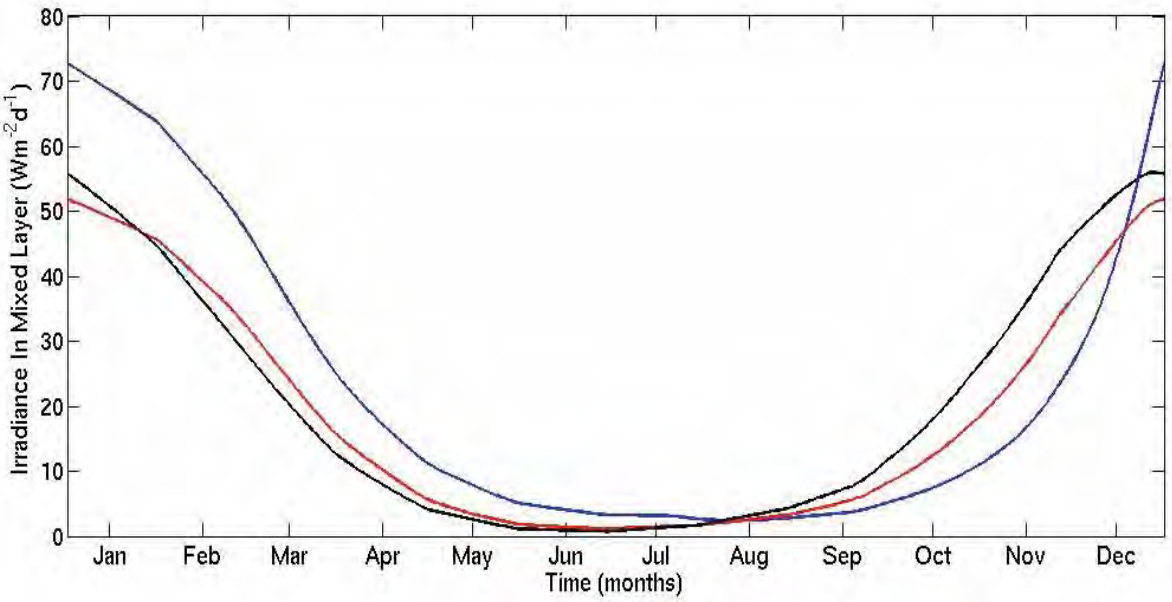

Figure 4.12: Photosynthetically available radiation in the water column of the mixed layer. The SAZ site (140°E, 46°S) is shown in blue, the PFZ site (140°E, 54°S) is shown in red and the AZ site (140°E, 61°S) is shown in black.

Under these conditions phytoplankton adaptation to low light should more notable in the PFZ and AZ than the SAZ, and greatest in the PFZ. Accordingly Boyd et al. (2001) found increased light harvesting requirements of cells in the PFZ at 54°S compared with those in the SAZ at 47°S in ship board experiments in the Australian sector of the Southern Ocean. Our estimates of α are in good agreement with notably higher estimates in the PFZ and AZ than the SAZ and the highest estimate in the PFZ (Table 4.2).

The differences seen between the SAZ, PFZ and AZ in the model estimates of photosynthetic efficiency and the differing light availability due to latitude and thickness of the mixed layer largely offset one another and therefore are not the cause of low phytoplankton biomass and production in the PFZ and AZ compared with the SAZ in this model.

4.5.3 Parameter estimates – maximum photosynthetic growth

The parameter estimates result in the highest maximum growth rates in the SAZ. The growth rate is considerably lower in the PFZ and declines even further in the AZ (Table 4.2).

The maximum light saturated growth, P_{max}, is based on the temperature dependent formula given by Eppley (1972), who noted that there are two general trends to growth rates: There is a gradual and exponential increase in growth with temperature up to about 40°C; growth rates below this temperature fall within an envelope and it is possible to plot a smooth curve showing the maximum expected value - the upper limit on the growth rate at a given temperature. The upper limit for $P_{max} = a \cdot b^T$ described by Eppley takes the parameters a = 0.8511 and b = 1.0654, which gives values of P_{max} between 0.8 and 1.8 d^{-1} for temperatures between -1 and 12°C - the range of temperatures covering the three optimisation sites in this study.

The maximum growth rate curve (Eppley, 1972) is plotted against temperature in Figure 4.13, along with the optimised growth rate curves for the three experiment sites. The PFZ and AZ growth rates show little temperature dependence and fall far below the maximum rates indicated by Eppley's formula, the SAZ growth rates also fall below the maximum however there is a clear temperature dependance. The maximum growth values given by Eppley are not expected to be realised under conditions of nutrient limitation or light limitation, where growth rates show little or no temperature dependence (Eppley, 1972). This indicates that there is either nutrient or light limitation, or a combination of both over the entire region and additional limitation south of the SAF. However we have already shown that light mostly affects the initial slope of the P-I curve, not the maximum growth rate, and the region is nutrient replete with respect to nitrogen.

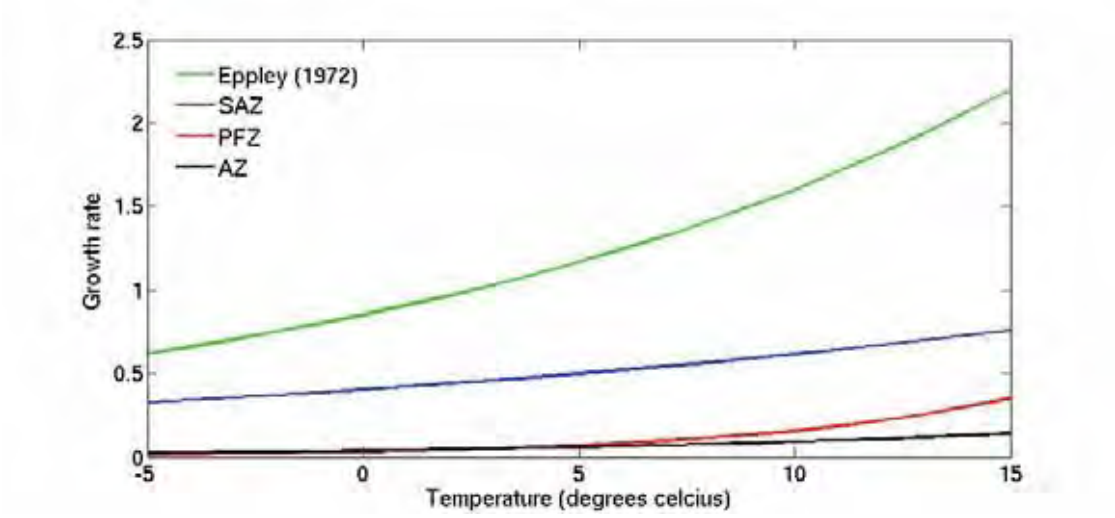

Figure 4.13: Variation in the maximum growth rate with temperature, the SAZ site (140°E, 46°S) is shown in blue, the PFZ site (140°E, 54°S) is shown in red and the AZ site (140°E, 61°S) is shown in black. The maximum growth rate curve defined by Eppley (1972) is shown in green.

In the initial parameterisation used by OG99 (Table 4.1) P_{max} takes a value of 1.1, 0.8 and $0.6\,d^{-1}$ for the mean temperatures in the SAZ, PFZ and AZ respectively. Schartau and Oschlies (2003a) subsequently optimised the model parameters from OG99 to simultaneously fit data from BATS, NABE and OWS-INDIA, their parameters result in values of P_{max} of 0.5, 0.4 and $0.3\,d^{-1}$ for the mean temperatures in the SAZ, PFZ and AZ respectively. Comparatively our estimates of maximum growth in the PFZ and AZ are very low, and indeed lower than would be expected from in situ estimates in the region (Griffiths, F.B., personal communication). This further indicates that there is a process not captured explicitly in the model which limits phytoplankton growth in the AZ and PFZ.

None of the optimisations in which forcing data was interchanged between regions resulted in a high estimate of growth in the AZ; the differences occur due to processes not explicitly represented by the model or its forcing. We therefore attribute the low estimates of P_{max} in the AZ and PFZ to limited supply of micronutrients. Hutchins et al.,

(2001) suggest that iron is the proximate limiting nutrient for chlorophyll production in the Australian sector of the Southern Ocean with silica playing a secondary role.

In situ measurements of dissolved iron concentrations in the Australian sector of the Southern Ocean from Sedwick et al. (2008) and Lannuzel et al. (in press) indicate a general north to south decrease. Sedwick et al. (2008) found concentrations of more than 0.3nM at ~140°E, 46°S, 0.08-0.12 at ~140°E, 54°S and uniformly low concentrations of less than 0.1nM south of the PF ~140°E, 61°S. Lannuzel et al. (in press) found dissolved iron concentrations of 0.27 ± 0.04 nmol/l at ~140°E, 46°S and 0.22 ± 0.02 nmol/l at ~146°E, 54°S. On the contrary, measurements of silic acid in the Southern Ocean show an increase in concentrations with increasing latitude ranging from <5 μM in the SAZ to >60 μM in the AZ (Coale et al., 2004). Therefore the most likely cause of the low estimates of P_{max} in the AZ and PFZ is limited supply of iron.

4.5.4 Parameter resolution

The error analysis reveals that for this model P_{max} is more important in fitting the model to the chlorophyll data than α (Figure 4.11). This is consistent with the findings of Galbraith et al. (2010) who similarly found the effect of light saturated photosynthesis rates negated the importance of photosynthetic efficiency particularly in the Southern Ocean, they suggest that because iron limitation reduces the maximum photosynthetic growth, the utility of photons would decrease under iron limitation, making light availability less important. Moore et al. (2007) studied iron-light interactions in the PFZ and found that in low-iron waters irradiance had little influence on phytoplankton biomass accumulation.

4.6 Conclusion

The HNLC regime of the Southern Ocean is potentially important in controlling CO_2 fluxes between the ocean and atmosphere. The causes of HNLC conditions has been the subject of much debate (Banse, 1996; Mitchell et al., 1991) with much of the attention focussing on the availability of iron (Coale et al., 1996; Boyd et al., 2000).

The phytoplankton photosynthetic parameters of a simple NPZD model have been optimised at three sites in the Australian sector of the Southern Ocean, spanning the Sub-Antarctic Zone, the Polar Frontal Zone and the Antarctic Zone. The optimised parameters give a good fit to Sea-WiFS surface chlorophyll data and result in realistic ecosystem dynamics as determined by the fluxes of nitrogen between model compartments which give *f*-ratios, primary productivity, and grazing estimates generally consistent with in-situ estimates.

The optimisations indicate that phytoplankton growth rates in the Polar Frontal Zone and Antarctic Zone are limited by some process not explicitly included in this model, with iron availability being the most likely candidate.

Photosynthetic efficiency is primarily determined by light availability in the mixed layer. The effect of changes in algal growth rates far outweighs the effect of changes in photosynthetic efficiency on the biological model solution, and thus differences to the ecosystem functioning caused by iron availability are of greater consequence than differences in surface irradiance and mixed layer depth.

Based on these optimisations we support the contention that micronutrient availability, such as iron, is the primary cause of the HNLC conditions in the Australian sector of the Southern Ocean.

Under future climate change scenarios the frequency and scale of aeolian dust emissions (e.g. from Australia) are predicted to increase (IPCC, 2007), and high latitude oceanic

stratification is predicted to increase (Matear and Hirst, 2003; Sarmiento et al., 2004). Atmospheric deposition is the dominant source of iron in the SAZ and vertical advection is relatively more important in the PFZ (Bowie et al. 2009). Based on the results of the optimisation experiments presented here this has the potential to impact future oceanic productivity by enhancing the differences in growth rates observed either side of the STF south of Australia, increasing the maximum phytoplankton growth rates in the SAZ and further reducing them in the PFZ and AZ. While increased stratification may increase available light and therefore phytoplankton growth in the mixed layer our sensitivity analysis indicates that this effect would be negated by a reduction in iron supply.

Chapter 5:

General Discussion

5.1 Summary

The work in this thesis contributes to scientific understanding of Southern Ocean plankton dynamics through biogeochemical modelling. The performance of an ecosystem model with respect to observations of surface chlorophyll has been improved in a number of data assimilation experiments. The results of our data assimilation experiments facilitate quantitative understanding of the factors determining zonal and meridional variability of phytoplankton biomass in the Southern Ocean.

A four component NPZD model was used for the experiments. The model configuration has been demonstrated to give a good representation of phytoplankton distributions in the North Atlantic by Schartau and Oschlies (2003a,b), however the parameters they used results in a poor fit to the annual cycle of phytoplankton biomass in the Southern Ocean. To improve the model performance the parameters were optimised by assimilating Sea-WiFS surface chlorophll data. Many optimisation techniques exist, and at present there is no consensus on which method is the most efficient and robust. Two stochastic optimisation algorithms, simulated annealing and the Metropolis-Hastings algorithm, were compared.

5.1.1 Simulated Annealing

Twin experiments suggest that simulated annealing would be favourable as a standard method of assimilating biological data into marine ecosystem models. The algorithm found the global minimum of the cost function, and the true parameters were recovered when assimilating synthetic observations of phytoplankton only. Calculation of the Hessian matrix provided easy analysis of the expected errors in the parameter estimates. The singular vectors of the Hessian matrix provided comprehensible information on how well the individual model parameters fit the data and also relationships between the parameter estimates.

Experiments assimilating Sea-WiFS surface chlorophyll data demonstrated that simulated annealing provides robust results, improving the model fit to chlorophyll observations

and providing parameter estimates generally consistent with estimates from a number of data sources that had not been used in the assimilation process. In our experiments the highly sensitive parameters were the maximum growth rate of phytoplankton, phytoplankton loss rate and zooplankton excretion rate. The least sensitive parameters were the detrital sinking rate and the half saturation constant of DIN uptake rate. Removing the least sensitive parameters from the optimisation can be advantageous as error propagation is reduced with little effect on how the model solution fits the data (Matear, 2004). Accordingly experiments assimilating Sea-WiFS data while optimising only a subset of parameters resulted in good agreement of the annual model trajectory with the surface chlorophyll observations, allowing conclusions to be drawn while isolating aspects of the model.

Many of the well constrained parameters were correlated with one another and could not be estimated independently. Validation of results with independent data is essential in any data assimilation experiment particularly when correlations among parameters result in non unique estimates and non linearity's mean convergence to a local, rather than global, minimum is possible. A number of ship based observations and experiments were used to assist the analysis of our results. Still more credibility would be afforded to our results if there were seasonal atmospheric iron deposition data, time series data, mooring data, and long term information on rates used as model parameters, such as the maximum growth of phytoplankton, and on mechanisms not explicitly optimised, such as the *f*-ratio. The estimated errors showed spatial variability both zonaly and meridionally emphasising the need for prudence when applying specific model parameters to multiple locations, and the need for increased observations spatially as well as temporally.

5.1.2 The Metropolis-Hastings algorithm

The Metropolis Hastings algorithm was effective for optimising only uncorrelated and well constrained parameters. Accurate estimates were obtained for only three parameters. This is similar to recent studies by Zhao and Lu (2009) and Xu et al. (2008). Both studies found 5 uncorrelated parameters in a model very similar to the one used here, using the

adjoint method. The difficulty in implementing the Metropolis-Hastings algorithm due to parameter correlations discouraged use of the method for experiments assimilating SeaWiFS data. However it has been demonstrated by Friedrichs et al. (2006; 2007) that optimising poorly constrained and correlated model parameters results in degraded predictive ability. Friedrichs et al. (2007) found that in parameter optimisations of a complex 24 component model the model ability to reproduce validation data was greatly improved if they optimised only 3 parameters rather than 14. Hence we would not rule out future experiments with the Metropolis-Hastings algorithm since the error estimation using this method is more mathematically stringent as it does not rely on linear approximations.

5.1.3 Phytoplankton dynamics in the Southern Ocean

Zonal variation in phytoplankton biomass south of Tasmania was examined by optimising the model parameters at two distinct locations in the Sub-Antarctic Zone. Several hypotheses were presented as to the cause of the differences in observed surface chlorophyll concentrations (Griffiths et al., in press). The optimal parameters and their effect on the modelled ecosystem functioning were compared between the two locations. The primary cause of meridional variation in phytoplankton biomass south of Australia was also considered. Bio-availability of iron was the principal hypothesis for the cause of the meridional differences in observed surface chlorophyll concentrations. The most reliable physiological indicator of iron availability was isolated by optimising the model parameters pertaining to the growth of phytoplankton. The optimisations were performed at three sites spanning the Sub-Antarctic Zone, Polar Frontal Zone and Antarctic Zone.

Our optimisations attest that an interplay of factors controls primary productivity in the Southern Ocean with bio-availability of iron limiting production, particularly south of the Sub-Antarctic Front and bio-availability of iron altering species composition within the Sub-Antarctic Zone. The overall picture is of an underlying community of small phytoplankton with the existence of a regeneration loop at all sites (mean annual *f*-ratios between 0.57 and 0.7 over all sites), and an additional diatom based food chain of varying

efficacy over the region. The regeneration loop is strongest in the waters south east of Tasmania (*f*-ratio of 0.57 at P3). The smaller phytoplankton thrive here since mixed layer ammonium concentrations are relatively high (0.47 μM; Cavagna et al., in press) and there is no iron limitation (dFe = 0.48 ± 0.10 nmol/l; Lannuzel et al., in press), but silicate concentrations are very low (<1 μM; Cavagna et al., in press).

South west of Tasmania the euphotic zone waters are nitrate replete but low in ammonium (0.05 – 0.45 μM; Cavagna et al., in press). Under these conditions production becomes dominated by larger phytoplankton (diatoms) (*f*-ratio of 0.7 at P1). However diatom growth is more effected by the concentration of iron which is lower here (dFe = 0.27 ± 0.04 nmol/l; Lannuzel et al., in press) and so summer phytoplankton concentrations are lower than further east.

At P3 the optimisation results in satisfactory estimates of recycling rates but underestimates primary production, zooplankton biomass and zooplankton grazing. Based on other studies (Mongin et al., in press) we hypothesise that seasonal variability in atmospheric iron deposition plays an important role in the seasonal evolution of phytoplankton and produces the late summer maximum in phytoplankton. An ecosystem model that includes seasonal variations in atmospheric deposition of iron may improve our modelling results at P3.

South of the Sub-Antarctic Front the phytoplankton community is dominated by the iron sensitive diatoms (Sohrin et al., 2000). They are adapted to the light conditions with increased light-harvesting characteristics compared to the SAZ phytoplankton (α = 0.044 in the SAZ, 0.6 in the PFZ and 0.35 in the AZ). This does not help to increase overall growth rate, production and biomass which is bounded by iron limitation (P_{max} = 0.63 in the SAZ, 0.06 in the PFZ and 0.04 in the AZ) since iron concentrations decrease with increasing latitude in this region (Sedwick et al., 2008).

Our experiments suggest that differences in observed chlorophyll result from biological differences rather than physical forcing. This implies that this model is not suitable for

coupling to a 3D circulation model to make basin scale estimates of biogeochemical processes and ecosystem functioning in the Southern Ocean. Our conclusions are drawn from optimisation experiments performed in a small number of locations south of Australia. It would be of interest to perform a number of individual optimisations, over a smaller spatial resolution, spanning the entire Southern Ocean. This would provide a comprehensive map of iron limitation and elucidate basic community composition in the Southern Ocean.

5.2 Discussion of model parameter estimates and validation data

The results presented assume the model configuration to be a truthful representation of the marine ecosystem. We have greatly simplified a complex reality to allow investigation of the core processes. The roles of iron, silica and ammonium production are discussed, none of which are explicitly included in the model. The use of a more complex model to research these ideas further may be intuitive, however presently there is barely enough data to assimilate and independently validate even this very simple model. There is a pressing need for observationalists and modellers to work together to collect comprehensive data sets to constrain biogeochemical models for the Southern Ocean.

In the Sub-Antarctic Zone accurate parameterisations of regenerated production are crucial to modelling phytoplankton biomass, and characterising the ecosystem functioning. In-situ estimates of atmospheric iron deposition, primary production, new production and *f*-ratios are essential for validating the model output. On a basin scale accurate parameterisations of maximum growth rates of phytoplankton are essential to modelling phytoplankton biomass in the Southern Ocean.

- *regenerated production*

Ammonia excreted by zooplankton may be an important source of nitrogen requirements for phytoplankton in the Sub-Antarctic Zone. Our results in Section 3.5.3 suggest that ammonia excreted by zooplankton provides 14 and 23% of the requirements of primary

production at P1 and P3 respectively (Figure 3.8b). Our error analysis in Section 3.5.2 shows that zooplankton excretion is one of the most sensitive model parameters, and therefore it is essential to have a reasonable estimate of this parameter to realistically model phytoplankton distributions. Field measurements of zooplankton excretion rates are required to support model predictions.

The error analysis in Section 3.5.2 shows that the phytoplankton loss rate representing an implicit description of the bacterial loop (μ_p) is also a very sensitive model parameter. This parameter was optimised to near zero at stations P1 and P3 indicating that the model results were notably improved by removing this phytoplankton loss rate (one of two phytoplankton mortality terms) from the model. This parameter was included in the model by SO03 to represent the fraction of phytoplankton's nitrogen rapidly remineralised in the euphotic zone. They hypothesised that this flux was important in their experiments at the oligotrophic BATS site. The role of bacterial loop is more significant in oligotrophic waters than eutrophic waters (Sarmiento and Gruber, 2006). Hoppe et al. (2002) found the ratio between bacterial production and primary production changed significantly from up to 40% in the equatorial Atlantic to 1-5% in the high latitude South Atlantic (Hoppe et al., 2002, Figure 2). We found that bacterial production represents an insignificant percentage of primary production in the SAZ and it was important to reduce the parameter value from the SO03 estimate of 0.04 d^{-1} to effectively zero in order to realistically model the annual cycle of phytoplankton.

It is important to note that this parameter estimate can not be uniquely determined. The estimate is correlated to the estimate of zooplankton excretion at both station P1 and station P3 and additionally to the mortality of zooplankton and the maximum growth rate of phytoplankton at station P1. Therefore in-situ measurements of ammonia excreted by bacteria as well as ammonia excreted by zooplankton would be beneficial in validating the regenerated production predicted by the model, and also our decision to remove this flux of the model for the experiments in Chapter 4.

- *phytoplankton growth*

The maximum growth rate of phytoplankton is a key process to modelling annual phytoplankton cycles in the Australian sector of the Southern Ocean. Changes to phytoplankton growth, indicative of changes in bio-availability of iron, can have a considerable effect on phytoplankton biomass and primary productivity. More in-situ estimates of maximum photosynthetic growth are essential for model validation. Comparatively estimates of maximum photosynthetic efficiency (the initial slope of the P-I curve) are less important for model validation (for this model). The model output is less sensitive to the choice of this parameter value, which is predominantly determined by light availability in the water column.

- *unconstrained parameters*

The modelled phytoplankton biomass shows virtually no sensitivity to the detrital sinking rate or the half saturation constant for DIN uptake rate. Measurements of these processes are not critical in modelling surface chlorophyll concentrations in the Australian region of the Southern Ocean. On the other hand the model cannot be used to accurately predict these processes and therefore quantifying sinking rates through methods such as sediment trap measurements is essential for obtaining estimates of carbon export in the Southern Ocean.

5.3 Future Research

The advantages and disadvantages of simulated annealing and the Metropolis-Hastings algorithm have been assessed independently, however it is possible that these methods may be used in a complimentary manner. Simulated annealing could be used to optimise all the model parameters and identify a subset of the most sensitive and uncorrelated ones. The Metropolis-Hastings algorithm could then be used to optimise this subset to provide a rigorous error estimation with the parameter estimates. Error estimation is central to the concept of data assimilation (Gregg et al., 2009). In our experiments, probing questions about ecosystems, the model predictions are regarded as hypotheses. The price of being wrong is minimal and the errors calculated from the Hessian matrix are certainly satisfactory. Marine ecosystem models are increasingly being used as tools

to support decision making (Stow et al., 2009). In high-stakes policy-making applications, error analysis is critical. When using models for future predictions an assessment of the sensitivity of the response to ranges in parameter estimates is essential. For such applications the combination of simulated annealing and the Metropolis-Hasting algorithm could be applicable.

Our experiments suggest that using this model the biological solution is more sensitive to the biological parameters than to the physical forcing. Similarly Losa et al. (2006) found that spatial biological parameterisations were more important in capturing the variability in chlorophyll observations of the North Atlantic than improvements to the model physics. Multiple optimisations in an ocean basin have been performed in a number of studies following several different approaches, such as independent optimisations, simultaneous optimisation or grouping stations. Hurtt and Armstrong (1999) found that different ecological processes must be considered to achieve a fit to observations at two sites in the North Atlantic (BATS and OWSI). Schartau and Oschlies (2003a,b) concluded that a simultaneous optimisation at three sites in the North Atlantic (BATS, OWSI and NABE) results in parameter estimates that are a compromise among local parameter estimates that would be obtained from three individual optimisations. Hemmings et al. (2004) found that a good fit to observations of the North Atlantic requires the domain to be split into two provinces with different parameter sets. Losa et al. (2004) found significant spatial variation in optimised parameters over the North Atlantic basin and reasoned that the use of different parameter vectors smoothed over the domain boundaries with interpolation techniques is the best way to apply the model on a basin wide scale. Future work should focus on a number of individual optimisations over the Southern Ocean domain to identify the factors influencing spatial patterns in surface chlorophyll concentration.

There have been numerous parameter optimisation experiments to improve the fit of a model to some set of observations, presenting the theoretical basis and the potential of data assimilation in marine ecosystem modelling. Thus far, few studies have focussed on

what we can learn from the optimised parameters, or used the results to form new/ test existing hypotheses on ecosystem functioning (Spitz et al., 2001; Friedrichs, 2002). In this thesis data assimilation is used as a tool to probe questions about marine biogeochemical dynamics. As methods such as simulated annealing become more established, parameter optimisations can become routine in biogeochemical modelling experiments. Thus I hope this work may inspire the focus of future parameter optimisation studies to be on what we learn about marine ecosystems as well as calibrating models to observations.

References

Aber, J. D. 1997. Why don't we believe the models? Bulletin of the Ecological Society of America, 78, 232–233.

Agawin, N.S.R., Duarte, C.M. and Agusti, S., 2000. Nutrient and temperature control of the contribution of picoplankton to phytoplankton biomass and production. Limnology and Oceanography, 45(3): 591-600.

Anderson, L.A., 2009. The seasonal nitrogen cycle in Wilkinson Basin, Gulf of Maine, as estimated by 1-D biological model optimization. Journal of Marine Systems, 78(1): 77-93.

Anderson, R.F. and Smith, W.O., 2001. The US Southern Ocean Joint Global Ocean Flux Study: Volume two. Deep-Sea Research Part II-Topical Studies in Oceanography, 48(19-20): 3883-3889.

Anderson, T.R. and Totterdell, I.J. 2004. Modelling the response of the biological pump to climate change. In: M. Follows and T. Oguz (Eds.), The Ocean Carbon Cycle and Climate. Kluwer Academic Publishers. The Netherlands, pp. 353-395.

Anderson, T.R., 2005. Plankton functional type modelling: running before we can walk? Journal of Plankton Research, 27(11): 1073-1081.

Athias, V., Mazzega, P. and Jeandel, C., 2000. Selecting a global optimization method to estimate the oceanic particle cycling rate constants. Journal of Marine Research, 58(5): 675-707.

Ayres, R.U. 1997. Integrated assessment of the grand nutrient cycles. Environmental modeling and assessment, 2, 3, 1420 – 2026.

Baird, M.E., Timko, P.G., Suthers, I.M. and Middleton, J.H., 2006. Coupled physical-biological modelling study of the East Australian Current with idealised wind forcing. Part 1: Biological model intercomparison. Journal of Marine Systems, 59(3-4): 249-270.

Bakker, D.C.E. et al., 2005. Iron and mixing affect biological carbon uptake in SOIREE and EisenEx, two Southern Ocean iron fertilisation experiments. Deep-Sea Research Part I-Oceanographic Research Papers, 52(6): 1001-1019.

Banse, K., 1996. Low seasonality of low concentrations of surface chlorophyll in the Subantarctic water ring: underwater irradiance, iron, or grazing? Progress in Oceanography, 37(3-4): 241-291.

Belkin, I.M. and Gordon, A.L., 1996. Southern Ocean fronts from the Greenwich meridian to Tasmania. Journal of Geophysical Research-Oceans, 101(C2): 3675-3696.

Bisset, W.P., Walsh, J.J., Dieterle, D.A., and Garder, K.L. 1999. Carbon cycling in the upper waters of the Sargasso sea : I. Numerical simulation of differential carbon and nitrogen fluxes. Deep-Sea Research I 46: 205-269.

Blain, S. et al., 2004. Availability of iron and major nutrients for phytoplankton in the northeast Atlantic Ocean. Limnology and Oceanography, 49(6): 2095-2104.

Bowie, A.R. et al., 2009. Biogeochemical iron budgets of the Southern Ocean south of Australia: Decoupling of iron and nutrient cycles in the subantarctic zone by the summertime supply. Global Biogeochemical Cycles, 23.

Boyd, P.W., 2002. Environmental factors controlling phytoplankton processes in the Southern Ocean. Journal of Phycology, 38(5): 844-861.

Boyd, P.W. et al., 2001. Control of phytoplankton growth by iron supply and irradiance in the subantarctic Southern Ocean: Experimental results from the SAZ Project. Journal of Geophysical Research-Oceans, 106(C12): 31573-31583.

Boyd, P.W. et al., 2000. A mesoscale phytoplankton bloom in the polar Southern Ocean stimulated by iron fertilization. Nature, 407(6805): 695-702.

Brock, T.D. 1981. Calculating solar radiation for ecological studies. Ecological Modelling, 14, 1-19.

Cavagna, A., Elskens, M., Griffiths, F.B., Jacquet, S.H.M., Dehairs, F., in Press. Contrasting regimes of productivity and potential for carbon export in the SAZ and PFZ south of Tasmania. Deep Sea Research Part II-Topical Studies in Oceanography.

Chai, F., Lindley, S.T. and Barber, R.T., 1996. Origin and maintenance of a high nitrate condition in the equatorial Pacific. Deep-Sea Research Part II-Topical Studies in Oceanography, 43(4-6): 1031-1064.

Chaigneau, A., Morrow, R.A. and Rintoul, S.R. 2004. Seasonal and interannual evolution of the mixed layer in the Antarctic Zone south of Tasmania. Deep-Sea Research Part I-Oceanographic Research Papers, 51(12): 2047-2072.

Chavez, F.P. et al., 1991. Growth-rates, grazing, sinking, and iron limitation of equatorial Pacific phytoplankton. Limnology and Oceanography, 36(8): 1816-1833.

Coale, K.H., 1991. Effects of iron, manganese, copper, and zinc enrichments on productivity and biomass in the Sub-Arctic Pacific. Limnology and Oceanography, 36(8): 1851-1864.

Coale, K.H. et al., 2004. Southern ocean iron enrichment experiment: Carbon cycling in high- and low-Si waters. Science, 304(5669): 408-414.

Coale, K.H. et al., 1996. A massive phytoplankton bloom induced by an ecosystem-scale iron fertilization experiment in the equatorial Pacific Ocean. Nature, 383(6600): 495-501.

Cox, P.M., Betts, R.A., Jones, C.D., Spall, S.A. and Totterdell, I.J., 2000. Acceleration of global warming due to carbon-cycle feedbacks in a coupled climate model. Nature, 408(6809): 184-187.

de Baar, H. J. W., and Boyd., P. M. 2000. The role of iron in plankton ecology and carbon dioxide transfer of the global oceans, p. 61–140. In Hanson, R. B., Ducklow, H. W. and Field, J. G., (eds.), The dynamic ocean carbon cycle: A midterm synthesis of the Joint Global Ocean Flux Study, International Geosphere Biosphere Programme Book Series. V. 5. Cambridge Univ. Press.

Denman, K.L., 2008. Climate change, ocean processes and ocean iron fertilization. Marine Ecology-Progress Series, 364: 219-225.

Denman, K.L. and Pena, M.A., 1999. A coupled 1-D biological/physical model of the northeast subarctic Pacific Ocean with iron limitation. Deep-Sea Research Part II-Topical Studies in Oceanography, 46(11-12): 2877-2908.

Denman, K.L. and Pena, M.A., 2002. The response of two coupled one-dimensional mixed layer/planktonic ecosystem models to climate change in the NE subarctic Pacific Ocean. Deep-Sea Research Part II-Topical Studies in Oceanography, 49(24-25): 5739-5757.

de Salas, M.F., Eriksen, R., Davidson, A.T., Wright, S.W., in press. Protistan communities in the Australian sector of the subantarctic zone during SAZ-Sense. Deep Sea Research Part II-Topical Studies in Oceanography.

Dilks, D.W., Canale, R.P. and Meier, P.G., 1992. Development of Bayesian Monte-Carlo techniques for water-quality model uncertainty. Ecological Modelling, 62(1-3): 149-162.

Doney, S.C., Glover, D.M. and Najjar, R.G., 1996. A new coupled, one-dimensional biological-physical model for the upper ocean: Applications to the JGOFS Bermuda Atlantic time-series study (BATS) site. Deep-Sea Research Part II-Topical Studies in Oceanography, 43(2-3): 591-624.

Douglas, S.E., Raven, J.A. and Larkum, W.D., 2003. The Algae and their general characteristics, p. 1-10. In Larkum, W.D., Douglas, S.E., Raven, J.A. (eds), Photosythesis in Algae. Kluwer Academic Publishers, P.O. Box 17, 3300 AA Dordrecht, The Netherlands.

Dowd, M. and Meyer, R., 2003. A Bayesian approach to the ecosystem inverse problem. Ecological Modelling, 168(1-2): 39-55.

Dugdale, R.C., Wilkerson, F.P. and Minas, H.J., 1995. The role of a silicate pump in driving new production. Deep-Sea Research Part I-Oceanographic Research Papers, 42(5): 697-719.

Eknes, M. and Evensen, G., 2002. An Ensemble Kalman filter with a 1-D marine ecosystem model. Journal of Marine Systems, 36(1-2): 75-100.

Eppley, R.W., 1972. Temperature and phytoplankton growth in sea. Fishery Bulletin, 70(4): 1063-1085.

Evans, G.T., 1999. The role of local models and data sets in the Joint Global Ocean Flux Study. Deep-Sea Research Part I-Oceanographic Research Papers, 46(8): 1369-1389.

Evans, G.T. and Parslow, J.S., 1985. A model of annual plankton cycles. Biological Oceanography, 3, 328-347.

Falkowski, P.G., Barber, R.T. and Smetacek, V., 1998. Biogeochemical controls and feedbacks on ocean primary production. Science, 281(5374): 200-206.

Falkowski, P.G. et al., 1988. The fate of a spring phytoplankton bloom - export or oxidation. Continental Shelf Research, 8(5-7): 457-484.

Fan, W. and Lv, X.Q., 2009. Data assimilation in a simple marine ecosystem model based on spatial biological parameterizations. Ecological Modelling, 220(17): 1997-2008.

Fasham, M.J.R., 1995. Variations in the seasonal cycle of biological production in Sub-Arctic oceans - a model sensitivity analysis. Deep-Sea Research Part I-Oceanographic Research Papers, 42(7): 1111-1149.

Fasham, M.J.R., Ducklow, H.W. and McKelvie, S.M., 1990. A nitrogen-based model of plankton dynamics in the oceanic mixed layer. Journal of Marine Research, 48(3): 591-639.

Fasham, M.J.R. and Evans, G.T., 1995. The use of optimization techniques to model marine ecosystem dynamics at the JGOFS station at 47-degrees-N 20-degrees-W. Philosophical Transactions of the Royal Society of London Series B-Biological Sciences, 348(1324): 203-209.

Fasham, M.J.R., Flynn, K.J., Pondaven, P., Anderson, T.R. and Boyd, P.W., 2006. Development of a robust marine ecosystem model to predict the role of iron in biogeochemical cycles: A comparison of results for iron-replete and iron-limited areas, and the SOIREE iron-enrichment experiment. Deep-Sea Research Part I-Oceanographic Research Papers, 53(2): 333-366.

Fennel, K., Abbott, M.R., Spitz, Y.H., Richman, J.G. and Nelson, D.M., 2003. Impacts of iron control on phytoplankton production in the modern and glacial Southern Ocean. Deep-Sea Research Part II-Topical Studies in Oceanography, 50(3-4): 833-851.

Fennel, K., Losch, M., Schroter, J. and Wenzel, M., 2001. Testing a marine ecosystem model: sensitivity analysis and parameter optimization. Journal of Marine Systems, 28(1-2): 45-63.

Fiechter, J. et al., 2009. Modeling iron limitation of primary production in the coastal Gulf of Alaska. Deep-Sea Research Part II-Topical Studies in Oceanography, 56(24): 2503-2519.

Fontana, C., Grenz, C., Pinazo, C., Marsaleix, P. and Diaz, F., 2009. Assimilation of SeaWiFS chlorophyll data into a 3D-coupled physical-biogeochemical model applied to a freshwater-influenced coastal zone. Continental Shelf Research, 29(11-12): 1397-1409.

Franck, V.M., Brzezinski, M.A., Coale, K.H. and Nelson, D.M., 2000. Iron and silicic acid concentrations regulate Si uptake north and south of the Polar Frontal Zone in the Pacific Sector of the Southern Ocean. Deep-Sea Research Part II-Topical Studies in Oceanography, 47(15-16): 3315-3338.

Friedrichs, M.A.M., 2001. A data assimilative marine ecosystem model of the central equatorial Pacific: Numerical twin experiments. Journal of Marine Research, 59(6): 859-894.

Friedrichs, M.A.M., 2002. Assimilation of JGOFS EqPac and SeaWiFS data into a marine ecosystem model of the central equatorial Pacific Ocean. Deep-Sea Research Part II-Topical Studies in Oceanography, 49(1-3): 289-319.

Friedrichs, M.A.M. et al., 2007. Assessment of skill and portability in regional marine biogeochemical models: Role of multiple planktonic groups. Journal of Geophysical Research-Oceans, 112(C8): 22.

Friedrichs, M.A.M., Hood, R.R. and Wiggert, J.D., 2006. Ecosystem model complexity versus physical forcing: Quantification of their relative impact with assimilated Arabian Sea data. Deep-Sea Research Part II-Topical Studies in Oceanography, 53(5-7): 576-600.

Galbraith, E. D., Gnanadesikan, A., Dunne, J. P. and Hiscock, M. R. 2010. Regional impacts of iron-light colimitation in a global biogeochemical model. Biogeosciences, Volume 7, Issue 3, pp.1043-1064

Gelman, A., Carlin, J.B., Stern, H.S., and Rubin, D.B. 2004. Bayesian Data Analysis (2nd edition). Chapman & Hall/CRC, Boca Raton. pp.696.

Gill, A.E. 1982. Atmosphere-Ocean Dynamics. International Geophysics Series. Academic Press, London, pp. 662.

Gille, S. 2002,. Warming of the Southern Ocean since the 1950s, Science, 295, 1275 – 1277.

Greene, R.M., Geider, R.J. and Falkowski, P.G., 1991. Effect of iron limitation on photosynthesis in a marine diatom. Limnology and Oceanography, 36(8): 1772-1782.

Gregg, W.W., 2008. Assimilation of SeaWiFS ocean chlorophyll data into a three-dimensional global ocean model. Journal of Marine Systems, 69(3-4): 205-225.

Gregg, W.W. et al., 2009. Skill assessment in ocean biological data assimilation. Journal of Marine Systems, 76(1-2): 16-33.

Gregg, W.W., Ginoux, P., Schopf, P.S. and Casey, N.W., 2003. Phytoplankton and iron: validation of a global three-dimensional ocean biogeochemical model. Deep-Sea Research Part II-Topical Studies in Oceanography, 50(22-26): 3143-3169.

Griffiths, F.B., Bowie, A.R., Dehairs, F., Trull, T.W., in press. The SAZ-Sense experiment: a biogeochemical comparison of Sub-Antarctic and Polar Frontal waters southwest and southeast of Tasmania. Deep Sea Research Part II-Topical Studies in Oceanography.

Griffiths, F.B., Howard, W., Wright, S., Tillbrook, B., Trull, T. 2006. Australian Antarctic Program - Application Custom Report. Science project 2720.

Gruber, N., Doney, S.C., Emerson, S.T., Gilbert, D., Kobayashi, T., Körtzinger, A., Johnson, G. C., Johnson, K.S., Riser, S.C., Ulloa, O. 2007. The Argo-Oxygen Program: A white paper to promote the addition of oxygen sensors to the international Argo Float Program, Version 5-1, Prepared for distribution to the Argo Steering Committee, February 14, 2007.

Harmon, R. and Challenor, P., 1997. A Markov chain Monte Carlo method for estimation and assimilation into models. Ecological Modelling, 101(1): 41-59.

Hallegraeff, G.M,, 2006. Plankton: A Critical Creation, Foot & Playsted, pp. 100.

Harrison, W.G. and Platt, T., 1986. Photosynthesis-irradiance relationships in polar and temperate phytoplankton populations. Polar Biology, 5(3): 153-164.

Hemmings, J.C.P., Barciela, R.M. and Bell, M.J., 2008. Ocean color data assimilation with material conservation for improving model estimates of air-sea CO2 flux. Journal of Marine Research, 66(1): 87-126.

Hemmings, J.C.P., Srokosz, M.A., Challenor, P. and Fasham, M.J.R., 2004. Split-domain calibration of an ecosystem model using satellite ocean colour data. Journal of Marine Systems, 50(3-4): 141-179.

Hemmings, J.C.P. 2009. A marine model optimization test-bed for ecosystem model evaluation: MarMOT version 1.0 description and user guide. National Oceanography Centre, Southampton. Research & Consultancy Report No. 67. 111pp.

Hense, I., Bathmann, U.V. and Timmermann, R., 2000. Plankton dynamics in frontal systems of the Southern Ocean. Journal of Marine Systems, 27(1-3): 235-252.

Hernandez-Leon, S., Fraga, C. and Ikeda, T., 2008. A global estimation of mesozooplankton ammonium excretion in the open ocean. Journal of Plankton Research, 30(5): 577-585.

Hill, S.L., Murphy, E.J., Reid, K., Trathan, P.N. and Constable, A.J., 2006. Modelling Southern Ocean ecosystems: krill, the food-web, and the impacts of harvesting. Biological Reviews, 81(4): 581-608.

Hiscock, M.R. et al., 2003. Primary productivity and its regulation in the Pacific Sector of the Southern Ocean. Deep-Sea Research Part II-Topical Studies in Oceanography, 50(3-4): 533-558.

Holm-Hansen, O., El-Sayed, S.Z., Franceschini, G.A. and Cuhel, R.L., 1977. Primary production and the factors controlling phytoplankton growth in the Southern Ocean. In: Llano, G.A. (ed.), Adaptations Within Antarctic Ecosystems: Proceedings of the Third SCAR Symposium on Antarctic Biology, pp. 11-50. Gulf Publishing Co., Houston, Texas.

Hurtt, G.C. and Armstrong, R.A., 1996. A pelagic ecosystem model calibrated with BATS data. Deep-Sea Research Part II-Topical Studies in Oceanography, 43(2-3): 653-683.

Hurtt, G.C. and Armstrong, R.A., 1999. A pelagic ecosystem model calibrated with BATS and OWSI data. Deep-Sea Research Part I-Oceanographic Research Papers, 46(1): 27-61.

Hutchins, D.A. et al., 2001. Control of phytoplankton growth by iron and silicic acid availability in the subantarctic Southern Ocean: Experimental results from the SAZ Project. Journal of Geophysical Research-Oceans, 106(C12): 31559-31572.

Johnson, K.S., Gordon, R.M. and Coale, K.H., 1997. What controls dissolved iron concentrations in the world ocean? Marine Chemistry, 57(3-4): 137-161.

Kamykowski, D. and Zentara, S.J., 1985. Nitrate and silicic-acid in the world ocean - patterns and processes. Marine Ecology-Progress Series, 26(1-2): 47-59.

Kantha, L.H., 2004. A general ecosystem model for applications to primary productivity and carbon cycle studies in the global oceans. Ocean Modelling, 6(3-4): 285-334.

Karakas, G. et al., 2009. Impact of particle aggregation on vertical fluxes of organic matter. Progress in Oceanography, 83(1-4): 331-341.

Kirkpatrick, S., Gelatt, C.D. and Vecchi, M.P., 1983. Optimization by simulated annealing. Science, 220(4598): 671-680.

Kohfeld, K.E., Le Quere, C., Harrison, S.P. and Anderson, R.F., 2005. Role of marine biology in glacial-interglacial CO2 cycles. Science, 308(5718): 74-78.

Kolber, Z.S. et al., 1994. Iron limitation of phytoplankton photosynthesis in the equatorial Pacific-Ocean. Nature, 371(6493): 145-149.

Kriest, I., 2002. Different parameterizations of marine snow in a 1D-model and their influence on representation of marine snow, nitrogen budget and sedimentation. Deep-Sea Research Part I-Oceanographic Research Papers, 49(12): 2133-2162.

Kruger, J., 1993. Simulated annealing - a tool for data assimilation into an almost steady model state. Journal of Physical Oceanography, 23(4): 679-688.

Ku, T.L., Luo, S.D., Kusakabe, M. and Bishop, J.K.B., 1995. RA-228-Derived nutrient budgets in the upper equatorial Pacific and the role of new silicate in limiting productivity. Deep-Sea Research Part II-Topical Studies in Oceanography, 42(2-3): 479-497.

Lai, X. et al., 2008. Spatial and temporal distribution of Fe, Ni, Cu and Pb along 140 degrees E in the Southern Ocean during austral summer 2001/02. Marine Chemistry, 111(3-4): 171-183.

Landry, M.R. et al., 1997. Iron and grazing constraints on primary production in the central equatorial Pacific: An EqPac synthesis. Limnology and Oceanography, 42(3): 405-418.

Lawson, L.M., Hofmann, E.E. and Spitz, Y.H., 1996. Time series sampling and data assimilation in a simple marine ecosystem model. Deep-Sea Research Part II-Topical Studies in Oceanography, 43(2-3): 625-651.

Le Quere, C., 2006. Reply to Horizons Article 'Plankton functional type modelling: running before we can walk' Anderson (2005): I. Abrupt changes in marine ecosystems? Journal of Plankton Research, 28(9): 871-872.

Le Quere, C. et al., 2005. Ecosystem dynamics based on plankton functional types for global ocean biogeochemistry models. Global Change Biology, 11(11): 2016-2040.

Le Quere, C. et al., 2007. Saturation of the Southern Ocean CO2 sink due to recent climate change. Science, 316(5832): 1735-1738.

Leblanc, K. et al., 2000. Particulate biogenic silica and carbon production rates and particulate matter distribution in the Indian sector of the Subantarctic Ocean, Southern Ocean Joint Global Ocean Flux Symposium (SO-JGOFS). Pergamon-Elsevier Science Ltd, Brest, France, pp. 3189-3206.

Lee, P.A. and de Mora, S.J., 1999. A review of dimethylsulfoxide in aquatic environments. Atmosphere-Ocean, 37(4): 439-456.

Lenton, A., Bopp, L. and Matear, R.J., 2009. Strategies for high-latitude northern hemisphere CO2 sampling now and in the future. Deep-Sea Research Part II-Topical Studies in Oceanography, 56(8-10): 523-532.

Levitus, S. 1982. Climatological Atlas of the World Ocean. NOAA Professional Paper 13. U.S. Department of Commerce, NOAA, NESDIS.

Leynaert, A., Tréguer, P., Nelson, D.M., Del Amo, Y., 1996. 32Si as a tracer of biogenic silica production: methodological improvements. In: Baeyens, J., Dehairs, F., Goeyens, L. (Eds), Integrated Marine System Analysis, Minute of the First Workshop Meeting. VUB, Brussels, Belgium, pp. 29–35.

Lourey, M.J. and Trull, T.W., 2001. Seasonal nutrient depletion and carbon export in the Subantarctic and Polar Frontal Zones of the Southern Ocean south of Australia. Journal of Geophysical Research-Oceans, 106(C12): 31463-31487.

Maier-Reimer, E. and Hasselmann, K. 1987. Transport & storage of CO_2 in the ocean - an inorganic ocean-circulation carbon cycle model. Climate Dynamics 2, 63 - 90.

Maier-Reimer, E., Mikolajewicz, U. and Winguth, A. 1996. Future ocean uptake of CO2: interaction between ocean circulation and biology. Climate Dynamics, 12, 711-721, 19.

Marinov, I., Gnanadesikan, A., Toggweiler, J.R. and Sarmiento, J.L., 2006. The Southern Ocean biogeochemical divide. Nature, 441(7096): 964-967.

Martin, J.H. et al., 1994. Testing the iron hypothesis in ecosystems of the equatorial Pacific-Ocean. Nature, 371(6493): 123-129.

Martin, J.H. and Fitzwater, S.E., 1988. Iron-deficiency limits phytoplankton growth in the northeast Pacific Subarctic. Nature, 331(6154): 341-343.

Martin, J.H., Gordon, R.M. and Fitzwater, S.E., 1990. Iron in Antarctic waters. Nature, 345(6271): 156-158.

Matear, R.J., 1995. Parameter optimization and analysis of ecosystem models using simulated annealing - a case-study at Station-P. Journal of Marine Research, 53(4): 571-607.

Matear, R.J. 2004. Data Assimilation into marine carbon models. In: M. Follows and T. Oguz (Eds.), The Ocean Carbon Cycle and Climate. Kluwer Academic Publishers. The Netherlands, pp. 353-395.

Matear, R.J., Hirst, A.C. 1999. Climate change feedback on the future oceanic CO2 uptake. Tellus Series B, Chemical and physical meteorology 51(3): 722-733.

Matear, R.J. and Hirst, A.C., 2003. Long-term changes in dissolved oxygen concentrations in the ocean caused by protracted global warming. Global Biogeochemical Cycles, 17(4).

Matsumoto, K., 2007. Biology-mediated temperature control on atmospheric pCO(2) and ocean biogeochemistry. Geophysical Research Letters, 34(20): 5.

Mattern, J.P., Dowd, M. and Fennel, K., Sequential data assimilation applied to a physical-biological model for the Bermuda Atlantic time series station. Journal of Marine Systems, 79(1-2): 144-156.

McClain, C.R., 2009. A Decade of Satellite Ocean Color Observations. Annual Review of Marine Science, 1: 19-42.

McNeil, B.I. and Matear, R.J., 2008. Southern Ocean acidification: A tipping point at 450-ppm atmospheric CO2. Proceedings of the National Academy of Sciences of the United States of America, 105(48): 18860-18864.

Menzel, D. W. and Ryther, J.H., 1960. The annual cycle of primary production in the Sargasso Sea off Bermuda. Deep-Sea Res. 6:351–367.

Metzl, N., Tilbrook, B. and Poisson, A., 1999. The annual fCO(2) cycle and the air-sea CO2 flux in the sub-Antarctic Ocean. Tellus Series B-Chemical and Physical Meteorology, 51(4): 849-861.

Miller, C.B. et al., 1991. Ecological dynamics in the Sub-Arctic Pacific, a possibly iron-limited ecosystem. Limnology and Oceanography, 36(8): 1600-1615.

Minas, H.J. and Minas, M., 1992. Net community production in high nutrient-low chlorophyll waters of the tropical and Antarctic Oceans - grazing vs iron hypothesis. Oceanologica Acta, 15(2): 145-162.

Mitchell, B.G. and Holm-Hansen, O., 1991. Observations and modeling of the Antarctic phytoplankton crop in relation to mixing depth. Deep-Sea Research, 38(8/9): 981-1,007.

Mongin, M., Chamberlain, M., Matear, R., in press, a. Potential iron sources into the Sub Antarctica Zone south of Australia: Sedimentary versus Aeolian input. Deep Sea Research Part II-Topical Studies in Oceanography.

Mongin, M., Moore, T., Matear, R., in press, b. Seasonality and variability of remotely sensed observations and mixed layer depth estimates in the Subantarctic and Polar Frontal zones. The settings of the SAZ-Sense project. Deep Sea Research Part II-Topical Studies in Oceanography.

Mongin, M., Nelson, D.M., Pondaven, P. and Treguer, P., 2006. Simulation of upper-ocean biogeochemistry with a flexible-composition phytoplankton model: C, N

and Si cycling and Fe limitation in the Southern Ocean. Deep-Sea Research Part II-Topical Studies in Oceanography, 53(5-7): 601-619.

Moore, C.M. et al., 2007. Iron-light interactions during the CROZet natural iron bloom and EXport experiment (CROZEX) I: Phytoplankton growth and photophysiology. Deep-Sea Research Part II-Topical Studies in Oceanography, 54(18-20): 2045-2065.

Moore, J.K., Doney, S.C., Kleypas, J.A., Glover, D.M. and Fung, I.Y., 2002. An intermediate complexity marine ecosystem model for the global domain. Deep-Sea Research Part II-Topical Studies in Oceanography, 49(1-3): 403-462.

Morrow, R., Valladeau, G. and Sallee, J.B., 2008. Observed subsurface signature of Southern Ocean sea level rise. Progress in Oceanography, 77(4): 351-366.

Neftel, A., Oeschger, H., Schwander, J., Stauffer, B. and Zumbrunn, R., 1982. Ice core sample measurements give atmospheric CO2 content during the past 40,000 yr. Nature, 295(5846): 220-223.

Nerger, L. and Gregg, W.W., 2007. Assimilation of SeaWiFS data into a global ocean-biogeochemical model using a local SEIK filter. Journal of Marine Systems, 68(1-2): 237-254.

Nowlin, W.D., Whitworth, T. and Pillsbury, R.D., 1977. Structure and transport of Antarctic Circumpolar Current at drake passage from short-term measurements. Journal of Physical Oceanography, 7(6): 788-802.

Odate, T. and Fukuchi, M., 1995. Distribution and community structure of picophytoplankton in the Southern Ocean during late austral summer of 1992. Proc. NIPR Symp. Polar Biol., Nat. Inst. Polar Res., 8, 86–100.

Oke, P.R., Brassington, G.B., Griffin, D.A. and Schiller, A., 2008. The Bluelink ocean data assimilation system (BODAS). Ocean Modelling, 21(1-2): 46-70.

Orsi, A.H., Whitworth, T. and Nowlin, W.D., 1995. On the meridional extent and fronts of the Antarctic Circumpolar Current. Deep-Sea Research Part I-Oceanographic Research Papers, 42(5): 641-673.

Oschlies, A. and Garcon, V., 1999. An eddy-permitting coupled physical-biological model of the North Atlantic - 1. Sensitivity to advection numerics and mixed layer physics. Global Biogeochemical Cycles, 13(1): 135-160.

Oschlies, A. and Schartau, M., 2005. Basin-scale performance of a locally optimized marine ecosystem model. Journal of Marine Research, 63(2): 335-358.

Pakhomov, E.A. and Froneman, P.W., 2004. Zooplankton dynamics in the eastern Atlantic sector of the Southern Ocean during the austral summer 1997/1998 - Part 2: Grazing impact. Deep-Sea Research Part II-Topical Studies in Oceanography, 51(22-24): 2617-2631.

Palmer, J.R. and Totterdell, I.J., 2001. Production and export in a global ocean ecosystem model. Deep-Sea Research Part I-Oceanographic Research Papers, 48(5): 1169-1198.

Pearce, I., Davidson, A.T., Thomson, P.G., Wright, S., van den Enden, R., in press. Marine microbial ecology in the Sub-Antarctic Zone: Rates of bacterial and phytoplankton growth and grazing by heterotrophic protists. Deep Sea Research Part II-Topical Studies in Oceanography.

Popova, E.E. et al., 2002. Coupled 3D physical and biological modelling of the mesoscale variability observed in North-East Atlantic in spring 1997: biological processes. Deep-Sea Research Part I-Oceanographic Research Papers, 49(10): 1741-1768.

Prunet, P., Minster, J.F., RuizPino, D. and Dadou, I., 1996. Assimilation of surface data in a one-dimensional physical-biogeochemical model of the surface ocean.1. Method and preliminary results. Global Biogeochemical Cycles, 10(1): 111-138.

Reynolds, R. W. and T. M. Smith, 1994. Improved Global Sea Surface Temperature Analyses Using Optimum Interpolation. J. Climate, 7, 929-948.

Riebesell, U. et al., 2007. Enhanced biological carbon consumption in a high CO2 ocean. Nature, 450: 545-U10.

Riebesell, U., Wolfgladrow, D.A. and Smetacek, V., 1993. Carbon-dioxide limitation of marine-phytoplankton growth-rates. Nature, 361(6409): 249-251.

Rintoul, S.R. and Bullister, J.L., 1999. A late winter hydrographic section from Tasmania to Antarctica. Deep-Sea Research Part I-Oceanographic Research Papers, 46(8): 1417-1454.

Rintoul, S.R. and Trull, T.W., 2001. Seasonal evolution of the mixed layer in the Subantarctic Zone south of Australia. Journal of Geophysical Research-Oceans, 106(C12): 31447-31462.

Robinson, A.R. and Lermusiaux, P.F.J., 2000. Overview of Data Assimilation, Harvard University Reports in Physical/Interdisciplinary Ocean Science #62, Harvard University.

Robinson, I.S. and Sanjuan-Calzado, V., 2006. The application of satellite ocean colour data to marine ecosystem models. Report D2.3.6 for the Marine Environment and Security for the European Area - Integrated Project (MERSEA-IP). Institut Français de Recherche pour l'Exploitation de la Mer - France, 40pp.

Ruiz, J., Prieto, L. and Ortegon, F., 2002. Diatom aggregate formation and fluxes: a modeling analysis under different size-resolution schemes and with empirically determined aggregation kernels. Deep-Sea Research Part I-Oceanographic Research Papers, 49(3): 495-515.

Ryabchenko, V.A., Fasham, M.J.R., Kagan, B.A. and Popova, E.E., 1997. What causes short-term oscillations in ecosystem models of the ocean mixed layer? Journal of Marine Systems, 13(1-4): 33-50.

Sarmiento, J,L. and Gruber, N., 2006. Ocean Biogeochemical Dynamics. Princeton University Press, Princeton, New Jersey 08540.

Sarmiento, J.L., Hughes, T.M.C., Stouffer, R.J. and Manabe, S., 1998. Simulated response of the ocean carbon cycle to anthropogenic climate warming. Nature, 393(6682): 245-249.

Sarmiento, J.L. and le Quéré, C. 1996. Oceanic carbon dioxide uptake in a model of century-scale global warming. Science, 274, 1346-1350.

Sarmiento, J.L. and Orr, J.C., 1991. 3-Dimensional simulations of the impact of Southern-Ocean nutrient depletion on atmospheric CO2 and ocean chemistry. Limnology and Oceanography, 36(8): 1928-1950.

Sarmiento, J.L. et al., 2004. Response of ocean ecosystems to climate warming. Global Biogeochemical Cycles, 18(3): 35.

Sarmiento, J.L. et al., 1993. A seasonal 3-dimensional ecosystem model of nitrogen cycling in the North-Atlantic euphotic zone. Global Biogeochemical Cycles, 7(2): 417-450.

Savoye, N. et al., 2004. Regional variation of spring N-uptake and new production in the Southern Ocean. Geophysical Research Letters, 31(3): 4.

Schartau, M. and Oschlies, A., 2003a. Simultaneous data-based optimization of a 1D-ecosystem model at three locations in the North Atlantic: Part I - Method and parameter estimates. Journal of Marine Research, 61(6): 765-793.

Schartau, M. and Oschlies, A., 2003b. Simultaneous data-based optimization of a 1D-ecosystem model at three locations in the North Atlantic: Part II - Standing stocks and nitrogen fluxes. Journal of Marine Research, 61(6): 795-821.

Schartau, M., Oschlies, A. and Willebrand, J., 2001. Parameter estimates of a zero-dimensional ecosystem model applying the adjoint method. Deep-Sea Research Part II-Topical Studies in Oceanography, 48(8-9): 1769-1800.

Sedwick, P.N., Bowie, A.R. and Trull, T.W., 2008. Dissolved iron in the Australian sector of the Southern Ocean (CLIVAR SR3 section): Meridional and seasonal trends. Deep-Sea Research Part I-Oceanographic Research Papers, 55(8): 911-925.

Sedwick, P.N. et al., 1999. Limitation of algal growth by iron deficiency in the Australian Subantarctic region. Geophysical Research Letters, 26(18): 2865-2868.

Simon, E. and Bertino, L., 2009. Application of the Gaussian anamorphosis to assimilation in a 3-D coupled physical-ecosystem model of the North Atlantic with the EnKF: a twin experiment. Ocean Science, 5(4): 495-510.

Six, K., and Maier-Reimer, E. 1996. Effects or plankton dynamics on seasonal carbon fluxes in an ocean general circulation model, Global Biogeochemical Cycles, 10, 559-583.

Smith, W.O. and Lancelot, C., 2004. Bottom-up versus top-down control in phytoplankton of the Southern Ocean. Antarctic Science, 16(4): 531-539.

Smith, W.O., Jr., and Nelson, D.M. 1985. Phytoplankton bloom produced by a receding ice edge in the Ross Sea: Spatial coherence with the density field. Science 227: 163-166.

Sohrin, Y. et al., 2000. The distribution of Fe in the Australian sector of the Southern Ocean. Deep-Sea Research Part I-Oceanographic Research Papers, 47(1): 55-84.

Sokolov, S. and Rintoul, S.R., 2002. Structure of Southern Ocean fronts at 140 degrees E. Journal of Marine Systems, 37(1-3): 151-184.

Sokolov, S. and Rintoul, S.R., 2007. On the relationship between fronts of the Antarctic Circumpolar Current and surface chlorophyll concentrations in the Southern Ocean. Journal of Geophysical Research-Oceans, 112(C7).

Spitz, Y.H., Moisan, J.R., Abbott, M.R. and Richman, J.G., 1998. Data assimilation and a pelagic ecosystem model: parameterization using time series observations. Journal of Marine Systems, 16(1-2): 51-68.

Street, J.H. and Paytan, A., 2005. Iron, phytoplankton growth and the carbon cycle, Biogeochemical Cycles of Elements. Metal Ions in Biological Systems, pp. 153-193.

Takahashi, T. et al., 2002. Global sea-air CO2 flux based on climatological surface ocean pCO(2), and seasonal biological and temperature effects. Deep-Sea Research Part II-Topical Studies in Oceanography, 49(9-10): 1601-1622.

Tarantola, A. 1987. Inverse Problem Theory. Elsevier Science, New York, NY.

Tarantola, A. 2005. Inverse Problem Theory and Methods for Model Parameter Estimation. SIAM: Society for Industrial and Applied Mathematics.

Taylor, A.H., Allen, J.I. and Clark, P.A., 2002. Extraction of a weak climatic signal by an ecosystem. Nature, 416(6881): 629-632.

Thacker, W.C., 1987. Three lectures on fitting numerical models to observations. External report GKSS 87/E/65, GKSS-Forschungszentrum Geesthacht, GmbHGeesthacht, Federal Republic of Germany.

Timmermans, K.R. et al., 1998. Iron stress in the Pacific region of the Southern Ocean: evidence from enrichment bioassays. Marine Ecology-Progress Series, 166: 27-41.

Toggweiler, J.R., Dixon, K. and Broecker, W.S., 1991. The Peru upwelling and the ventilation of the South-Pacific thermocline. Journal of Geophysical Research-Oceans, 96(C11): 20467-20497.

Totterdell, I. J., Armstrong, R. A., Drange, H. et al. 1993. Trophic resolution. In Evans,

G. T. and Fasham, M. J. R. (eds), Towards a Model of Ocean Biogeochemical Processes. NATO ASI, Vol. I 10. Springer-Verlag, Berlin, pp. 71–92.

Treguer, P. and Jacques, G., 1992. Dynamics of nutrients and phytoplankton, and fluxes of carbon, nitrogen and silicon in the Antarctic Ocean. Polar Biology, 12(2): 149-162.

Trewby, M., ed. 2002. Antarctica : an encyclopedia from Abbott ice shelf to zooplankton. Auckland: David Bateman Ltd.

Trull, T.W., Sedwick, P.N., Griffiths, F.B. and Rintoul, S.R., 2001. Introduction to special section: SAZ Project. Journal of Geophysical Research-Oceans, 106(C12): 31425-31429.

Tsuda, A. et al., 2007. Evidence for the grazing hypothesis: Grazing reduces phytoplankton responses of the HNLC ecosystem to iron enrichment in the western subarctic pacific (SEEDS II). Journal of Oceanography, 63(6): 983-994.

Tsuda, A. et al., 2003. A mesoscale iron enrichment in the western Subarctic Pacific induces a large centric diatom bloom. Science, 300(5621): 958-961.

Vaillancourt, R.D., Marra, J., Barber, R.T. and Smith, W.O., 2003. Primary productivity and in situ quantum yields in the Ross Sea and Pacific Sector of the Antarctic Circumpolar Current. Deep-Sea Research Part II-Topical Studies in Oceanography, 50(3-4): 559-578.

Vallino, J.J., 2000. Improving marine ecosystem models: Use of data assimilation and mesocosm experiments. Journal of Marine Research, 58(1): 117-164.

van Oijen, T. et al., 2004. Light rather than iron controls photosynthate production and allocation in Southern Ocean phytoplankton populations during austral autumn. Journal of Plankton Research, 26(8): 885-900.

Volk, T., and Hoffert, M.I. 1985. Ocean carbon pumps: analysis of relative strengths and efficiencies in ocean-driven atmospheric CO_2 changes, in E. T. Sundquist and W. S. Broecker (eds) The Carbon Cycle and Atmospheric CO_2: Natural Variations Archean to Present, pp. 99-110, Geophysical Monograph 32, American Geophysical Union, Wash., D.C.

Wall, M.E., Rechtsteiner, A., Rocha, L.M. 2002. Singular Value Decomposition and Priciple Component Analysis. In: Berrar, D.P., Dubitzky, W. and Granzow, M.

(Eds.), A Practical Approach to Microarray Data Analysis. Springer, New York, pp.91-109.

Walsh, J. 1976. Herbivory as a factor in patterns of nutrient utilisation in the sae. Limnology and oceanography 21, 1-13.

Wells, M.L., Price, N.M. and Bruland, K.W., 1995. Iron chemistry in seawater and its relationship to phytoplankton - a workshop report. Marine Chemistry, 48(2): 157-182.

Westwood, K.J., Griffiths, F.B., Webb, J., in press. Primary productivity in the sub-Antarctic south of Tasmania, Australia; SAZ-Sense survey, 2007. Deep Sea Research Part II-Topical Studies in Oceanography.

Wright, S., Van den Enden, R., Pearce, I., Doblin, M., in press. Phytoplankton pigmentsin the Sub-Antarctic and Polar frontal zones of Tasmania. Deep-Sea Research Part II-Topical Studies in Oceanography.

Wright, S.W. et al., 1996. Analysis of phytoplankton of the Australian sector of the Southern Ocean: Comparisons of microscopy and size frequency data with interpretations of pigment HPLC data using the 'CHEMTAX' matrix factorisation program. Marine Ecology-Progress Series, 144(1-3): 285-298.

Wroblewski, J. S., Sarmiento, J.L. and Flierl. G.R., 1988. An ocean basin scale model of plankton dynamics in the North Atlantic 1. Solutions for the climatological oceanographic conditions in May. Global Biogcochem. Cycles 2: 199-2 18.

Xu, Q., Lin, H., Liu, Y.G., Lv, X.Q. and Cheng, Y.C., 2008. Data assimilation in a coupled physical-biological model for the Bohai Sea and the Northern Yellow Sea. Marine and Freshwater Research, 59(6): 529-539.

Zahariev, K., Christian, J.R. and Denman, K.L., 2008. Preindustrial, historical, and fertilization simulations using a global ocean carbon model with new parameterizations of iron limitation, calcification, and N-2 fixation. Progress in Oceanography, 77(1): 56-82.

Zhao, Q. and Lu, X., 2008. Parameter estimation in a three-dimensional marine ecosystem model using the adjoint technique. Journal of Marine Systems, 74(1-2): 443-452.